21985

National Library of Canada | Bibliothèque nationale du Canada | **CANADIAN THESES ON MICROFICHE** | ***THÈSES CANADIENNES SUR MICROFICHE***

NAME OF AUTHOR/*NOM DE L'AUTEUR* JOZEF STRAUS

TITLE OF THESIS/*TITRE DE LA THÈSE* SOME TUNNELING STUDIES in NORMAL METAL-INSULATOR-METAL JUNCTIONS

UNIVERSITY/*UNIVERSITÉ* UNIVERSITY of ALBERTA

DEGREE FOR WHICH THESIS WAS PRESENTED/*GRADE POUR LEQUEL CETTE THÈSE FUT PRÉSENTÉE* PhD

YEAR THIS DEGREE CONFERRED/*ANNÉE D'OBTENTION DE CE DEGRÉ* 1974

NAME OF SUPERVISOR/*NOM DU DIRECTEUR DE THÈSE* DR J.G. ADLER

Permission is hereby granted to the NATIONAL LIBRARY OF CANADA to microfilm this thesis and to lend or sell copies of the film.

The author reserves other publication rights, and neither the thesis nor extensive extracts from it may be printed or otherwise reproduced without the author's written permission.

L'autorisation est, par la présente, accordée à la BIBLIOTHÈQUE NATIONALE DU CANADA de microfilmer cette thèse et de prêter ou de vendre des exemplaires du film.

L'auteur se réserve les autres droits de publication; ni la thèse ni de longs extraits de celle-ci ne doivent être imprimés ou autrement reproduits sans l'autorisation écrite de l'auteur.

DATED/*DATÉ* 18th of July 74 SIGNED/*SIGNÉ* Jozef Straus

PERMANENT ADDRESS/*RÉSIDENCE FIXÉ*
PHYSICS DEPT.
UNIVERSITY of ALBERTA
EDMONTON, ~~CA~~ ALBERTA

NL-91 (11-73)

THE UNIVERSITY OF ALBERTA

RELEASE FORM

NAME OF AUTHOR: Jozef Straus

TITLE OF THESIS: Some Tunneling Studies in Normal Metal-Insulator-Metal Junctions

DEGREE FOR WHICH THESIS WAS PRESENTED: Ph. D.

YEAR THIS DEGREE GRANTED: 1974

Permission is hereby granted to THE UNIVERSITY OF ALBERTA LIBRARY to reproduce single copies of this thesis and to lend or sell such copies for private, scholarly or scientific research purposes only.

The author reserves other publication rights, and neither the thesis nor extensive extracts from it may be printed or otherwise reproduced without the author's written permission.

(Signed) Jozef Straus

PERMANENT ADDRESS:

1343 Meadowlands Drive
#1205, Seneca Towers
Ottawa, Ontario

DATED: July 16, 1974

THE UNIVERSITY OF ALBERTA

SOME TUNNELING STUDIES IN NORMAL METAL-INSULATOR-METAL JUNCTIONS

by

Ⓒ JOZEF STRAUS

A THESIS

SUBMITTED TO THE FACULTY OF GRADUATE STUDIES AND RESEARCH
IN PARTIAL FULFILLMENT OF THE REQUIREMENTS FOR THE DEGREE
OF DOCTOR OF PHILOSOPHY
IN
PHYSICS

DEPARTMENT OF PHYSICS

EDMONTON, ALBERTA

FALL, 1974

© JOZEF STRAUS 1978

THE UNIVERSITY OF ALBERTA

FACULTY OF GRADUATE STUDIES AND RESEARCH

The undersigned certify that they have read, and recommend to the Faculty of Graduate Studies and Research, for acceptance, a thesis entitled SOME TUNNELING STUDIES IN NORMAL METAL-INSULATOR-METAL JUNCTIONS submitted by Josef Straus in partial fulfillment of the requirements for the degree of Doctor of Philosophy.

Supervisor

J. S. Rogers

Peter S Turner

External Examiner

Date: July 16, 1974

TO MY LOVING PARENTS

ABSTRACT

A theory (Trofimenkoff, et al, 1972) of a non-equilibrium electron tunneling in normal metal-insulator-metal junctions has been proposed to explain the presence of a small (∿1%) conductance reduction around zero bias. In particular, the related structure in σ and $d\sigma/dV$ have been accounted for by the blocking of otherwise available electron states due to finite electron relaxation times in metal electrodes. Detailed measurements on Mg/Mg, Mg/Au and Al/Al junctions have been performed and the results compared with predictions of the theory. In all cases a satisfactory agreement between the theory and the experiment was found. The inclusion of non-equilibrium phonons in metal electrodes has been suggested as a further refinement of the theory.

Measurements on some Mg/Mg and Mg/Au junctions have shown an additional oscillatory type structure in the derivative of the conductance. The occurrence of the structure has been found to be independent of metal electrodes, and barrier layers. Under the influence of external perturbations such as warming the junctions to room temperature, applying DC bias up to 1 eV and passing currents along the metal electrodes, the properties of the junctions were irreversibly altered. This suggests that impurity contamination of

the barrier is responsible for the observed structure.

Tunneling experiments have been performed in an attempt to observe the quantization of allowed energy levels in Bi films. The structure in Bi/Bi junctions,however, could not be correlated with the film thickness, thus rendering the results negative. As a byproduct of the investigation, a phonon spectrum of Bi has been determined.

ACKNOWLEDGEMENTS

I wish to express my deep gratitude to Dr. J.G. Adler, my research supervisor, for his cheerful encouragement and guidance throughout the course of this project. My introduction into the world of an experimentalist could not have been accomplished without his patience and instructive help.

I wish to thank Dr. H.J. Kreuzer for many illuminating and valuable discussions pertaining to the theory of zero bias anomaly. I am also thankful to Dr. P.S. Turner for examination of films by an electron microscope. I am grateful to the technical staff of the Physics Department for supplying liquid helium and assisting in construction of evaporators and cryostats. My special thanks are due to Mr. D.P. Mullin for his help and cooperation throughout the course of my work in the laboratory. I also wish to thank Mr. R. Teshima for his computer programming assistance.

It is a pleasure to acknowledge the alternating financial support of the Physics Department, National Research Council and the support arising from the Izaak Walton Killam Memorial Fund.

Finally, I am thankful to Mrs. Mary Yiu for her patience and excellent typing performance of this thesis.

TABLE OF CONTENTS

Page

CHAPTER 1 THEORETICAL DISCUSSION 1
1.1 Introduction 1
1.2 Theory of elastic tunneling 1
1.3 Theory of inelastic tunneling 10

CHAPTER 2 THE ZERO BIAS ANOMALY 14
2.1 Introduction 14
2.2 Non-equilibrium theory of tunneling 18
2.3 Description of the model 19
2.4 Scattering mechanism 24
2.5 Predictions of the theory 32

CHAPTER 3 EXPERIMENTAL TECHNIQUES 50
3.1 Sample preparation 50
3.2 Formation of tunnel barriers 53
3.3 Film thickness determination 56
3.4 Temperature measurement and control 58
3.5 Production of low temperatures 62
3.6 Measurement of tunneling characteristics 62

CHAPTER 4 EXPERIMENTAL RESULTS 69
4.1 Introduction 69
4.2 The problem of the background 69
4.3 General considerations in extracting τ_B, τ_i and τ_{drift}. 82

Page

CHAPTER 4 (cont'd)

4.4 Comparison of the theory with the experiment 86

4.5 Discussion 120

CHAPTER 5 RESONANT ELECTRON TUNNELING 128

5.1 Introduction 128

5.2 Experimental investigations of oscillations 131

5.3 Analysis of the experimental data 159

5.4 Resonant tunneling through impurity states 164

5.5 Discussion 172

CHAPTER 6 TUNNELING INTO BISMUTH 179

6.1 Quantum size effect in Bi 179

6.2 General considerations 184

6.3 Discussion of results 185

6.4 Phonons in Bi 193

6.5 Other interesting effects 202

CHAPTER 7 SUMMARY AND CONCLUSIONS 206

7.1 Discussions 206

7.2 Suggestions for further work 209

BIBLIOGRAPHY 212

APPENDIX I 219

APPENDIX II 226

LIST OF TABLES

		Page
Table 3.1	Selection of materials for evaporation	54
Table 6.1	Thickness and periodicity of oscillations	182
Table 6.2	Identification of phonon peaks in a Bi/Bi junction	200
Table 6.3	Identification of phonon peaks in Mg/Bi	201
Table 6.4	Identification of phonon peaks in Al/Bi	201

LIST OF FIGURES

Figure		Page
1.1	Transfer Hamiltonian model.	3
1.2	Schematic energy level diagram for tunneling between normal metals.	11
2.1	Conductance curves for junctions with various electrodes.	15
2.2	Schematic diagram of scattering processes.	20
2.3	Illustration of a deblocking by magnetic field.	28
2.4	$\delta\sigma$ vs V and $\frac{1}{\sigma_o}\frac{d\delta\sigma}{dV}$ vs V at T = 0 K ($\alpha^2F = a_1\omega^2$).	36
2.5	$\delta\sigma$ vs V and $\frac{1}{\sigma_o}\frac{d\delta\sigma}{dV}$ vs V at T = 0 K ($\alpha^2F = a_2\omega^2$).	38
2.6	$\delta\sigma$ vs T at V = 0 mV ($\alpha^2F = a_1\omega$).	42
2.7	$\delta\sigma$ vs T at V = 0 mV ($\alpha^2F = a_2\omega^2$).	44
2.8	V_{max} vs T and $\frac{1}{\sigma_o}\frac{d\delta\sigma_e}{dV}\Big\|_{V_{max}}$ vs T ($\alpha^2F = a_1\omega$).	46
2.9	V_{max} vs T and $\frac{1}{\sigma_o}\frac{d\delta\sigma_e}{dV}\Big\|_{V_{max}}$ vs T ($\alpha^2F = a_2\omega^2$).	48
3.1	Layout of the sample.	51
3.2	Schematic diagram of the cryostat.	60
3.3	Simplified bridge configuration.	63
3.4	Schematic diagram of the data acquisition system.	67
4.1	σ vs V for a Mg/Mg junction for various temperatures.	70
4.2	$\frac{1}{\sigma_o}\frac{d\sigma}{dV}$ vs V for a Mg/Mg junction for various temperatures.	72

Figure | Page

4.3 $\delta\sigma$ vs V for a Mg/Mg junction for various temperatures. 75

4.4 $\frac{1}{\sigma_o}\frac{d\delta\sigma}{dV}$ vs V for a Mg/Mg junction for various temperatures. 77

4.5 Experimental σ_{odd}/σ_o vs V. 80

4.6 Theoretical fit to experimentally determined V_{max} vs T and $\frac{1}{\sigma_o}\frac{d\delta\sigma e}{dV}\Big|_{V_{max}}$ vs T for a Mg/Mg junction. 87

4.7 Theoretical fit to experimentally determined $\delta\sigma/\sigma_o$ vs T for a Mg/Mg junction at V = 0 mV. 90

4.8 Theoretical and experimental $\frac{1}{\sigma_o}\frac{d\delta\sigma_e}{dV}$ vs V for a Mg/Mg junction. 92

4.9 σ vs V for O85A Mg/N_2/Au for various temperatures. 95

4.10 σ vs V for O85B Mg/N_2/Au for various temperatures. 97

4.11 Theoretical fit to experimentally determined V_{max} vs T and $\frac{1}{\sigma_o}\frac{d\delta\sigma_e}{dV}\Big|_{V_{max}}$ vs T for O85B1 and O85B2. 99

4.12 Theoretical and experimental $\frac{1}{\sigma_o}\frac{d\delta\sigma_e}{dV}$ vs V for a Mg/N_2/Au junction. 101

4.13 $\delta\sigma/\sigma_o$ vs T at V = 0 mV, for two junctions with different thickness of metal electrodes. 104

4.14 Theoretical fit to experimentally determined V_{max} vs T and $\frac{1}{\sigma_o}\frac{d\delta\sigma_e}{dV}\Big|_{V_{max}}$ vs T for an Al/Al junction. 107

Figure		Page
4.15	$\delta\sigma$ vs V for an Al/Al junction for various temperatures.	109
4.16	Theoretical fit to experimentally determined V_{max} vs T and $\frac{1}{\sigma_o}\frac{d\delta\sigma_e}{dV}\Big\|_{V_{max}}$ vs T for an Al/Al junction.	112
4.17	Theoretical and experimental $\frac{1}{\sigma_o}\frac{d\delta\sigma_e}{dV}$ vs V for an Al/Al junction.	114
4.18	Illustration of the appearance of the energy gap in an Al/Al junction.	116
4.19	$\sigma(0)$ vs T for 851 Al/Al, 691 Al/Al.	118
5.1	$\frac{1}{\sigma_o}\frac{d\sigma}{dV}$ vs V for 877A Mg/Au.	129
5.2	σ vs V for 883A Mg/Mg.	132
5.3	$\frac{1}{\sigma_o}\frac{d\sigma}{dV}$ vs V for 883A Mg/Mg.	134
5.4	Temperature smearing of oscillations in 867B Mg/Au.	138
5.5	σ vs V for 875B Mg/Au.	140
5.6	σ/σ_o vs V, $1d\sigma/\sigma_o dV$ vs V for 875 Mg/Mg/Au.	142
5.7	σ vs V for 95A Mg/N_2/Au.	145
5.8	$\frac{1}{\sigma_o}\frac{d\sigma}{dV}$ vs V for 95A Mg/N_2/Au.	147
5.9	σ/σ_o vs V for O8OB Mg/Au before and after annealing.	151
5.10	$\frac{1}{\sigma_o}\frac{d\sigma}{dV}$ vs V for O8OB Mg/Au before and after annealing.	153
5.11	$\sigma/\sigma(0)$ vs V for J107B Mg/N_2/Au before and after applying high bias across the junction.	155

Figure | Page

5.12 $\frac{1}{\sigma_o}\frac{d\sigma}{dV}$ vs V for J107B Mg/N_2/Au before and after applying high bias across the junction. 157

5.13 Schematic potential diagram for a junction with an impurity lying inside the barrier. 165

5.14 σ_R/σ_N vs V. 169

5.15 Spin splitting of an impurity level. 174

6.1 σ/σ_o vs V for 001, 007, 016 Bi/Bi junctions. 186

6.2 $\frac{1}{\sigma_o}\frac{d\sigma}{dV}$ vs V for 001, 007, 016 Bi/Bi junctions. 188

6.3 $\frac{1}{\sigma_o}\frac{d\sigma}{dV}$ vs V for 007 Bi/Bi. 191

6.4 Phonons in Bi/Bi. 194

6.5 Phonons in Mg/Bi. 196

6.6 Phonons in Al/Bi. 198

6.7 Normalized conductance of typical Al/Bi, Mg/Bi and Bi/Bi junctions. 203

CHAPTER 1

THEORETICAL DISCUSSION

1.1 Introduction

The concept of a particle tunneling from a classically allowed region of space through a classically forbidden region, into the second allowed region was one of the early predictions of Schrödinger's wave equation.

The possibility that a tunnel current may flow between metals separated by a vacuum was first considered by Frenkel (Frenkel, 1930). Sommerfeld and Bethe (Sommerfeld and Bethe, 1933) extended Frenkel's calculation to the case in which the vacuum was replaced by a thin insulating layer. The actual physical fabrication of such a system was delayed until 1960 when the thin film technology had sufficiently advanced allowing Fisher and Giaver (Fisher, Giaver, 1961) to build a tunnel structure using aluminum-aluminum-oxide-aluminum. The results of their experiments stimulated a sequence of measurements on both normal and superconducting tunnel junctions with far reaching results leading to a better understanding of electron transport phenomena in metals.

1.2 Theory of elastic tunneling

Bardeen (Bardeen, 1961) has regarded the tunneling process as a transition of an electron across the barrier which itself acts as a perturbing potential. The composite metal-insulator-metal system is described by Hamiltonians H_1, H_2 of the left and right hand metals and one electron eigenstates ψ_1 and ψ_2 which are weakly coupled together by a perturbation U (fig.1.1). By taking a linear combination of ψ_1 and ψ_2 we seek then a modified solution to the time dependent Schrödinger equation. Knowing ψ_1 and ψ_2 the transition matrix element M_{12} of the Hamiltonian between states ψ_1 and ψ_2 can then be calculated using the method of time dependent perturbation theory.

The transition probability P_{12} per unit time of an electron in a state ψ_1 to a state ψ_2 is then given by Fermi golden rule

$$P_{12} = \frac{2\pi}{\hbar} |M_{12}|^2 \rho_2 f_1^o (1 - f_2^o) \tag{1.1}$$

where ρ_2 is the density of final states in the metal 2, f_1^o and f_2^o are the Fermi-Dirac probabilities of occupation of states ψ_1 and ψ_2.

As an approximation for the electron current density between the two metals, an independent particle model is used. It is assumed that the metal-insulator interface is planar and that the component of the wave number parallel to the plane of the barrier, $k_{||}$, is

Fig. 1.1

Transfer Hamiltonian Model

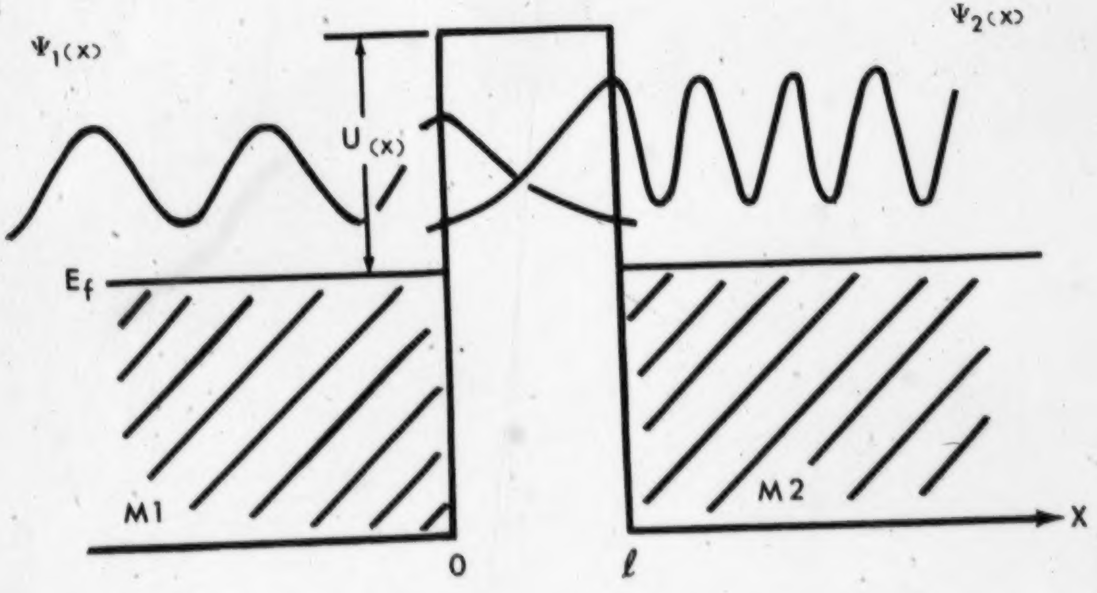
$\Psi_1(x)$
$\Psi_2(x)$
$U_{(x)}$
E_f
M1
M2
0
ℓ
X

conserved before and after the transmission. The total energy of the electron of course, is conserved and this is implied when writing eq. (1.1). To obtain the tunneling current from metal 1 to metal 2, P_{12} is summed over all states 1 of fixed $k_{||}$, summed over $k_{||}$, multiplied by 2 for spin and by charge e of the electron. The sum over states 1 may be replaced by an integral over energy at fixed wave number $k_{||}$. Subtracting the current from metal 2 to metal 1, one obtains for the net current

$$I = \frac{4\pi e}{\hbar} \sum_{k_{||}} \int_0^\infty |M_{12}|^2 \rho_1(E_x)\rho_2(E_x+eV)[f^o(E)-f^o(E+eV)]dE_x \qquad (1.2)$$

where

$$f^o(E) = \frac{1}{1 + e^{(E-E_{f1})/K_BT}}$$

and ρ_i, i = 1,2, represents a one dimensional density of states, associated with the motion perpendicular to the barrier

$$\rho_i = \frac{L}{\pi} \left(\frac{\partial E}{\partial k_{x_i}}\right)^{-1} \qquad i = 1,2 \qquad (1.3)$$

where L gives the length of the metal. Unless otherwise stated all energies are measured with reference to the bottom of the conduction band of metal 1. Because of the independent particle model, we can write E as

$$E = E_x + E_{||}$$

with

$$E_{||} = \frac{\hbar^2 k_{||}^2}{2m} \quad , \qquad E_x = \frac{\hbar^2 k_x^2}{2m} \quad .$$

The functional form of the matrix element $|M_{12}|^2$ depends on the profile of the barrier potential used for the calculation of electron transmission probability. Harison, (Harrison, 1961) applying a WKB approximation found that

$$|M_{12}|^2 = \frac{D(E,E_{||})}{4\pi^2 \rho_1 \rho_2} \tag{1.4}$$

where the barrier transmission coefficient D is given by

$$D(E,E_{||}) = \exp(-2 \int_0^{\ell} \sqrt{\frac{2m}{\hbar^2} (U(x)-(E-E_{||})}\, dx) \ . \tag{1.5}$$

Substituting eq. (1.4) for $|M_{12}|^2$ into eq. (1.2) we obtain

$$I = \frac{2e}{\hbar} \sum_{k_{||}} \int_0^{\infty} D(E,E_{||})\,(f^o(E) - f^o(E+ eV)\ dE_x \tag{1.6}$$

and find that the density of states factors appearing in eq. (1.2) have cancelled with the matrix element so that the tunneling current does not explicitly depend on them. The absence of density of states in eq. (1.6) is a result of the independent particle model, which enabled the separation of the electron wave number into parallel and perpendicular components with respect to the plane of the barrier and the replacement of the sum over the normal components by an integral over energy E_x. Furthermore, the WKB approximation is restricted only to regions where the fractional change in the electron wavelength is small i.e. $\frac{\delta\lambda}{\lambda} << 1$. This is not satisfied for electrons near the band edge, having small kinetic energy. Therefore, as Harrison points out, band edges and energy gaps may introduce an observable structure in the tunneling current.

The form of the matrix element eq. (1.3) and its use in eq. (1.5) implies that the tunneling is from one quasi-continuous band of states, through the barrier into another quasi-continuous band. If, on the other hand, ρ_2 is a set of localized surface states or impurity states, the resulting matrix element is no longer proportional to ρ_2^{-1} but rather to τ^{-1}, the lifetime of the state (Penley, 1962), and the density of such states does not cancel. In general, if the rate limiting quantity in the tunneling process is the electron velocity, and if the velocity is inversely proportional to the density of states, which is characteristic of a band of single particle states, then the tunneling current does not contain information about the density of states. But, if the tunneling process is primarily via traps and defect states in the insulator, which can be characterized by a lifetime τ, the density of states should not cancel.

Eq. (1.6) can be cast into a more convenient form by converting the sum over $k_{||}$ to an integral over $k_{||}$ and then to an integral over $E_{||}$, with $d^2k_{||} = \frac{m}{2\pi\hbar^2}\, dE_{||}$.

$$I = \frac{4\pi meA}{h^3} \int_0^{\infty} \int_0 [f^o(E) - f^o(E + eV)] D(E, E_{||})\, dE_x dE_{||} . \qquad (1.7)$$

The upper limit on the integration over $dE_{||}$ can be determined from the condition that the component of the wave number parallel to the plane of the barrier $k_{||}$ and the electron energy E are conserved during transition. Exchanging the order of integration in eq. (1.7) and noting that $D(E, E_{||}) = D(E_x)$ and $\partial E_{||}/\partial E = 1$ we obtain

$$I = \frac{4\pi meA}{h^3} \int_0^{\infty} [f^o(E) - f^o(E + eV)]\, dE \int_0^{E} D(E_x)\, dE_x \qquad (1.8)$$

where A is the effective junction area.

For illustration, we calculate the tunneling current at T = 0 K. Since

$$f^o(E) - f^o(E + eV) = 0 ,$$

unless

$$E_{f1} - eV < E < E_{f1}$$

when

$$f^{o}(E) - f^{o}(E+eV) = 1$$

eq. (1.8) reduces to:

$$I = \frac{4\pi meA}{h^{3}} \int_{E_{f1}-eV}^{E_{f1}} dE \int_{0}^{E} D(E_{x})\, dE_{x} \qquad (1.9)$$

or

$$I = \frac{4\pi meA}{h^{3}} (eV) \int_{0}^{E_{f1}} D(E_{x})\, dE \qquad (1.10)$$

providing that $eV << E_{f1}$. The current is therefore ohmic at low biases. The current at $T \neq 0$ K can be connected to the current at $T = 0$ K (Stratton, 1962) by

$$\frac{I(V,T)}{I(V,0)} = \frac{\pi CK_{B}T}{\sin \pi CK_{B}T} \qquad (1.11)$$

where C is a constant dependent on the barrier height and thickness. The expected variation of the current with temperature is more apparent in eq. (1.11) (Maissel, Glang, 1970)

$$\Delta I(V,T) = \frac{I(V,T) - I(V,0)}{I(V,0)} = 3\times10^{-9}\ \frac{(\ell.T)^{2}}{\Phi} \qquad (1.12)$$

where ℓ is in Å, and T and Φ (average barrier potential) are in conventional units. For typical parameters $\phi = 1$ eV, $\ell = 30$ Å, $T = 5$ K,

$$\Delta I(V,T) \sim 10^{-5}$$

which is negligible.

1.3 Inelastic tunneling

Tunneling which involved a loss of energy by tunneling to localized impurities in the barrier was first reported by Jacklevic and Lambe (Jacklevic and Lambe, 1966). In studying Al-insulator-Pb tunnel junctions, they have noticed increases in the conductance of the junctions at characteristic voltages corresponding to vibrational frequencies $\hbar\omega$ of molecular species contained in the insulating region of the junction. The energy level diagram on fig. 1.2 allows a visualization as to how such processes can lead to increases in conductance.

Fig. 1.2 represents a tunnel junction energy level diagram where the Fermi levels of the two metals are separated by the energy eV where V is the applied voltage. For simplicity let us assume that the system is at T = 0 K which means that the Fermi levels are sharp and the impurity present in the barrier is in its ground state. Electrons may tunnel elastically from metal 1 to metal 2 (process a). If a new mechanism exists so that an electron can lose energy $\hbar\omega$ to a localized impurity in the barrier as it is tunneling (process b) a new channel will open up. This new channel is possible only if there exist empty states in metal 2 at an energy $\hbar\omega$ less than E_1. This becomes possible when $eV \geq \hbar\omega$.

Fig. 1.2

Schematic energy level diagram for tunneling between normal metals:

a) elastic tunneling

b) inelastic tunneling.

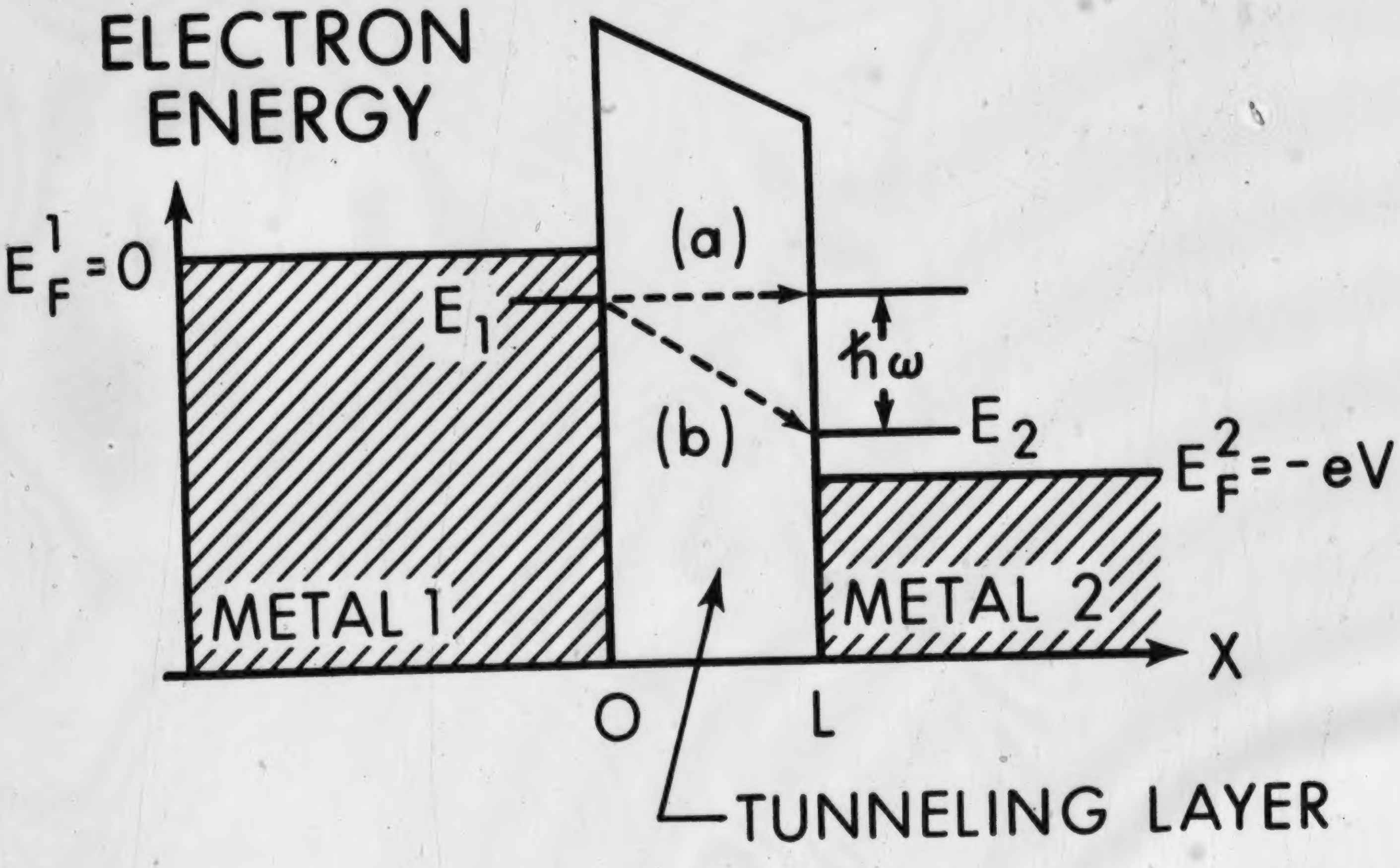
ELECTRON ENERGY
$E_F^1 = 0$
E_1
(a)
(b)
$\hbar\omega$
E_2
$E_F^2 = -eV$
METAL 1
METAL 2
X
O
L
TUNNELING LAYER

This onset of a new tunneling channel results in a steplike increase in the conductance and δ function like structure in the derivative of the conductance. A finite temperature will smear the Fermi surface of both metals and thus it will smear the δ function like structure although it will be centered around $eV = \hbar\omega$. The energy loss of the tunneling electron is not limited only to losses to localized impurities. In fact, as it was shown by Giaver and Zeller (Giaver and Zeller, 1968) and others, inelastic excitations due to phonons of the barrier (Adler, 1969), phonons of metal electrode (Rowell et al, 1969) itself, surface plasmons (Tsui, 1969), magnons (Tsui, et al, 1971) are possible.

CHAPTER 2

THE ZERO BIAS ANOMALY

2.1 Introduction

The description of a tunnel junction at small biases ($eV << \Phi$) as an ohmic element (eq. 1.10) is found to be adequate only when analyzing I-V curves. Conductance measurements using derivative techniques to an accuracy of $\sim$1 % have shown that the conductance of a tunnel junction up to 500 meV is roughly parabolic

$$\sigma(V) = \alpha + \beta V + \gamma V^2 \quad . \tag{2.1}$$

Theoretical calculations (Brinkman et al, 1969) have explained the offset of the parabola from zero bias as being due to the barrier asymmetry arising from different work functions of the metal electrodes. Offsets larger than 50 meV were attributed to the distortion of the barrier potential due to impurities trapped in the junction. The parabolic fit by eq. (2.1) is considered to be approximate in the sense that it helps to determine the background conductance level for any additional structure which may appear superimposed on the tunnel characteristics. Fig. 2.1 illustrates such a case (Chen, Adler, 1970). The set of

Fig. 2.1

Normalized condutance curves for junctions with various electrodes. The curves are displaced vertically by 0.1 for clarity. The scales for Al-Al, Al-Mg junctions should be multiplied by two. The insert shows the sizes of zero bias anomalies of some junctions.

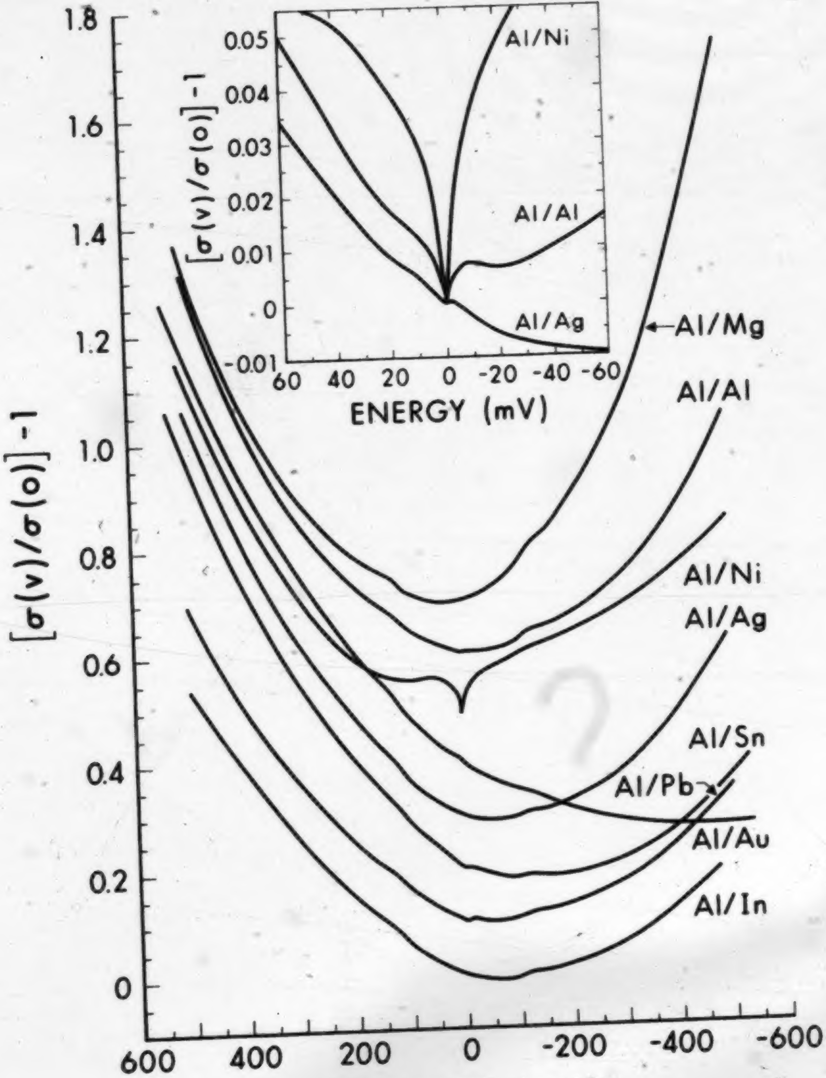
[σ(v)/σ(o)] -1
1.8
1.6
1.4
1.2
1.0
0.8
0.6
0.4
0.2
0
600
400
200
0
-200
-400
-600
ENERGY (mV)
Al/Mg
Al/Al
Al/Ni
Al/Ag
Al/Sn
Al/Pb
Al/Au
Al/In
0.05
0.04
0.03
0.02
0.01
0
-0.01
60
40
20
0
-20
-40
-60
Al/Ni
Al/Al
Al/Ag

curves for different junctions is roughly parabolic with weak conductance increases at 118 meV due to inelastic excitation of aluminum hydrate (Geiger et al, 1969).

The insert in fig. 2.1 shows a structure around zero bias (commonly called the zero bias anomaly), the detection of which requires conductance measurements with a resolution to one part in 10^4. Disregarding the relatively large conductance dip for the Al/Ni junction, which is associated with the magnetic properties of the nickel electrode (Rowell, 1969), small conductance decreases (< 1 %) around zero bias in normal metal-insulator-junctions (seen here in Al/Al and Al/Ag junctions) were for a long time unexplained. The structure does not fall into any other previously investigated classes of zero bias anomalies explained on the basis of metallic inclusions (Giaver, Zeller, 1968) or magnetic impurities inside the insulating layer (Rowell, Shen, 1967).

A recent theory (Trofimenkoff et al, 1972) through a nonequilibrium treatment of the tunneling process has shown that the appearance of the low bias conductance minimum in M-I-M junctions is closely related to the finite electron relaxation rates in metal electrodes.

In what follows, we shall present the theoretical model of describing the non-equilibrium tunneling process with its predictions which are relevant to experimental verification.

2.2 Non-equilibrium theory of tunneling

A conventional theory of tunneling (Chapter 1) assumes that the tunneling electron is in thermal equilibrium with the rest of the electrons inside the metal. This is expressed by using the equilibrium Fermi-Dirac distribution function, f^o, in the calculation of the tunneling current.

Consider, however, the following argument. An electron which penetrates the barrier finds itself at certain energy level in the host metal. At He^4 temperatures, the final state of the electron is such that even at small imposed biases ~ 1 meV, it is energetically well above the thermally smeared Fermi sea ($1\ K = 86\ \mu V$). The existing non-equilibrium situation is neutralized only after a short period of time which is characterized by the relaxation processes in the metal. During the time the excited state is occupied, by the virtue of Pauli exclusion principle, all incoming electrons are effectively blocked from entering the same state. If the decay times of the excitation were of the same order of magnitude as the time an electron decides to penetrate the barrier, the blocking of the available states would manifest itself by a strong decrease in the conductance of the tunnel junction. The use of equilibrium Fermi-Dirac distribution function is then equivalent to an assumption that the thermalization is immediate. In other words, the relaxation times of the interactions are assumed to be equal to zero.

To obtain quantitative predictions of the above mentioned process, a non-equilibrium distribution function has to be found, characteristic of the existing situation in the metal electrode. This is done by solving a transport model for the tunnel current, based upon the Boltzmann equation.

2.3 Description of the model

With reference to fig. 2.2, assume that an electron tunnels from a state ψ_1 into a state ψ_2. By the virtue of Pauli exclusion principle the final state ψ_2 is unavailable for tunneling as long as it is occupied. However, through various scattering processes, the electron is scattered out of the occupied state. The competing mechanisms of filling and emptying the states soon establish across the junction a steady state in which the rate of change of the distribution function with time is zero, $\partial f/\partial t = 0$.

21983-2

Fig. 2.2

Schematic diagram of scattering processes:

a) electron in a forward direction

b) inelastic scattering by phonon emission
   or absorption

c), d) elastic impurity scattering

e) specular boundary scattering

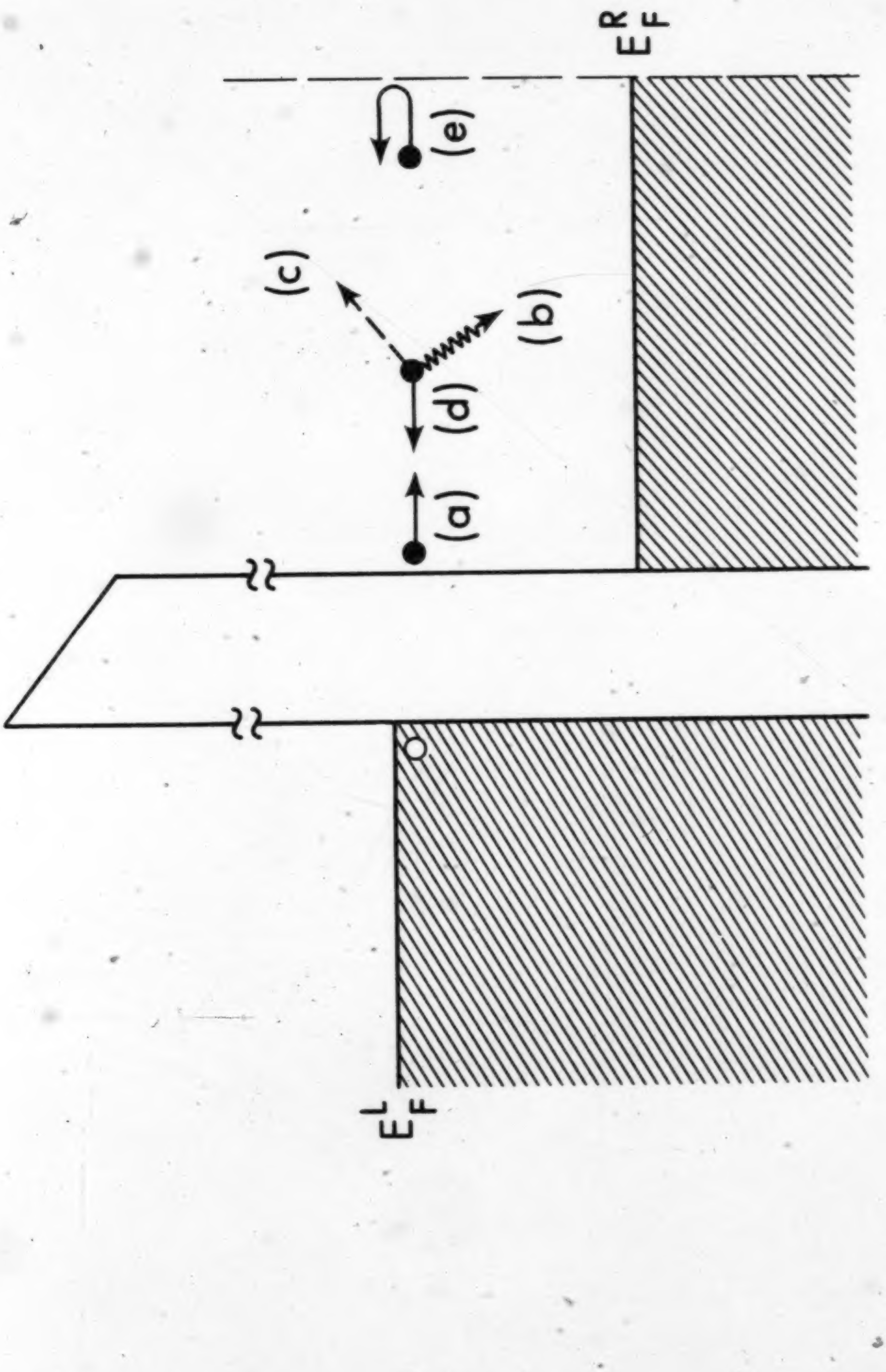

E_F^R
(a)
(b)
(c)
(d)
(e)
E_F^L

Balancing the rate of change of the distribution function in metal 2 due to incoming $(\partial f_2/\partial t)_{1\rightarrow 2}$ and outgoing $(\partial f_2/\partial t)_{2\rightarrow 1})$ electron flux with losses due to scattering processes, $(\partial f_2/\partial t)_{\text{scatt}}$ we have:

$$\left(\frac{\partial f_2}{\partial t}\right) = 0 = \left(\frac{\partial f_2}{\partial t}\right)_{1\rightarrow 2} + \left(\frac{\partial f_2}{\partial t}\right)_{2\rightarrow 1} + \left(\frac{\partial f_2}{\partial t}\right)_{\text{scatt}} . \tag{2.2}$$

In relaxation time approximation

$$\left(\frac{\partial f}{\partial t}\right)_{\text{scatt}} = - \frac{\Delta f}{\tau} \tag{2.3}$$

where Δf is the deviation of f from equilibrium

$$f = f^{o} + \Delta f \tag{2.4}$$

and τ is a time characteristic of scattering processes which bring f back to equilibrium. With the help of Fermi golden rule,eq. (2.2) is written as

$$\frac{\partial f_2}{\partial t} = \frac{2\pi}{\hbar} |M_{12}|^2 \rho_1 f_1 (1 - f_2) - \frac{2\pi}{\hbar} |M_{12}|^2 \rho_1 f_2 (1 - f_1) - \frac{\Delta f_2}{\tau_2} \tag{2.5}$$

or

$$\frac{\Delta f_2}{\tau_2} = \frac{2\pi}{\hbar} |M_{12}|^2 \rho_1 (f_1 - f_2) . \tag{2.6}$$

By symmetry a similar equation is written for f_1

$$\frac{\Delta f_1}{\tau_1} = \frac{2\pi}{\hbar} |M_{12}|^2 \rho_2 (f_2 - f_1) . \tag{2.7}$$

Since the relevant quantity which enters the calculation of the tunneling current is the difference in the distribution functions (eq. 1.8), the two equations above are solved in that form:

$$f_1 - f_2 = \frac{f_1^o - f_2^o}{1 + \frac{2\pi}{h}|M_{12}|^2[\rho_1\tau_2 + \rho_2\tau_1]} \quad . \qquad (2.8)$$

On the basis of experimental evidence, we expect that the deviations from equilibrium are small. This permits to rewrite eq. (2.8)

$$f_1 - f_2 = (f_1^o - f_2^o)(1 - \frac{2\pi}{h}|M_{12}|^2[\rho_1\tau_2 + \rho_2\tau_1]) . \qquad (2.9)$$

Therefore instead of the usual difference in the equilibrium distribution functions ($f_1^o - f_2^o$), (eq. (1.8), the above relationship between f_1 and f_2 should be used in the calculation of the tunneling current. In the next section we shall consider the nature of the scattering processes, in order to determine the different relaxation mechanisms present in the metal.

2.4 Scattering mechanism

An electron in the metal undergoes a number of collisions which in general may alter its energy and momentum. Inelastic scattering due to phonon emission and absorption is characterized by a temperature and energy dependent relaxation time $\tau(\varepsilon,T)$. A first order calculation applied to an interacting electron-phonon gas (Wilkins, 1968) gives the following result:

$$\frac{1}{\tau_{ep}(\varepsilon,T)} = \frac{2\pi}{\hbar}\int_0^\infty d(\hbar\omega)\,\alpha^2(\hbar\omega)F(\hbar\omega)\,[2N^o(\hbar\omega) + 1 + f^o(\varepsilon+\hbar\omega) - f^o(\varepsilon-\hbar\omega)] \qquad (2.10)$$

where ε is the excitation energy measured relative to the Fermi level. α^2F is a product function involving the electron-phonon coupling function $\alpha^2(\hbar\omega)$ and the phonon density of states $F(\hbar\omega)$. The equilibrium distribution function for the phonons is given by

$$N^o = \frac{1}{e^{\frac{\hbar\omega}{k_BT}} - 1} \quad . \qquad (2.11)$$

Since the evaporated films are polycrystalline and thus have a characteristic of an isotropic material, the relaxation time τ_{ep} is assumed to be isotropic.

To facilitate a comparison of the theory with the experiment it is necessary to investigate the behaviour of τ_{ep} at low temperatures and low excitation energies. Approximating α^2F at low frequencies by a power law behaviour

$$\alpha^2F = a_n\omega^n \qquad n = \text{integer}$$

$$a_n = \text{constant}$$

Wattamaniuk (Wattamaniuk, 1972) found that

$$\frac{1}{\tau_{ep}(\varepsilon)} = \frac{\pi a_1}{\hbar}\,(\varepsilon^2 + (\pi k_BT)^2] \tag{2.12}$$

for n = 1, whereas for n = 2

$$\frac{1}{\tau_{ep}(\varepsilon)} \xrightarrow[\varepsilon\to 0]{} \frac{2\pi a_2}{\hbar}\,7\xi(3)(k_BT)^3 \tag{2.13}$$

$$\frac{1}{\tau_{ep}(\varepsilon)} \xrightarrow[T\to 0]{} \frac{2\pi a_2}{\hbar}\,\frac{|\varepsilon|^3}{3} \tag{2.14}$$

where $\xi(x)$ is a Riemann zeta function.

The two limiting cases of τ_{ep} appear as a result of a controversy which at the present time exists on the low energy limit of α^2F. At low frequencies $F(\omega)$ in the Debye approximation varies as ω^2. Therefore for $n = 2, \alpha^2(\hbar\omega)$ is a constant. Experimental results (Goy, Castaing, 1973) point to this behaviour. Theoretical calculations (Carbotte, Dynes, 1968; Allen, Cohen, 1970) indicate a possible linear behaviour of α^2F due to Umklapp processes. We shall consider both cases separately, hoping that the experimental results will favour one limit.

Lacking detailed knowledge about the structure of evaporated films, scatterings due to lattice defects, impurities and diffuse boundaries are characterized by a constant relaxation time τ_i i.e. the scattering is considered to be energy and temperature dependent.

Another mechanism by which the blocking of the incoming electron flow is decreased,is obtained by an application of a magnetic field perpendicular to the direction of the tunnel current.

An electron which penetrates the barrier will travel away from it and can propagate across the film before being scattered. Assuming specular reflection at the boundary, the electron is reflected back with a reversed momentum. Upon reaching the metal-insulator interface, it may again be reflected specularly, thus reversing the momentum back to the original one. If the travel time over the length of the film is much less than the time an electron decides to penetrate the barrier or the scattering time, then the electron effectively remains in its quantum state and contributes to the blocking. For typical metals at energies close to the Fermi level $V_f \sim 10^8$ cm/sec and for a 1000 Å film, the travelling time back and forth is $\sim 2\times 10^{-13}$ sec which is at least two orders of magnitude less than the relaxation times due to electron-phonon interaction ($\sim 10^{-11}$ sec at He^4 temperatures).

In the presence of the magnetic field (Fig. 2.3), oriented perpendicularly to the direction of the tunnel current flow, the Lorentz force induced drift provides a mechanism, whereby the specularly reflected electrons move down the electrode and ultimately move away from the tunneling area. In a classical picture, the relaxation time associated with this process is then equated to the time it takes an electron to drift out of the junction area and thus be removed from the forward blocking direction. It is assumed that at low biases the magnetic field introduces no appreciable changes in the Fermi surface of the metal which could affect the tunnel current. The validity of this assumption is confirmed by the experimental results.

With reference to Fig. 2.3, $\overline{AA}$ represents the metal-insulator interface, which is at distance L away from the other end of the film. A magnetic field of B kG produces a circular motion with radius

$$R = \frac{mcV_f}{e} \quad , \tag{2.15}$$

where c is speed of a light, and V_f is the velocity of the electron at the Fermi level. During the time

21985

Fig. 2.3

Schematic illustration of magnetic field induced drift velocity of a tunneling electron.

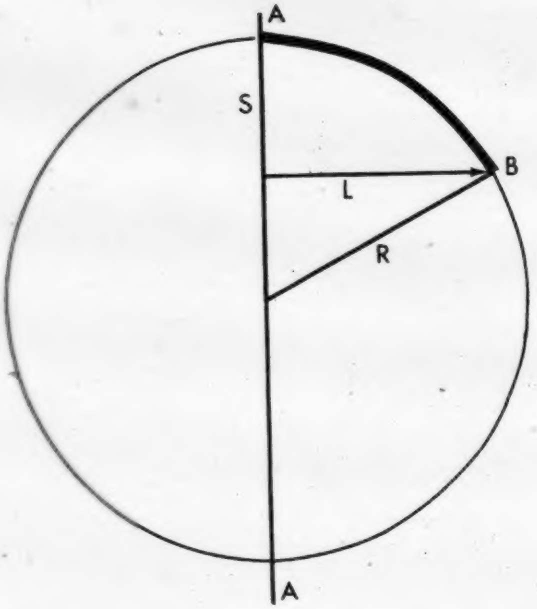
A
S
B
L
R
A

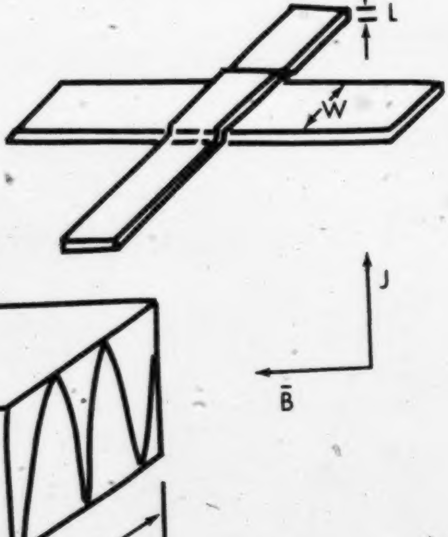
L
W

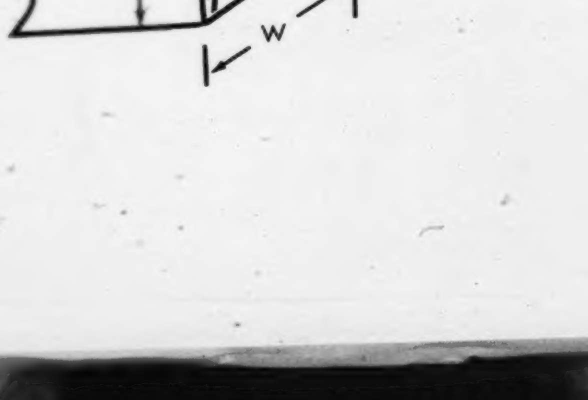
J
$\bar{B}$
L
W

$\tau_{AB} = \frac{\overline{AA}}{V_f}$, the electron drifts down the electrode a distance S

$$S = R - \sqrt{R^2 - L^2} \tag{2.16}$$

Approximating AB by a chord $\overline{AB}$

$$\overline{AA} = \sqrt{S^2 + L^2} \tag{2.17}$$

τ_{AB} becomes:

$$\tau_{\overline{AA}} = \frac{\sqrt{S^2 + L^2}}{V_f} \quad . \tag{2.18}$$

The drift velocity is given as:

$$V_{drift} = \frac{S}{\tau_{\overline{AA}}} = \frac{SV_f}{\sqrt{S^2 + L^2}} \tag{2.19}$$

and thus if w denotes the width of the film;

$$\tau_{drift} = \left(\frac{V_{drift}}{w}\right)^{-1} = \frac{w\sqrt{2}}{V_f} \left[1 - \sqrt{1 - \frac{L^2}{R^2}}\right]^{-1/2} \quad . \tag{2.20}$$

For L = 1000 Å and R(60 kG) = 20000 Å, $L/R << 1$ and we can expand the square root in eq. (2.20) in powers of L/R. Keeping the first non-zero term we have:

$$\tau_{drift}(B) = \frac{2mc}{eB} \left(\frac{w}{L}\right) \quad . \tag{2.21}$$

The final result shows that the effect of a magnetic field is to reduce the blocking by a rate which depends entirely on the geometry of the junction via the $(\frac{w}{L})$ ratio.

A magnetic field applied parallel to the tunnel current provides no Lorentz force on the electron and thus should have no effect on the size of the zero bias anomaly.

Recapitulating, we have considered three possible mechanisms which may scatter electrons from a given state:

a) Energy and temperature dependent electron-phonon scattering time.

b) Temperature and energy independent impurity scattering time, which includes contributions from lattice defects and diffuse boundaries.

c) Scattering due to magnetic field induced drift velocity of the tunneling electron.

Since the probability of a scattering is inversely proportional to the relaxation time and since the different scattering mechanisms are independent of each other, we can write

$$\frac{1}{\tau} = \frac{1}{\tau_{ep}} + \frac{1}{\tau_i} + \frac{1}{\tau_{drift}} \quad , \qquad (2.22)$$

where τ is the effective relaxation time of an excited electron.

2.5 Predictions of the theory

Substituting eq. (2.9) into eq. (1.8) the total tunneling current I is given as

$$I = I_o + \delta I \ , \tag{2.23}$$

where I_o is the equilibrium current and δI is the blocking current

$$\delta I = \frac{4\pi meA}{h^3} \int_0^\infty (f^o(E) - f^o(E + eV))\,dE \int_0^{E_x} D^2(E_x)$$

$$\cdot \left[\frac{1}{2\pi h} \frac{\tau_1(E-E_{f1})}{\rho_1(E_x)} + \frac{\tau_2}{2\pi h} \frac{(E - E_{f1} + eV)}{\rho_2(E_x + eV)} \right] . \tag{2.24}$$

When writing the above equation we assume that the energy dependence of the relaxation time is coming only from the energy dependence of the electron-phonon counterpart.

Notice the dependence of δI in the square of the barrier transmission coefficient, thus making δI a sensitive function of the insulator thickness. Furthermore the density of states factors did not cancel out as it happened in the calculation of the equilibrium tunneling current I_o. A density of states, rapidly varying with energy, could then produce a structure in δI. However, for small applied bias, where experimentally the blocking current is observed, the density of states is a smooth function of energy, the variation of which would not be expected to have significant effect on δI. In fact, we can replace the ratio $\frac{1}{2\pi h}\frac{D}{\rho_i}$, $i = 1,2$, by its value at the Fermi level providing $eV \ll E_{fi}$, $i = 1,2$

$$\frac{D}{2\pi\hbar\rho_i} = \frac{D(E_{fi})}{2L_i} V_{fi} = \frac{1}{\tau_{Bi}}\,, \quad i=1,2 \tag{2.25}$$

where V_{fi} is the Fermi velocity and L_i is the thickness of the metal i. τ_B is the tunneling lifetime of an electron in i^th electrode.

Referencing the energies to the Fermi level of the left hand metal, and realizing that due to the difference in the Fermi functions the only significant contribution to δI arises from energies close to the Fermi level, we rewrite eq. (2.24) as

$$\delta I = -\frac{\sigma_o}{e}\int_{-\infty}^{+\infty}\left[F^o(\varepsilon) - F^o(\varepsilon + eV)\cdot\left(\frac{\tau_1(\varepsilon)}{\tau_{B1}} + \frac{\tau_2(\varepsilon + eV)}{\tau_{B2}}\right)\right] d\varepsilon \tag{2.26}$$

where

$$F^o(\varepsilon) = \frac{1}{e^{\varepsilon/k_BT} + 1}$$

and σ_o is the ideal zero bias conductance as defined in eq. (1.10)

$$\sigma_o = \frac{4\pi me^2A}{h^3}\int_0^{E_{f1}} D(E_x)\, dE_x\ . \tag{2.27}$$

Eq. (2.26) can be further simplified realizing that τ, the effective relaxation time is an even function of the excitation energy since τ_{ep} by definition (eq. 2.10) is even. Using

$$F^{o}(\varepsilon) - F^{o}(\varepsilon + eV) = -F^{o}(-\varepsilon - eV) - F^{o}(-\varepsilon) \quad (2.28)$$

we rewrite eq. (2.26) as:

$$\delta I = -\frac{\sigma_o}{e} \int_{-\infty}^{\infty} \left[F^{o}(\varepsilon) - F^{o}(\varepsilon + eV)\right] \cdot \left[\frac{\tau_1(\varepsilon)}{\tau_{B1}} + \frac{\tau_2(\varepsilon)}{\tau_{B2}}\right] d\varepsilon \quad (2.29)$$

The blocking conductance $\delta\sigma(V) = \delta I(V)/dV$, normalized to zero bias is given as:

$$\frac{\delta\sigma(V)}{\sigma_o} = -\int_{-\infty}^{\infty} d\varepsilon \left[-\frac{\partial F^{o}(\varepsilon)}{\partial \varepsilon}\right] \cdot \left[\frac{\tau_1(\varepsilon + eV)}{\tau_{B1}} + \frac{\tau_2(\varepsilon + eV)}{\tau_{B2}}\right]. \quad (2.30)$$

It may be easily verified that $\delta\sigma(V)$ is an even function of the applied bias V. Therefore, it is symmetric around zero bias.

In further discussions we assume that the junction is symmetric and that the applied magnetic field is equal to 0 kG. We write then

$\tau_B = \tau_{B1} = \tau_{B2}$ and $\tau_1(\varepsilon) = \tau_2(\varepsilon) = \tau(\varepsilon)$.

At 0 K we can evaluate the blocking conductance in a closed form,

$$\frac{\delta\sigma(V)}{\sigma_o} = -\frac{2\tau(eV)}{\tau_B} \tag{2.31}$$

where

$$\frac{1}{\tau} = \frac{1}{\tau_i} + \frac{1}{\tau_{ep}(eV,T=0)} \ . \tag{2.32}$$

Recalling eqs. (2.12)-(2.14), we write

$$\frac{\delta\sigma(V)}{\sigma_o} = -\frac{2/\tau_B}{\frac{1}{\tau_i} + \left(\frac{\pi a_1}{\hbar}\right)(eV)^2} \tag{2.33}$$

for $\alpha^2 F = a_n \omega^n$, $n = 1$, and

$$\frac{\delta\sigma(V)}{\sigma_o} = -\frac{2/\tau_B}{\frac{1}{\tau_i} + \left(\frac{2\pi a_2}{3\hbar}\right)|eV|^3} \tag{2.34}$$

for $n = 2$. Figs.2.4 and 2.5 illustrate the blocking conductance and its derivative $d\delta\sigma(V)/dV$ for $n = 1$ and $n = 2$. For finite temperatures the integral in eq. (2.30) has to be calculated numerically. We write eq. (2.30) then as

$$\frac{\delta\sigma(V)}{\sigma_o} = -\int_{-\infty}^{\infty} \frac{dx}{(e^x+1)(e^{-x}+1)} \left\{ \frac{\tau_1(xk_BT + eV)}{\tau_{B1}} + \frac{\tau_2(xk_BT + eV)}{\tau_{B2}} \right\} \ . \tag{2.35}$$

The derivative of the blocking conductance $\frac{1}{\sigma_o}\frac{d\delta\sigma(V)}{dV}$ is given by

21985

Fig. 2.4

Blocking conductance and its derivative at $T=0$ K (assuming $\alpha^2F = a_n\omega^n$, $n = 1$).

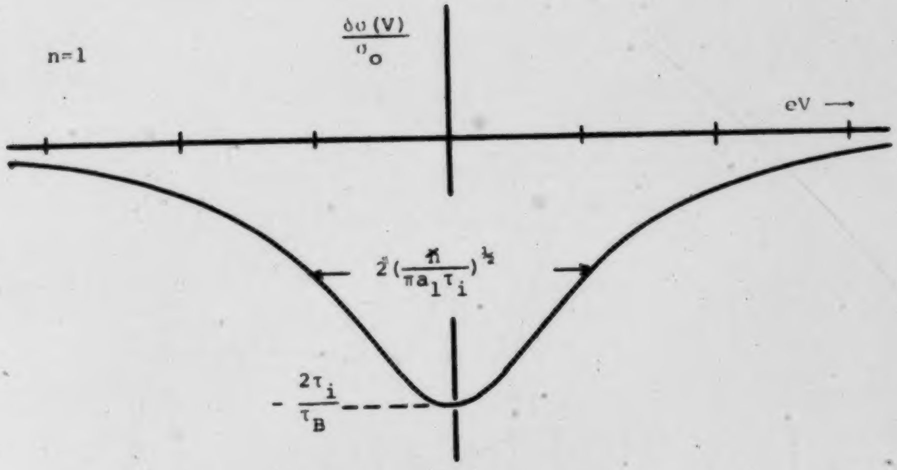
n=1
$\frac{\delta\sigma(V)}{\sigma_o}$
eV →
$2(\frac{\hbar}{\pi a_1\tau_i})^{\frac{1}{2}}$
$-\frac{2\tau_i}{\tau_B}$

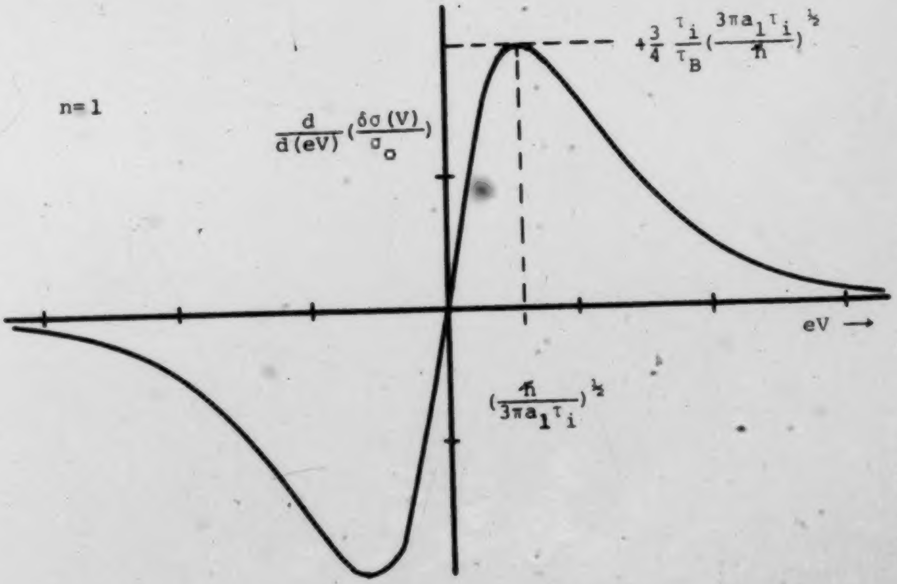
n=1
$+\frac{3}{4}\frac{\tau_i}{\tau_B}(\frac{3\pi a_1\tau_i}{\hbar})^{\frac{1}{2}}$
$\frac{d}{d(eV)}(\frac{\delta\sigma(V)}{\sigma_o})$
eV →
$(\frac{\hbar}{3\pi a_1\tau_i})^{\frac{1}{2}}$

21985

Fig. 2.5

Blocking conductance and its derivative at T=0 K (assuming $\alpha^2F = a_n\omega^n$, $n = 2$).

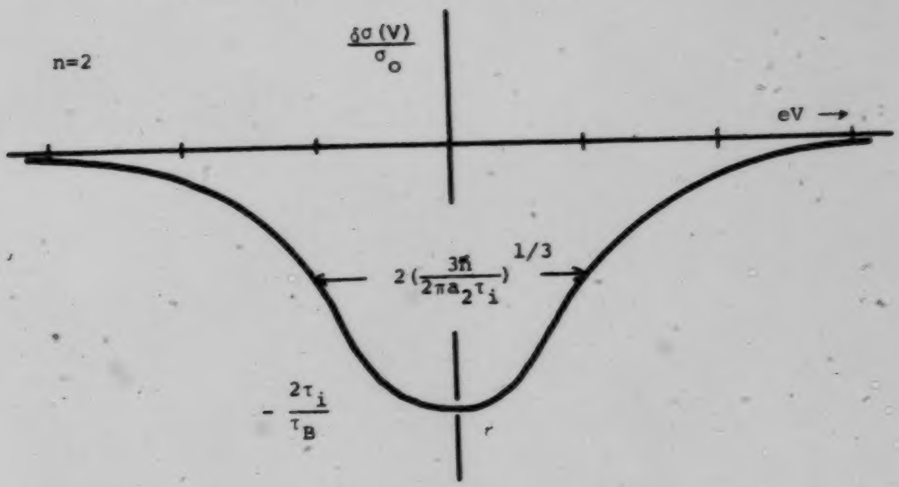
n=2
$\frac{\delta\sigma(V)}{\sigma_o}$
eV →
$2\left(\frac{3\hbar}{2\pi a_2\tau_i}\right)^{1/3}$
$-\frac{2\tau_i}{\tau_B}$

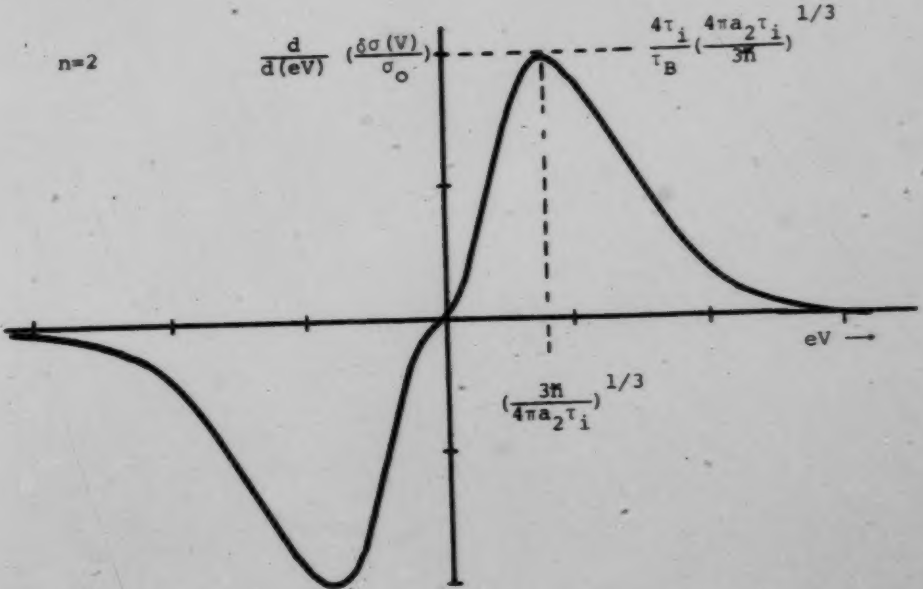
n=2
$\frac{d}{d(eV)}\left(\frac{\delta\sigma(V)}{\sigma_o}\right)$
$\frac{4\tau_i}{\tau_B}\left(\frac{4\pi a_2\tau_i}{3\hbar}\right)^{1/3}$
eV →
$\left(\frac{3\hbar}{4\pi a_2\tau_i}\right)^{1/3}$

$$\frac{1}{\sigma_o}\frac{d\delta\sigma(V)}{dV} = \int_{-\infty}^{\infty} \frac{1}{(e^{x}+1)(e^{-x}+1)} [S_1(xk_BT + eV)$$

$$+ S_2(xk_BT + eV)] \qquad (2.36)$$

where

$$S(\varepsilon) = -\frac{d}{dV}\left[\frac{\tau(\varepsilon)}{\tau_B}\right] \quad . \qquad (2.37)$$

To parameterize the theoretical curves for $T \neq 0$ K, it is convenient to introduce a parameter Γ_n, given by:

$$\Gamma_n^j = \frac{\hbar}{\pi\tau_i a_n^j} \qquad \begin{array}{l} j = 1,2 \\ n = 1,2 \end{array} \qquad (2.38)$$

This follows directly from the limiting behaviour of the effective relaxation time at low temperatures.

$$\tau \sim \frac{1}{\frac{\hbar}{\pi a_1 \tau_i} + \varepsilon^2 + (\pi k_B T)^2} \quad \text{for} \quad \alpha^2 F \sim \omega \qquad (2.39)$$

and

$$\tau \sim \frac{1}{\frac{\hbar}{\pi a_2 \tau_i} + \frac{2|\varepsilon|^3}{3}} \quad \text{for} \quad T \to 0 \qquad (2.40)$$

$$\tau \sim \frac{1}{\frac{\hbar}{\pi a_2 \tau_i} + 14\xi(3)(k_B T)^3} \quad \text{for} \quad \varepsilon \to 0$$

$$\text{if} \quad \alpha^2 F \sim \omega^2 \qquad (2.41)$$

Figs. 2.6 and 2.7 illustrate the behaviour of the blocking conductance at zero bias for a symmetrical junction as a function of temperature. A more sensitive comparison of the theory with the experiment is obtained by examining the behaviour of the maxima (minima) in $\frac{1}{\sigma_o} \frac{d\delta\sigma}{dV}$ with temperature. Figs. 2.8 and 2.9 show that the maximum in $\frac{1}{\sigma_o} \frac{d\sigma}{dV}$ decreases in size as the temperature increases. The data calculations were normalized to 1 K. The corresponding peak positions shift to a higher bias.

The application of a magnetic field leads only to a renormalization of the scattering time associated with the impurities.

$$\frac{1}{\tau_i} + \frac{1}{\tau_{i,drift}} = \frac{1}{\tau_i}(1 + \frac{\tau_i}{\tau_{drift}}) \quad . \qquad (2.42)$$

This for example, at T = 0 K, and for $\alpha^2F \sim \omega$, results in a shift of the position, V_{max}, of the maximum in $\frac{1}{\sigma_o} \frac{d\delta\sigma}{dV}$. Using eq. (2.33) we find

$$V_{max}(B) = V_{max}(0)(1 + \frac{\tau_i}{\tau_{drift}})^{1/2} \quad . \qquad (2.43)$$

There is a corresponding change in the peak height:

$$\frac{1}{\sigma_o} \frac{d\delta\sigma(V_{max},B)}{dV} = \frac{1}{\sigma_o} \frac{d\delta\sigma(V_{max},0)}{dV} (1 + \frac{\tau_i}{\tau_{drift}})^{-3/2} \quad . \qquad (2.44)$$

21985

Fig. 2.6

Temperature dependence of the blocking conductance at zero bias ($\alpha^2F = a_1\omega$).

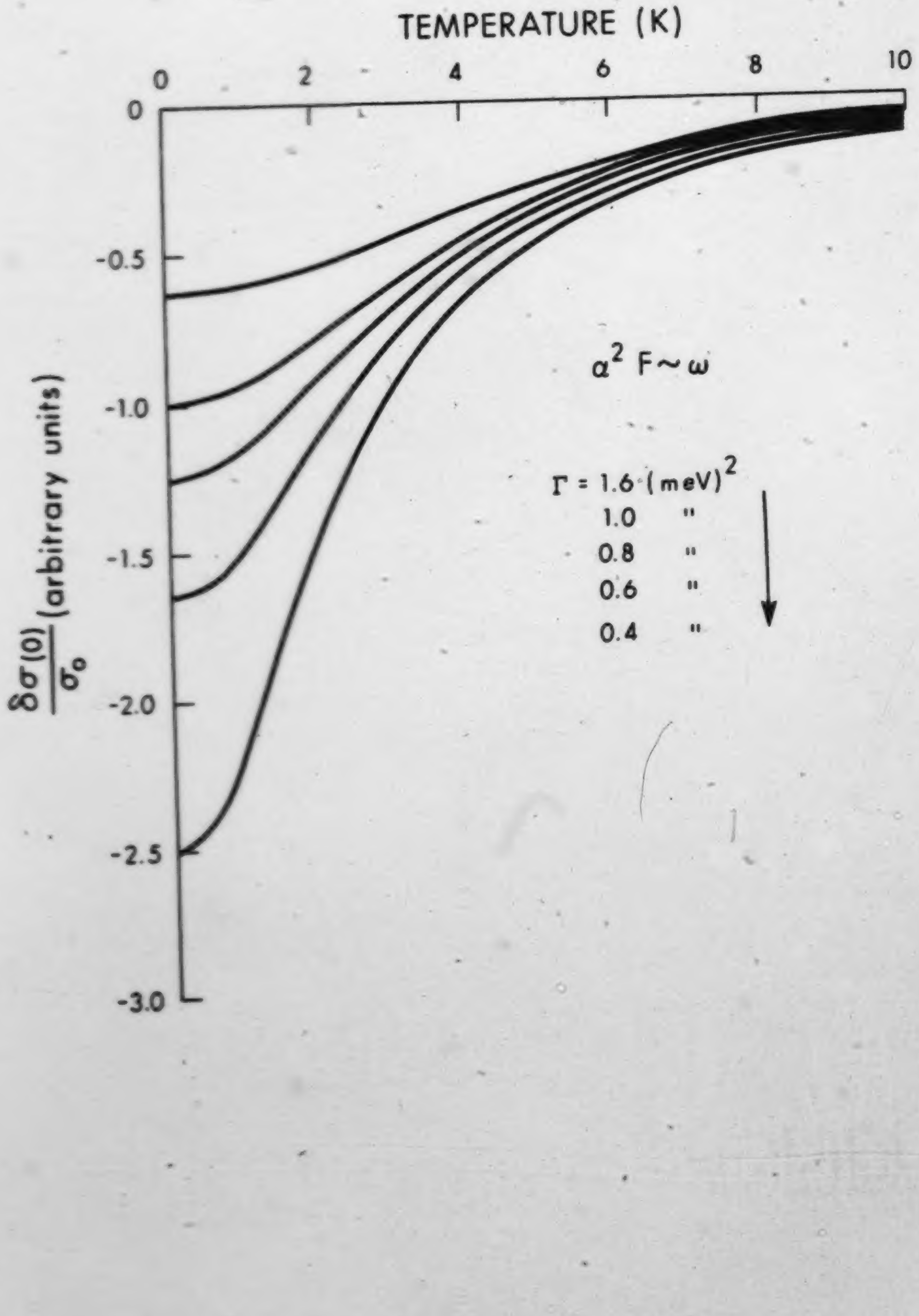
TEMPERATURE (K)
0
2
4
6
8
10
0
-0.5
-1.0
-1.5
-2.0
-2.5
-3.0
$\frac{\delta\sigma(0)}{\sigma_o}$ (arbitrary units)
$\alpha^2 F \sim \omega$
Γ = 1.6 (meV)^2
1.0 "
0.8 "
0.6 "
0.4 "

Fig. 2.7

Temperature dependence of the blocking conductance at zero bias ($\alpha^2F = a_2\omega^2$).

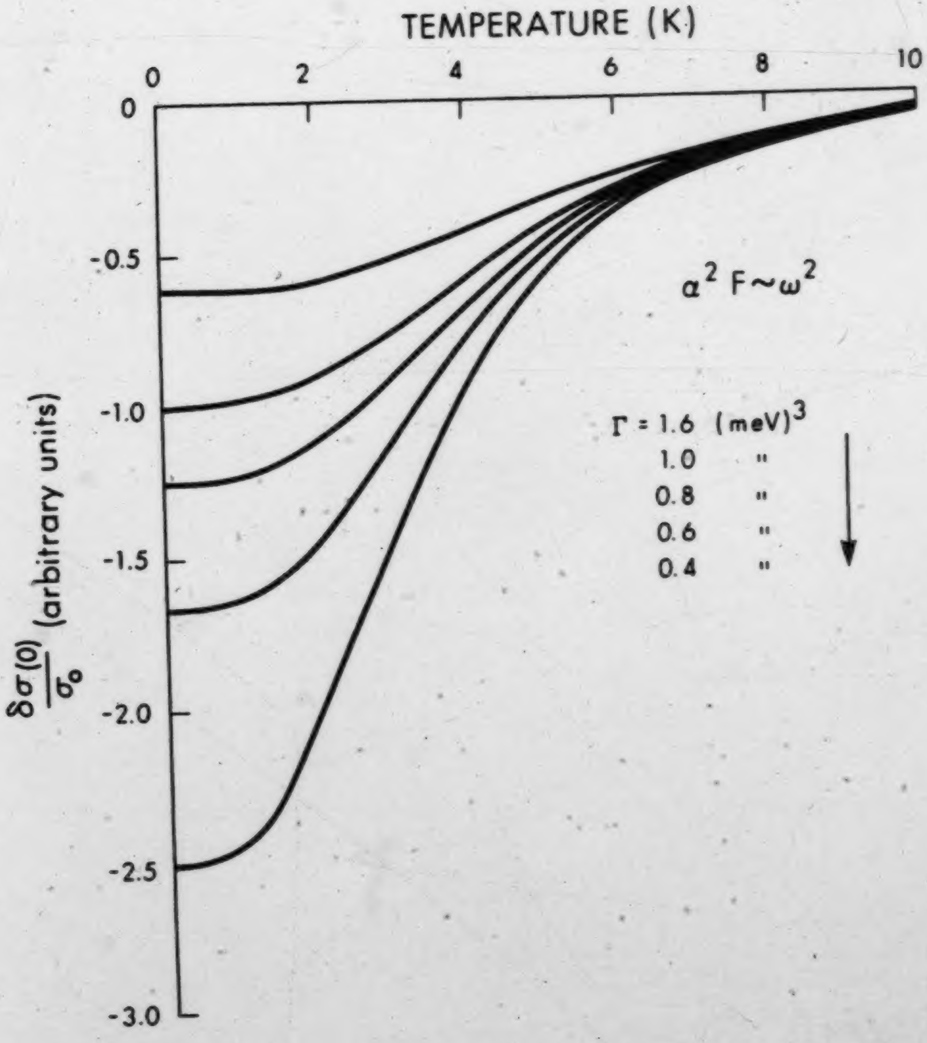
TEMPERATURE (K)
0
2
4
6
8
10
0
-0.5
-1.0
-1.5
-2.0
-2.5
-3.0
$\frac{\delta\sigma(0)}{\sigma_o}$ (arbitrary units)
$\alpha^2 F \sim \omega^2$
Γ = 1.6 (meV)^3
1.0 "
0.8 "
0.6 "
0.4 "

Fig. 2.8

Temperature dependence of peak positions, V_{max} (upper diagram) and peak amplitudes $\frac{1}{q_0}\frac{d\delta\sigma_e}{dV}\Big|_{V_{max}}$ (lower diagram) for different values of Γ ($\alpha^2F = a_1\omega$).

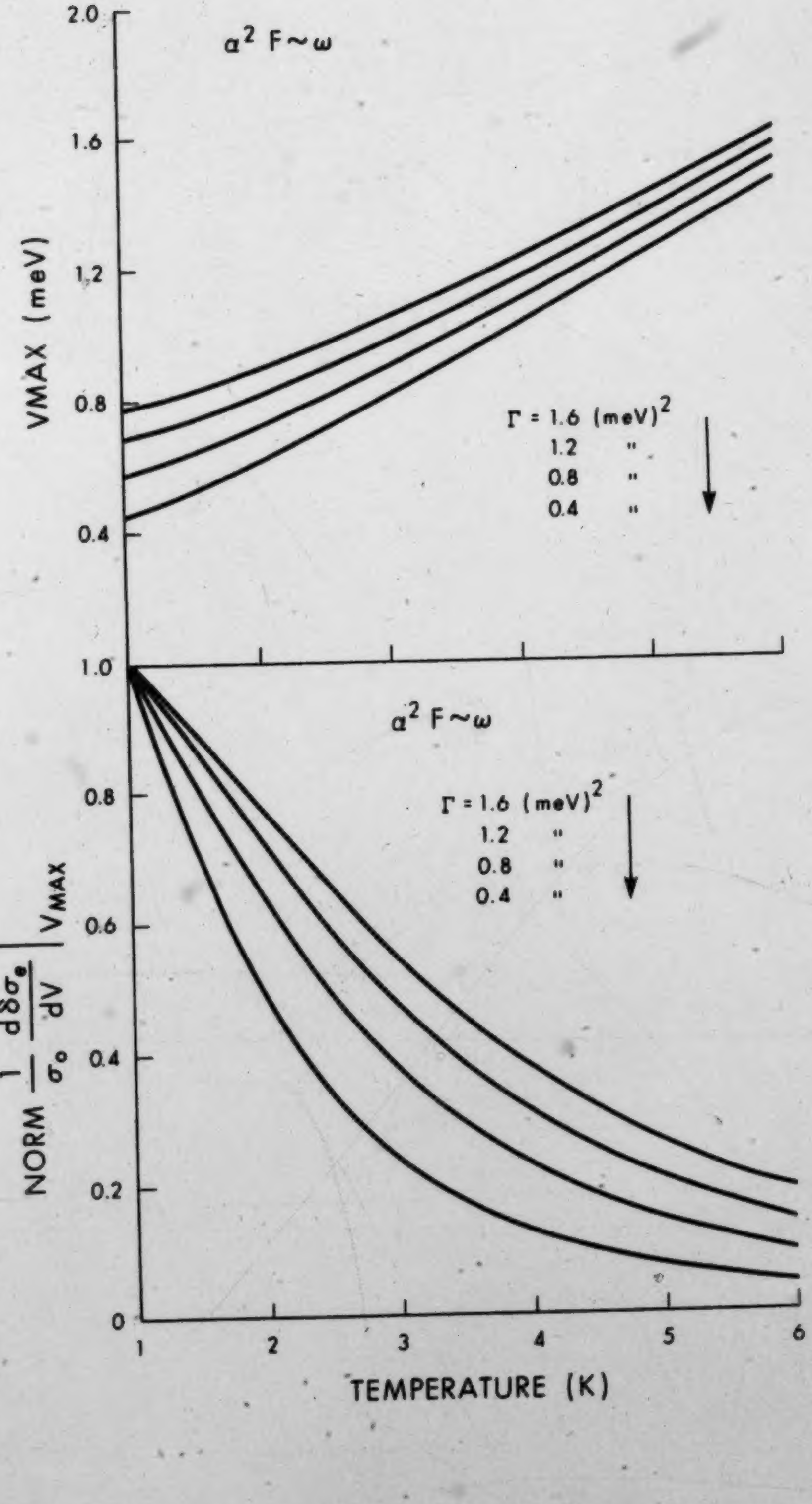
$\alpha^2 F \sim \omega$
VMAX (meV)
2.0
1.6
1.2
0.8
0.4
$\Gamma = 1.6\ (\text{meV})^2$
1.2 "
0.8 "
0.4 "
$\alpha^2 F \sim \omega$
$\text{NORM}\ \frac{1}{\sigma_o}\frac{d\delta\sigma_e}{dV}\Big|_{V_{MAX}}$
1.0
0.8
0.6
0.4
0.2
0
$\Gamma = 1.6\ (\text{meV})^2$
1.2 "
0.8 "
0.4 "
1
2
3
4
5
6
TEMPERATURE (K)

Fig. 2.9

Temperature dependence of peak positions, V_{max} (upper diagram) and peak amplitudes $\frac{1}{\sigma_o} \left. \frac{d\delta\sigma_e}{dV} \right|_{V_{max}}$ (lower diagram) for different values of Γ ($\alpha^2 F = a_2 \omega^2$).

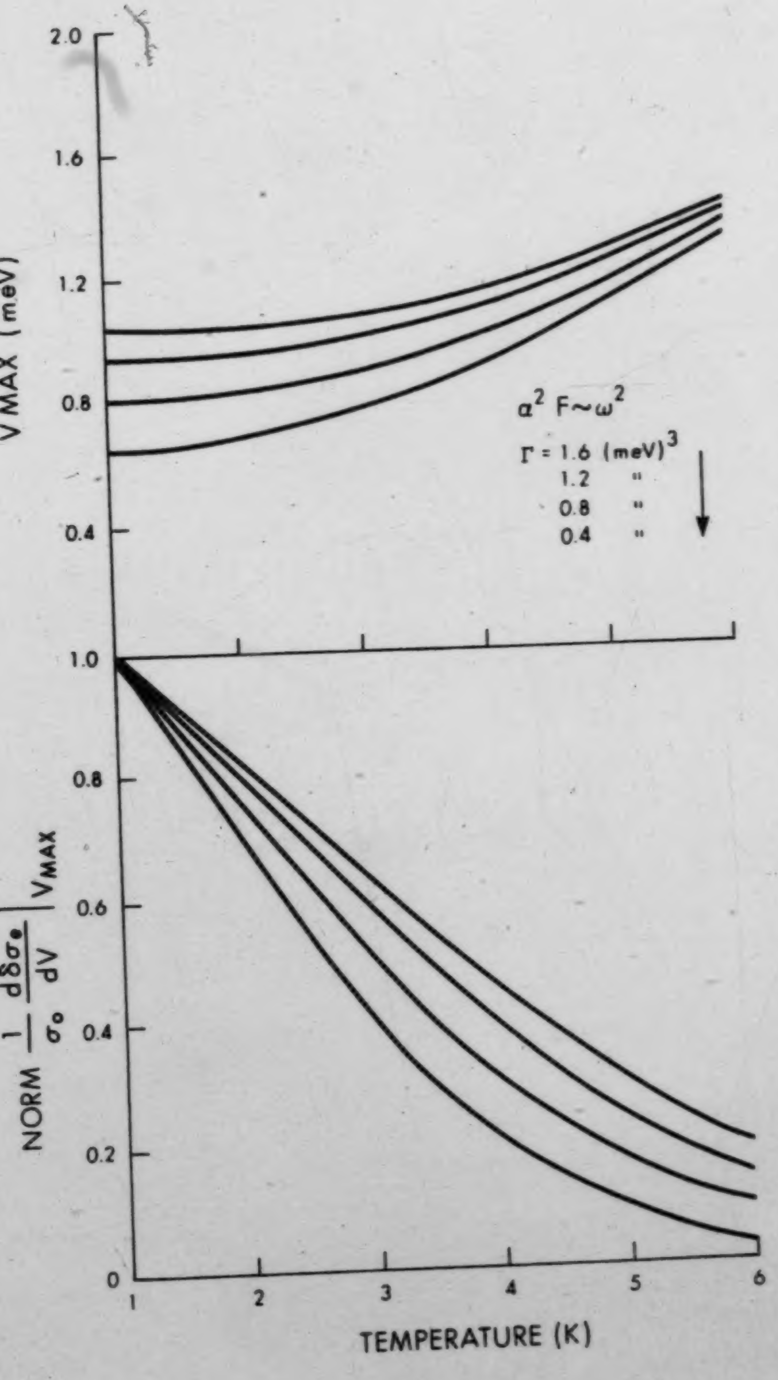
2.0
1.6
1.2
0.8
0.4
V MAX (meV)
$\alpha^2 F \sim \omega^2$
Γ = 1.6 (meV)^3
1.2 "
0.8 "
0.4 "
1.0
0.8
0.6
0.4
0.2
0
NORM $\frac{1}{\sigma_0} \frac{d\delta\sigma_e}{dV} \Big|_{V_{MAX}}$
1
2
3
4
5
6
TEMPERATURE (K)

CHAPTER 3

EXPERIMENTAL TECHNIQUES

3.1 Sample preparation

The preparation of tunnel junctions was carried out in a vacuum system by an evaporation of metals onto a suitable substrate. There are basically three steps involved in the process of preparation. First a metal film (base layer) of required thickness is deposited. A thin insulating layer is then formed on the top of the evaporated film. Finally a cross-strip of an another metal is evaporated, thus forming a composite metal-insulator-metal (MIM) system. Evaporated layers of In or Ag served as contacts for electrical connection.

The junctions were prepared on Fisher brand microscopic glass slides cut to a 1/2 inch square. The slides were washed with a detergent, air dried and flame polished. For some Bi/Bi junctions freshly cleared mica was used, washed in methyl alcohol. The substrates were further cleaned by exposing them to the plasma of glow discharge (Holland, 1961) prior to film deposition. The size of the substrates allowed to make two junctions with a common base layer without breaking the vacuum.

The films were evaporated from a resistively heated nonvolatile support (filament) through a pattern

21985

Fig. 3.1

Layout of the Sample

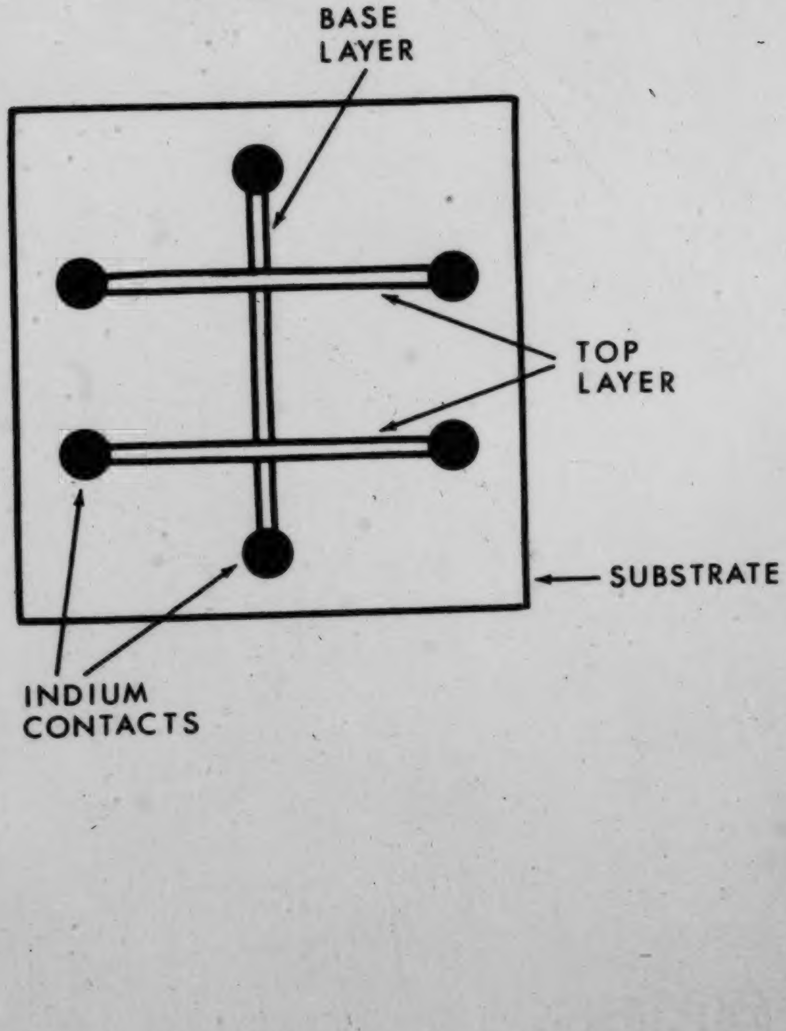
BASE LAYER
TOP LAYER
SUBSTRATE
INDIUM CONTACTS

forming mask, in close vicinity of which the substrate was placed. The filaments were mounted on a rotating carousel which allowed a proper indexing of the evaporated material. Cylindrical quartz chimneys placed around them prevented a mutual cross-contamination of the metals. Table 3.1 lists the selection of filaments for evaporation. The distance between the vapour source and the substrate was 7 inches.

The vacuum chamber, enclosed in an 18 inch bell jar, was pumped by an oil diffusion pump with a liquid nitrogen cold trap backed by a mechanical pump. A zeolite trap was installed between the mechanical pump and the rest of the system. The system was ready for the evaporation after 1 hour of evacuation with a pressure lower than 2×10^{-6} torr.

3.2 Formation of tunnel barriers

A glow discharge technique (Miles and Smith, 1963) was used to prepare tunnel junctions of Mg and Al. It consists of setting up a discharge between two aluminum electrodes while the pressure of the system was maintained between 100-600 torr of either 99.5% pure oxygen or nitrogen of the same purity (for Mg only). The aluminum electrodes were 2 inches wide, separated 1/2 inch

Table 3.1

Selection of Materials for Evaporation

Metal	Purity	Supplier	Evaporation Source
Al	59	A.D. Mackay	F8-3X.030 W coil
Mg	59	Johnson Mattey	S17A-.005 Ta covered boat
Bi	69	Cominco	S39-.005 Ta S39-.005 Mo boat
Pb	69	Cominco	S39-.005 Mo boat
Au	59	Cominco	S39-.005 Mo S9A-.005 W boat

Evaporation sources supplied by R.D. Mathis Company apart and placed 2 inch above the holder containing the glass slide with a freshly evaporated metal film. The polarity of the applied DC voltage was such that the evaporator which was conductively connected with one of the electrodes was at positive potential with respect to the second electrode. The thickness of a tunnel barrier grown by this method depended on the time the discharge was maintained, pressure in the system and the current flowing through the electrodes. For a successful preparation of a tunnel barrier it was important to keep a stable discharge without random fluctuations. Presumably the rapidly varying electric field produced pinholes in the thin insulator. The oxidation of Mg for 1-3 minutes in 100-200 torr of O_2, with a glow discharge current of 5-15 mA was sufficient to produce tunnel junctions with resistances of nominally 200 Ω. Al required a longer oxidation time (5-10 minutes) and higher pressure (400 torr), while the current was 5-15 mA. To prepare junctions in nitrogen environment, the discharge had to be kept for 40-80 minutes with currents up to 40 mA and pressures ranging between 400-600 torr.

Repeated experiments of producing an oxide of Bi by the glow discharge technique ended in failure. However, a method of thermal oxidation (Hapase et al, 1967) yielded thick enough oxides to produce junctions having resistances around 200 Ω. The oxidation procedure was as follows: After the deposition of the Bi film the vacuum was broken and the substrate was placed in an oven at 180°-220°C for 2 hours. Following this, the substrate was again placed in the substrate holder and the vacuum chamber re-evacuated for the evaporation of the cross-film.

3.3 Film thickness determination

The thickness of films during vacuum deposition was monitored by Sloan DTM-3 (Sloan Instr. Corp.) quartz crystal monitor. The measurement utilizes a principle that the resonance frequency of a piezoelectric crystal depends on the mass of the material deposited on the surfaces of the crystal (Eschbach and Kruidhoff, 1965). The monitor therefore consists of a crystal placed adjacent to a substrate onto which the film is deposited and the electrical equipment for measuring the change in its resonance frequency. Eq. (3.1) relates the thickness L of the deposited metal to the measured frequency shift Δf (Stockbridge, 1966)

$$L = C_1C_2 \frac{\Delta f}{\rho} = \frac{C\Delta f}{\rho} \tag{3.1}$$

$$C = C_1C_2$$

C_1 is a constant dependent on the thickness and cut of the piezoelectric crystal, C_2 depends on the geometry of the distribution of the deposit over the crystal and ρ is the density of the material. The validity of eq. (3.1) is restricted to mass deposits which are at most 5% of the mass of the crystal itself (Steckelmacher, 1965). For all practical purposes this condition was satisfied. Since the density of thin films is different from that of the bulk due to voids in the film (Hartman, 1965) it is best to determine the mass sensitivity ratio C/ρ for each given material experimentally, combining the shift in the resonance frequency of the crystal with an optical thickness measurement using Tolansky interferrometer (Tolansky, 1960).

The interferometer consists of two slightly inclined optical flats, one of them supporting the film which forms a step on the substrate. When the second optical flat is brought in contact with the film surface and the interferometer illuminated with a parallel monochromatic beam at normal incidence, dark fringes are observed which trace out the points of equal air-gap thickness. Their separation is $\lambda/2$ where λ is the wavelength of the monochromatic light. The fringes show a displacement as they pass over the film step edge. The displacement d expressed as a function of $\lambda/2$ fringe spacing gives the film thickness.

$$L = \frac{d}{\text{fringe spacing}} \frac{\lambda}{2} . \qquad (3.2)$$

In order that the phase change on reflection from the two sides of the step will be the same, it is necessary to coat the film as well as the exposed glass surface with the same reflecting silver layer.

Vrba (Vrba, 1971) has described these measurements in greater detail. The experimentally determined values of C/ρ are the following:

Al - 940 Å/Kc

Mg - 1480 Å/Kc

Bi - 268 Å/Kc

Pb - 235 Å/Kc

Au - 127 Å/Kc

The uncertainties in the mass sensitivity determination are approximately 5% and are of interferometric and geometric origin.

3.4 Temperature measurement and control

The temperatures were determined by a combination of vapour pressure and germanium resistance thermometer measurements. A 1958 scale of temperatures (Dijk et al, 1960) was used to convert the vapour pressure to temperature. Above the boiling of He^4, a germanium thermometer (Scientific Instruments, # 10372) was used with a computer generated polynomial fit of the form

$$\frac{1}{T} = \sum_{k=0}^{n} a_k H_k (\ln R) \qquad (3.3)$$

where a_k is the k^{th} expansion coefficient, H_k - the Chebyshev polynomial of order k, T - temperature, R - resistance of the thermometer.

By a controlled regulation of the He^4 vapour pressure, temperatures between 1 K and 4.2 K were obtained. Sommers (Sommers, 1954) described a convenient manostat which employs a thin teflon diaphragm, which bows out when there is a pressure difference across it, thus blocking the pumping orifice. The temperature fluctuations using this manostat did not exceed 5 mK around a preset value. A solid state temperature controller designed by Dr. Adler and Dr. Rogers was used to regulate temperatures above 4.2 K. The circuit is of the conventional Wheatstone bridge type, using a germanium thermometer as its sensing element and providing a proportional heater feedback to the regulated bath. It was capable of maintaining constant temperature within ±1 mK at 5 K. The power dissipation in the thermometer was less than 10^{-8} W.

Fig. 3.2

Schematic diagram of the cryostat

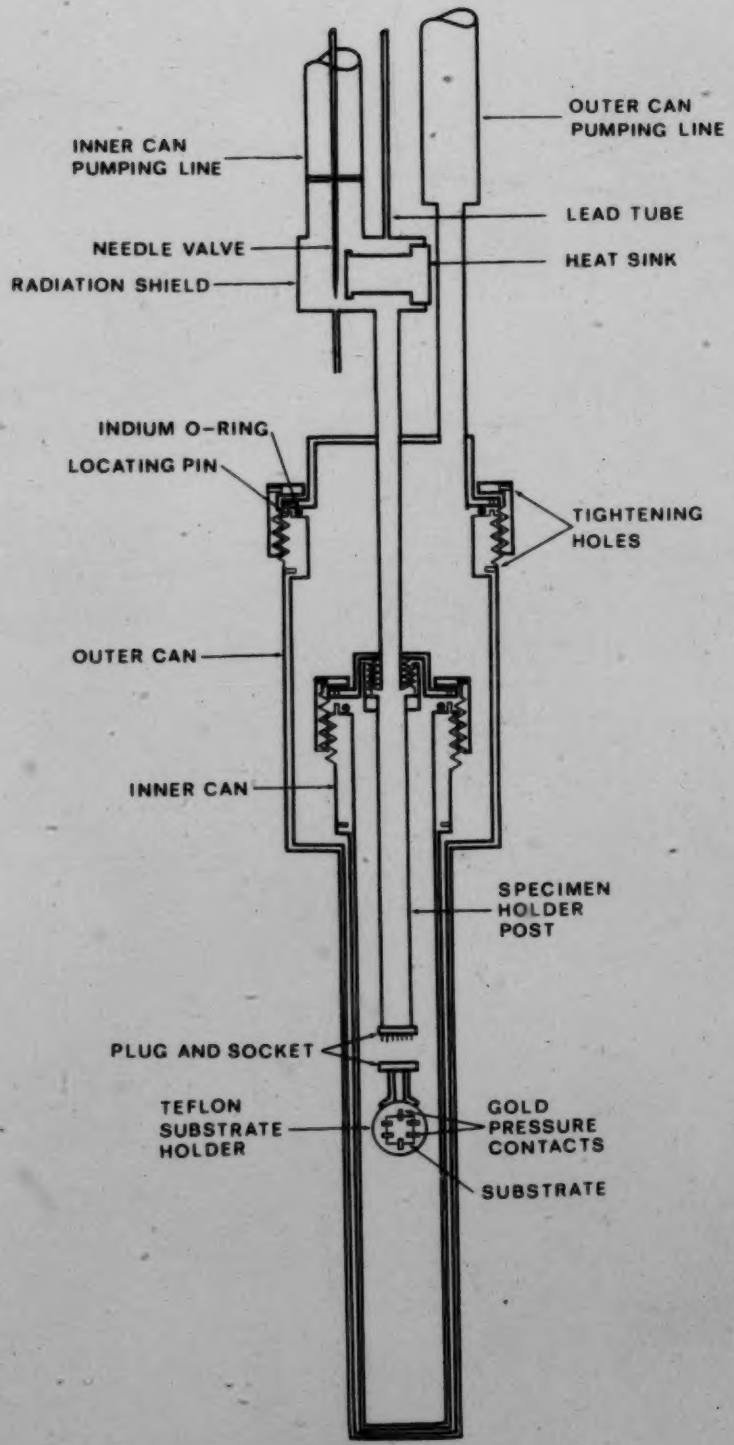
INNER CAN PUMPING LINE
OUTER CAN PUMPING LINE
LEAD TUBE
NEEDLE VALVE
HEAT SINK
RADIATION SHIELD
INDIUM O-RING
LOCATING PIN
TIGHTENING HOLES
OUTER CAN
INNER CAN
SPECIMEN HOLDER POST
PLUG AND SOCKET
TEFLON SUBSTRATE HOLDER
GOLD PRESSURE CONTACTS
SUBSTRATE

3.5 Production of low temperatures

A conventional He^4 cryostat facilitated measurements on tunnel junctions at low temperatures. A schematic diagram of the cryostat is illustrated on fig. 3.2. Indium O-rings with Apiezon N grease were used to seal the vacuum and sample chambers. The cryostat was designed to fit into the bore of a 70 kG superconducting magnet. By pumping on the helium liquid level, in the sample chamber, temperatures as low as 1 K were attained.

3.6 Measurement of tunneling characteristics

A system using a combination of harmonic detection and bridge techniques (Adler and Jackson, 1966) suitably interfaced to an online mini-computer facility for an analog and digital recording was used in obtaining the relevant information on tunnel junctions. These are the dynamical conductance $\sigma = dI/dV$ and its derivative $d\sigma/dV = d^2I/dV^2$. The principle of harmonic detection method can be understood by considering fig. 3.3.

In this circuit the tunnel junction serves as one arm of an ac Wheatstone bridge, the other arm being a variable resistor R_d. Assuming that the bridge is close to its balance the current through its arms is nearly identical. In the voltage region where the tunnel junctions are investigated, they behave as weakly

Fig. 3.3

Simplified bridge configuration

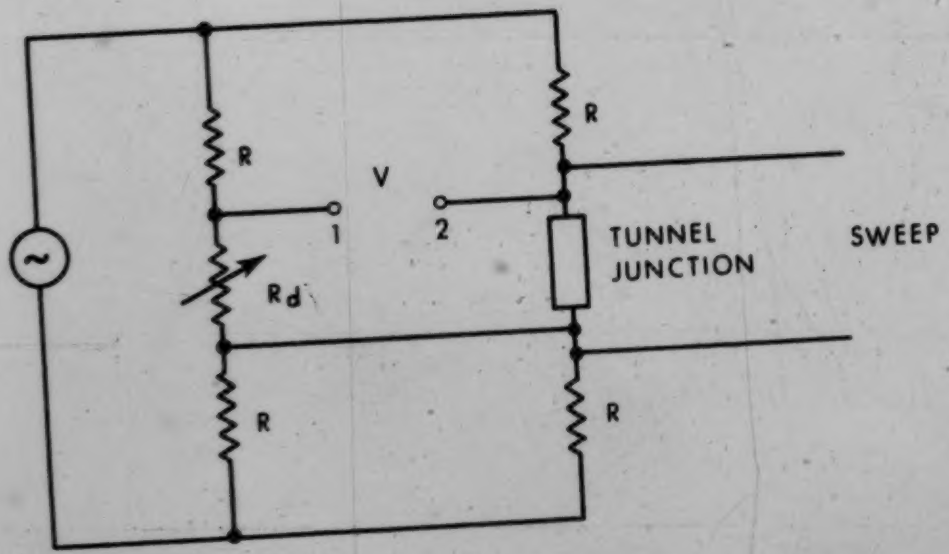
R
R
V
1
2
~
Rd
TUNNEL
JUNCTION
SWEEP
R
R

nonlinear passive elements. If the small current modulation amplitude δ is kept constant, then the voltage V across the junction can be written in terms of a Taylor's series

$$V(I) = V(I_o) + \left(\frac{dV}{dI}\right)_{I_o} \delta \cos \omega t + \frac{1}{2} \left(\frac{d^2V}{dI^2}\right)_{I_o} \delta^2 \cos^2 \omega t + \ldots\ldots \tag{3.4}$$

or

$$V(I) = V(I_o) + \left(\frac{dV}{dI}\right)_{I_o} \delta \cos \omega t + \frac{1}{4} \left(\frac{d^2V}{dI^2}\right)_{I_o} (1 + 2 \cos 2\omega t) + \tag{3.5}$$

where $V(I_o)$ is the DC-bias across the junction and ω is the modulating angular frequency. The voltage across the variable resistor R_d which has a linear I-V characteristics is given by

$$V_d = (I_o + \delta \cos \omega t) R_d \quad . \tag{3.6}$$

Thus the difference in potential between points 1 and 2, V_{12}, has components at the modulating frequency ω and its various harmonics. The signal at the fundamental frequency, $V_{12}(\omega)$, is proportional only to the departure of the dynamic resistance $\left(\frac{dV}{dI}\right)_{I_o}$ from R_d and the second harmonic component, $V_{12}(2\omega)$, is proportional to $\left(\frac{d^2V}{dI^2}\right)_{I_o}$. Both these components are measured by means of a phase sensitive detector.

$$V_{12}(\omega) = \delta[R_d - (\frac{dV}{dI})_{I_o}] \cos \omega t \qquad (3.7)$$

$$V_{12}(2\omega) = \frac{1}{4} \delta^2 (\frac{d^2V}{dI^2})_{I_o} \cos 2\omega t \quad . \qquad (3.8)$$

A direct calibration of $\frac{dV}{dI}$ curve enables the computation of the dynamical conductance $\sigma = \frac{dI}{dV}$. Ideally, the second derivative $\frac{d^2I}{dV^2} = \frac{d\sigma}{dV}$ is then calculated using the identity:

$$\frac{d^2I}{dV^2} = -\sigma^3 \cdot \frac{d^2V}{dI^2} \quad . \qquad (3.9)$$

The presence of a second harmonic distortion in the modulation supply complicates the above relation. This necessitates a use of a different numerical method in calibrating $\frac{d\sigma}{dV}$. The mathematical details of the analysis of this problem are given in Appendix I with an earlier version of our data acquisition system. The present system which employs an online mini-computer and its peripherals allows a fast evaluation of the incoming data. The complete description of the new data acquisition system was given in a technical report (Adler, Straus, 1974).

Fig. 3.4

Schematic diagram of the data acquisition system

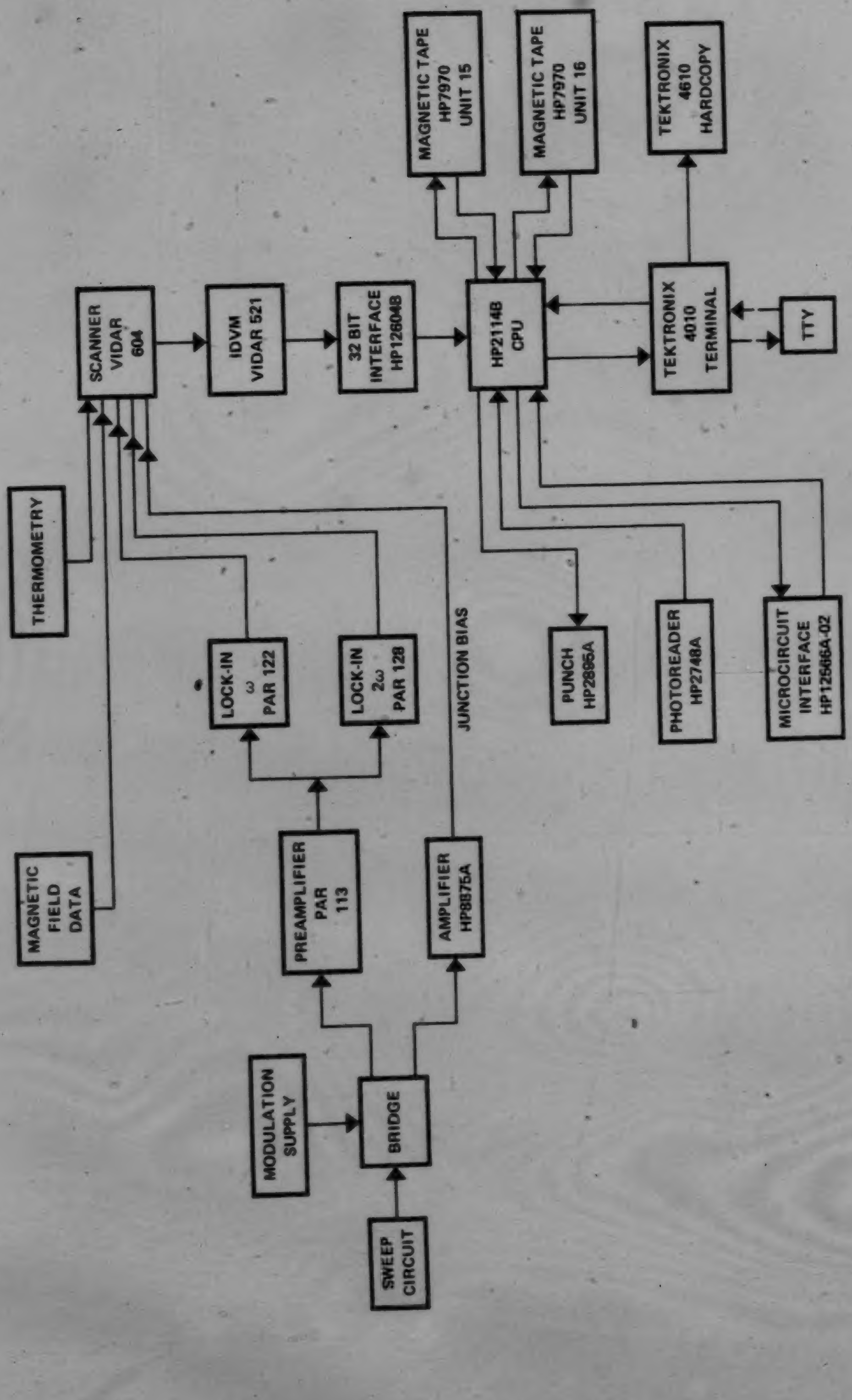
SWEEP CIRCUIT
MODULATION SUPPLY
BRIDGE
PREAMPLIFIER PAR 113
AMPLIFIER HP8875A
MAGNETIC FIELD DATA
THERMOMETRY
LOCK-IN ω PAR 122
LOCK-IN 2ω PAR 128
JUNCTION BIAS
SCANNER VIDAR 604
IDVM VIDAR 521
32 BIT INTERFACE HP12604B
HP2114B CPU
PUNCH HP2895A
PHOTOREADER HP2748A
MICROCIRCUIT INTERFACE HP12566A-02
MAGNETIC TAPE HP7970 UNIT 15
MAGNETIC TAPE HP7970 UNIT 16
TEKTRONIX 4010 TERMINAL
TEKTRONIX 4610 HARDCOPY
TTY

CHAPTER 4

EXPERIMENTAL RESULTS

4.1 Introduction

To test the theory with the experiment we have prepared a series of tunnel junctions using different metals as their electrodes. The thickness of these ranged between 500-50000 Å. The insulating layers of the junctions were prepared either by oxidation or nitrification (for Mg only). Some junctions were deliberately doped with oil to reduce the probability of making a sample with spurious oscillations in their characteristics. Junctions having these, will be discussed in a separate chapter.

4.2 The Problem of the Background

A typical measurement of the conductance of a Mg/oil/Mg junction to a 5 meV range is shown in fig. 4.1 for several different temperatures. As the temperature increases, the conductance minimum decreases with a simultaneous loss in the sharpness of the anomaly. The second derivative measurement for the same junction is shown in the next figure. Here, the maximum of $d\sigma/dV$ with higher temperatures decreases

Fig. 4.1

Temperature dependent conductance for a Mg/Mg junction.

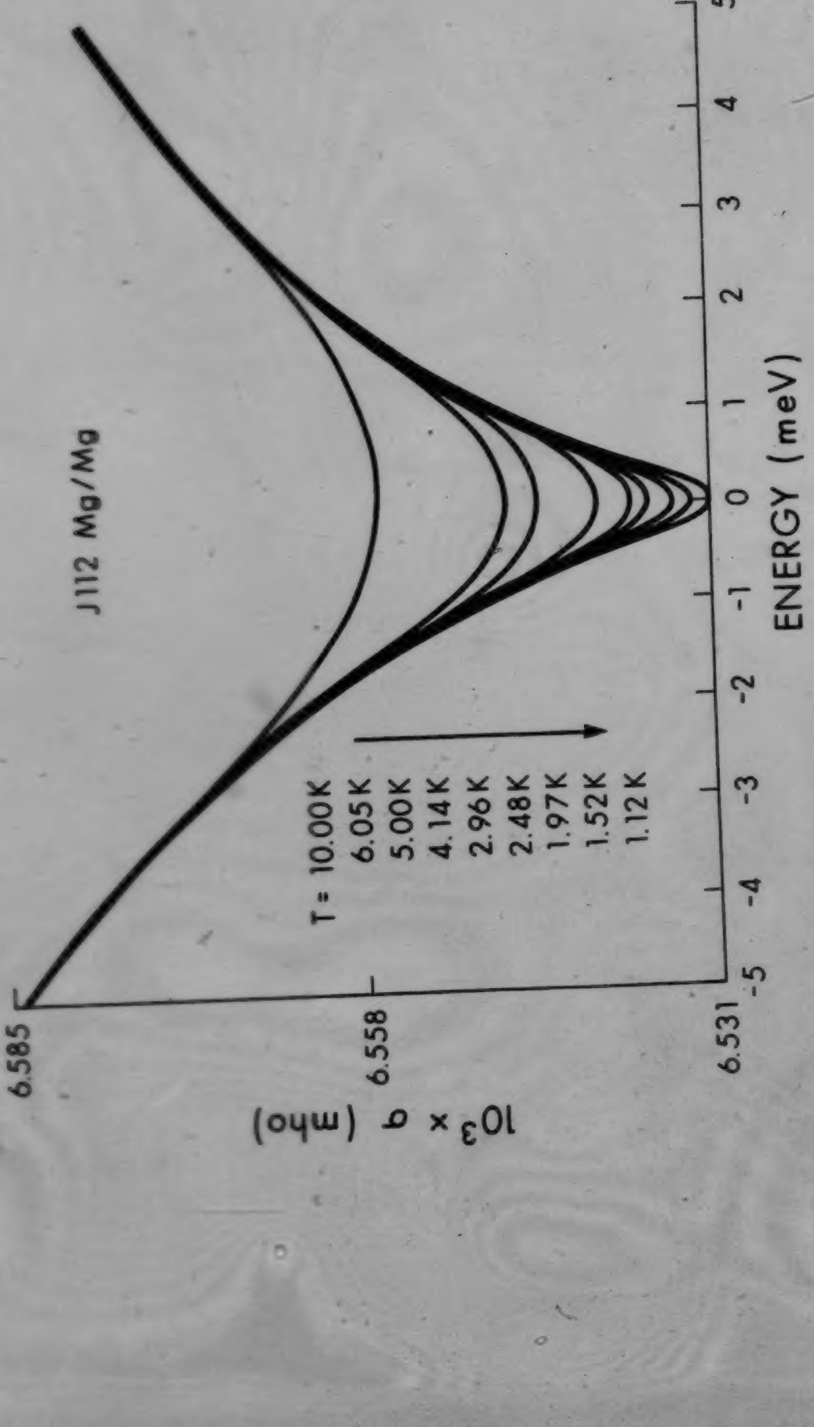
J112 Mg/Mg
T = 10.00K
6.05K
5.00K
4.14K
2.96K
2.48K
1.97K
1.52K
1.12K
$10^3 \times g$ (mho)
6.585
6.558
6.531
-5
-4
-3
-2
-1
0
1
2
3
4
5
ENERGY (meV)

Fig. 4.2

Temperature dependent normalized derivative of the conductance for a Mg/Mg junction.

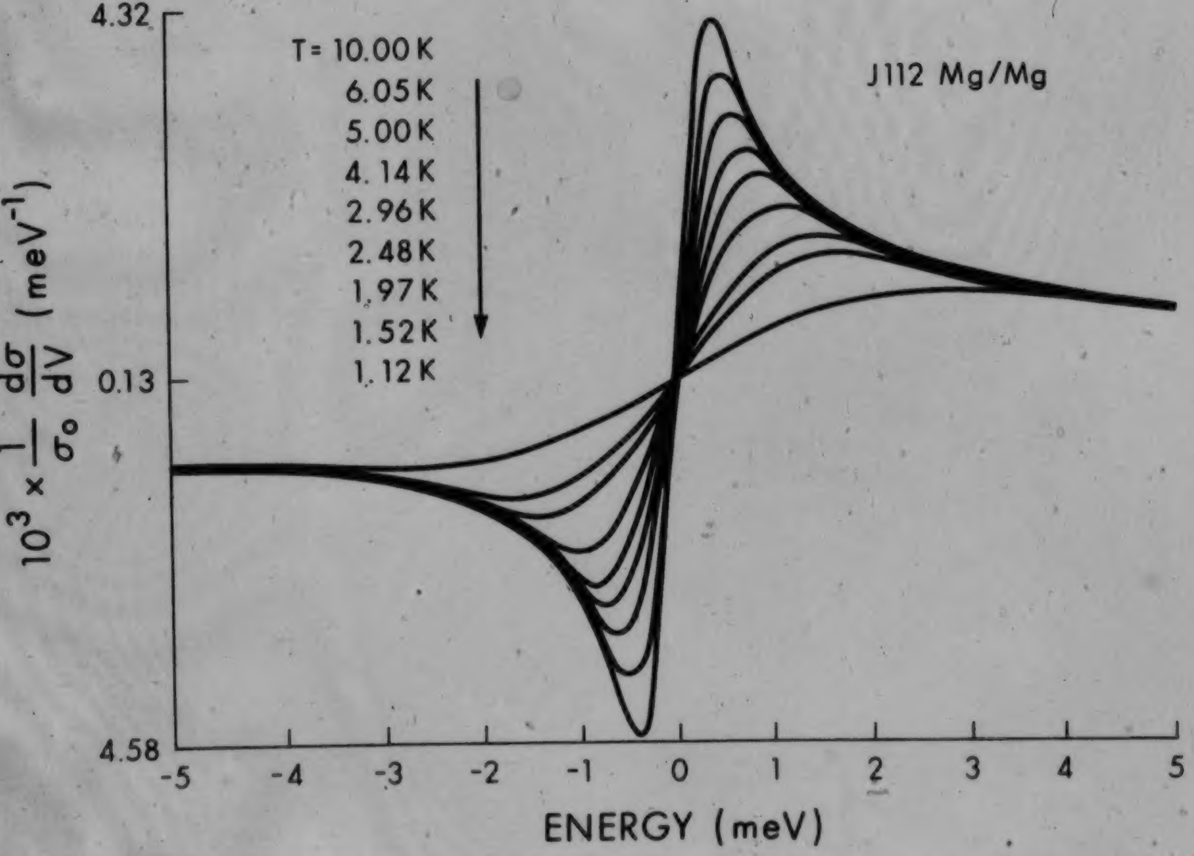
T= 10.00 K
6.05 K
5.00 K
4.14 K
2.96 K
2.48 K
1.97 K
1.52 K
1.12 K
J112 Mg/Mg
$10^3 \times \frac{1}{\sigma_o} \frac{d\sigma}{dV}$ (meV^{-1})
4.32
0.13
4.58
-5
-4
-3
-2
-1
0
1
2
3
4
5
ENERGY (meV)

(for a positive applied bias) while its position shifts to a higher voltage.

The conductance curve in fig. 4.1 has a slight asymmetry about the origin. We assume that this asymmetry arises from the ideal background conductance as discussed earlier (section 2.1). To eliminate the background, which we consider to be temperature independent at least between 1-10 K, we have adopted the following two procedures.

Let us first recall fig. 2.6, where we notice that at higher temperatures, the dip in conductance due to blocking is essentially equal to zero. Therefore by subtracting the conductance measured at the highest temperature (10 K) from the ones measured at lower temperatures where the blocking is still effective, we can isolate the pure "blocking conductance $\delta\sigma$". This technique was successfully applied for the junction shown earlier. Fig. 4.3 and fig. 4.4 illustrate the resulting curves.

For junctions where the high temperature curve was not obtained we have considered the following alternative: Let us suppose that the experimental conductance may be represented by an expression of the form

$$\sigma(V) = \sigma_o + \sigma_1 V + \sigma_2 V^2 + \delta\sigma(V,T) \qquad (4.1)$$

Fig. 4.3

Temperature dependence of the blocking conductance for a Mg/Mg junction after subtracting the background.

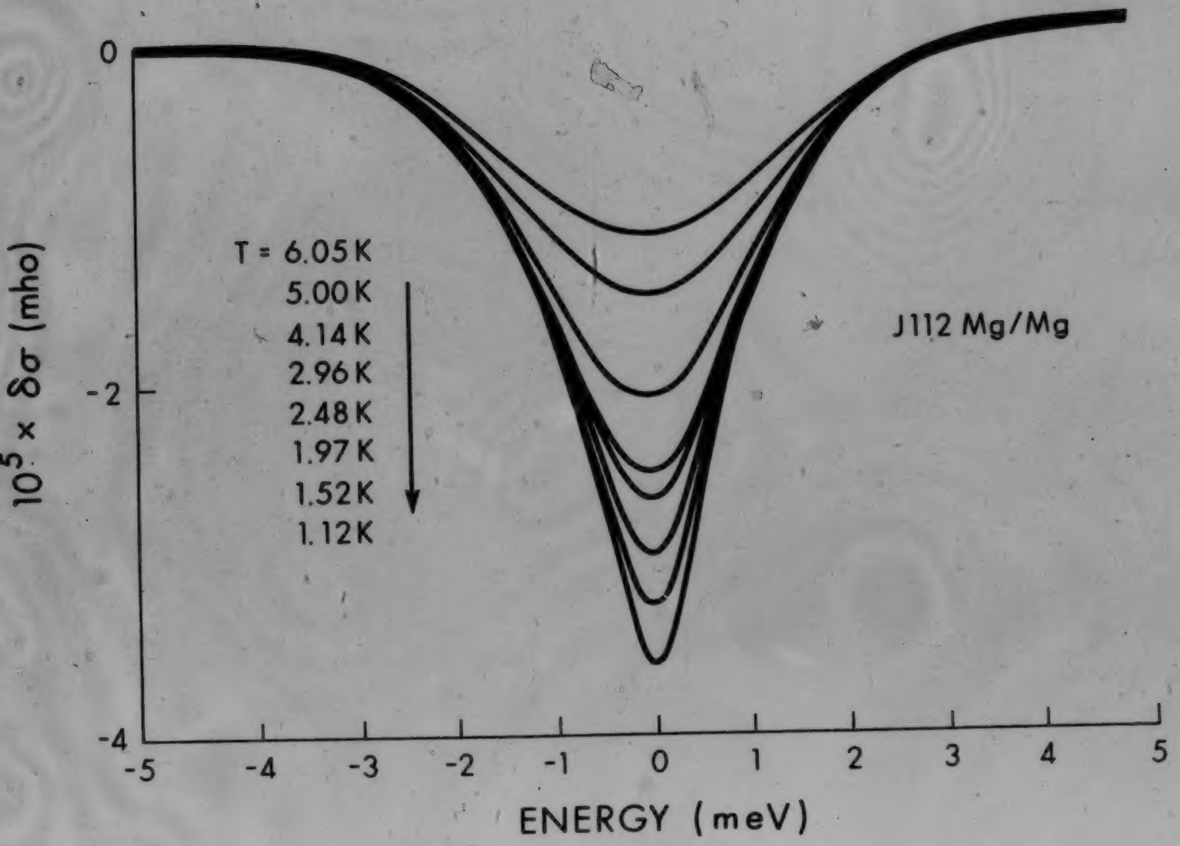
0
-2
-4
$10^5 \times \delta\sigma$ (mho)
-5
-4
-3
-2
-1
0
1
2
3
4
5
ENERGY (meV)
T = 6.05 K
5.00 K
4.14 K
2.96 K
2.48 K
1.97 K
1.52 K
1.12 K
J112 Mg/Mg

Fig. 4.4

Temperature dependence of the normalized derivative of the blocking conductance for a Mg/Mg junction after subtracting the background.

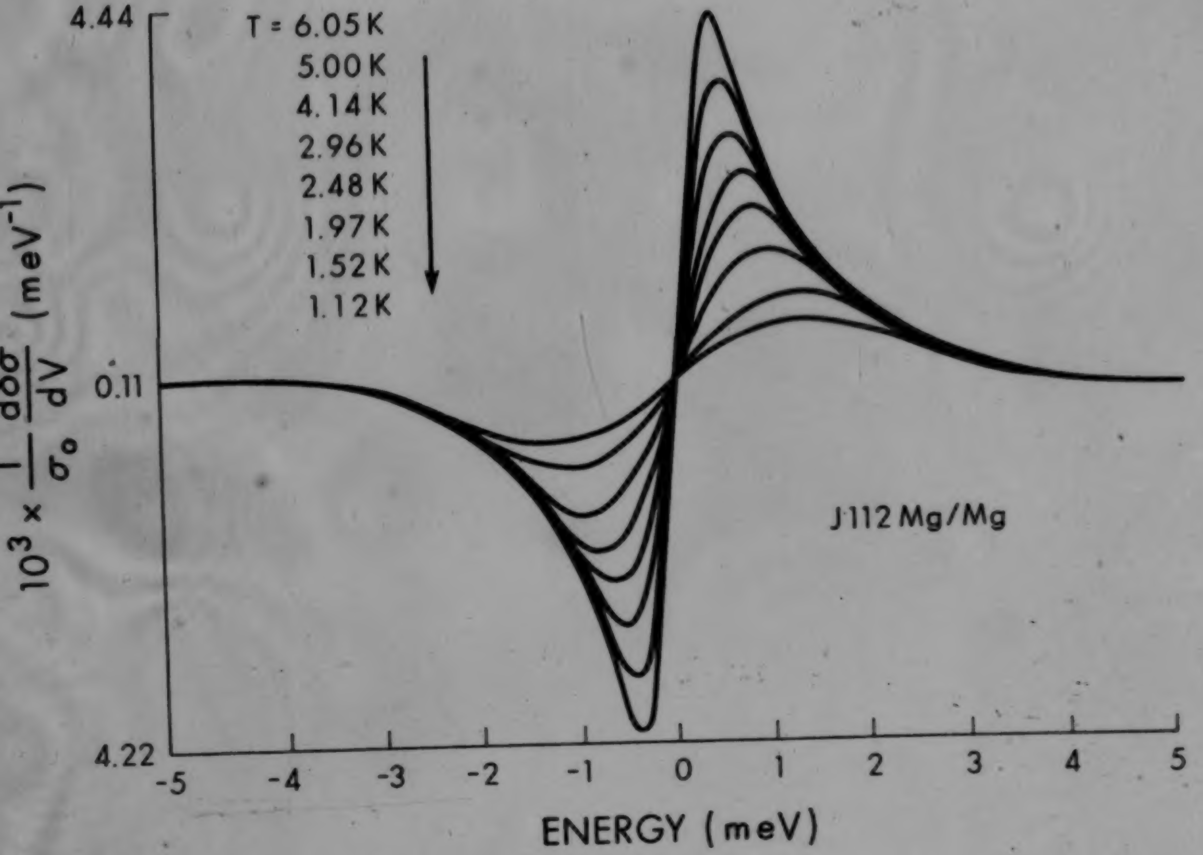
4.44
0.11
4.22
$10^3 \times \frac{1}{\sigma_o} \frac{d\delta\sigma}{dV}$ (meV^{-1})
T = 6.05 K
5.00 K
4.14 K
2.96 K
2.48 K
1.97 K
1.52 K
1.12 K
J112 Mg/Mg
-5
-4
-3
-2
-1
0
1
2
3
4
5
ENERGY (meV)

where the first three terms constitute the ideal temperature independent background. Then by taking the even part of the conductance

$$\frac{\sigma_e(V)}{\sigma_o} = \frac{I}{\sigma_o}\left(\frac{\sigma(V)+\sigma(-V)}{2}\right) = \frac{\sigma_2}{\sigma_o}V^2 + \frac{\delta\sigma}{\sigma_o}(V_1T) + 1 \ . \qquad (4.2)$$

We eliminate the linear term. The assumption that σ_1 is temperature independent is verified by forming the odd part of the conductance

$$\sigma_{odd} = \frac{\sigma(V)-\sigma(-V)}{2} = \sigma_1 V \qquad (4.3)$$

and plotting it as function of the bias voltage for different temperatures. The resulting curve should be a straight line independent of the temperature. This really is the case, as fig. 4.5 demonstrates. To eliminate the quadratic term σ_2V^2, a more detailed knowledge about the background is needed which unfortunately we do not have. We can, however, use the fact that the blocking at 4-5 meV is negligible because of the short lifetimes of the excitations. Therefore it is appropriate to subtract from the even part of the second derivative

$$\frac{d\sigma_e}{dV} = 2\sigma_2 V + \frac{d\delta\sigma(V,T)}{dV} \qquad (4.5)$$

Fig. 4.5

Experimental odd conductance

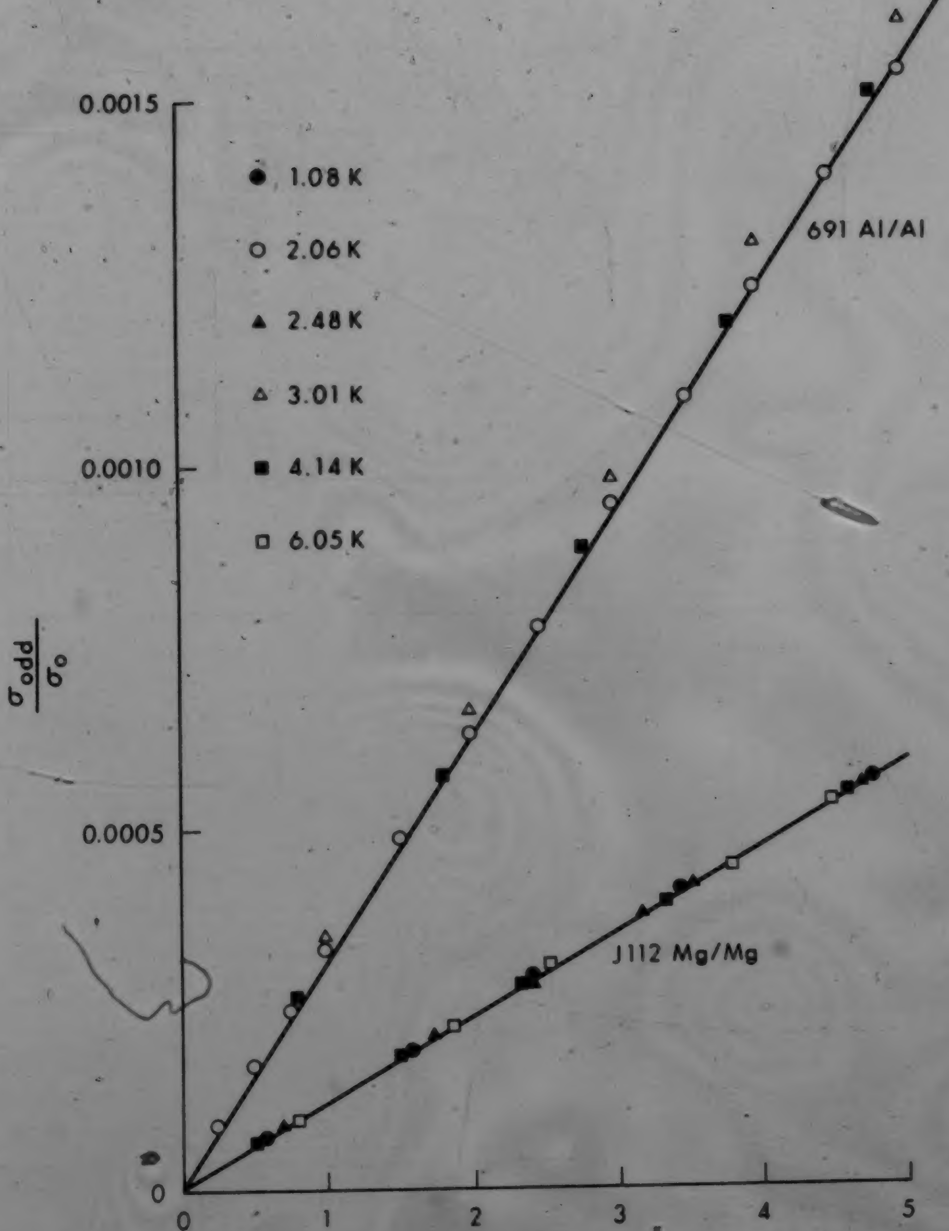
● 1.08 K
○ 2.06 K
▲ 2.48 K
△ 3.01 K
■ 4.14 K
□ 6.05 K
691 Al/Al
J112 Mg/Mg
$\frac{\sigma_{odd}}{\sigma_o}$
0.0015
0.0010
0.0005
0
0
1
2
3
4
5
ENERGY (meV)

a line, passing through the origin, with a slope which brings the measured $d\sigma_e/dV$ to zero at 4-5 meV. We estimate that this technique may introduce at the most a 5% uncertainty in the determination of the peak magnitudes in $d\sigma_e/dV$.

4.3 General Considerations in Extracting τ_B, τ_i and τ_{drift}

A successful theory of the zero bias anomaly should be able to predict the lineshape of the conductance dip and its general behaviour with temperature or magnetic field.

Let us consider first the case of a zero magnitic field. The usual procedure in comparing the experimental data with the theory is to fit the measured curve at a fixed temperature and extract the necessary parameters characterizing the anomaly. These are τ_B - the tunneling time and τ_i - the impurity scattering time. We assume that the coupling strength of the electron phonon interaction is known beforehand. Having obtained τ_B and τ_i, the theoretical curves are then calculated for different temperatures and compared to the measured ones. In practice, it is more sensitive and accurate to fit the zero bias anomaly to the experimentally determined derivative of the even part of the conductance $\frac{1}{\sigma_o}\frac{d\delta\sigma_e}{dV}$. The curve is fitted with respect to the peak height and its peak position in terms of Γ and the ratio of τ_i/τ_B. For the sake of completeness we rewrite eq. (2.30) in these terms (assuming that $\alpha^2F = a_1\omega$)

$$\frac{1}{\sigma_o}\delta\sigma_e = -\frac{2\tau_i\cdot\Gamma_1}{\tau_B}\int_0^\infty \frac{dx}{(e^x+1)(e^{-x}+1)}\left(\frac{1}{(\Gamma_1+(xk_BT+eV)^2+(\pi k_BT)^2)}\right.$$

$$\left.+\frac{1}{(\Gamma_1+(eV-xk_BT)^2+(\pi k_BT)^2}\right) . \qquad (4.6)$$

The derivative of even conductance is given as

$$\frac{1}{\sigma_o}\frac{d\delta\sigma_e}{dV} = \frac{4\tau_i\Gamma_{1e}}{\tau_B}\int_0^\infty \frac{dx}{(e^x+1)(e^{-x}+1)}\left(\frac{(xk_BT+eV)}{(\Gamma_1+(xk_BT+eV)^2+(\pi k_BT)^2)^2}\right.$$

$$\left.+\frac{(eV-xk_BT)}{(\Gamma_1+(eV-xk_BT)^2+(\pi k_BT)^2)^2}\right) . \qquad (4.7)$$

When writing the above equations we have again assumed that the junction is symmetric with respect to its relaxation processes and tunneling times. This simplifying assumption, as well, was used in the analysis of the experimental data. From the theoretical point of view, it is hard to justify this, even for samples prepared with the same electrodes, having the same thickness. Generally, the films can have different grain sizes and imperfections. In addition, the two interface planes adjoining the insulating layer can be contaminated with different impurities. This all, leads to a tunnel junction with non-symmetrical tunneling and scattering times. Considering eq. (2.30) we should then write the part enclosed in brackets as

$$\frac{1}{\tau_{B1}}\left[\frac{1}{(\Gamma_1^1+\varepsilon^2+(\pi k_B T)^2)}+\frac{\tau_{B1}}{\tau_{B2}}\cdot\frac{a_1^1}{a_1^2}\frac{1}{(\Gamma_1^2+\varepsilon^2+(\pi k_B T)^2)}\right] \qquad (4.8)$$

from which it follows that generally we can use three parameters Γ_1^1, Γ_1^2 and λ

$$\lambda = \frac{\tau_{B1}}{\tau_{B2}}\cdot\frac{a_1^1}{a_1^2} \qquad (4.9)$$

to fit the temperature dependence of the experimental data. The fourth parameter τ_{B1} adjusts the peak amplitudes. With a three parameter fit we have to consider the interference between the two terms in (4.8) which can be responsible in creating an additional peak in $d\delta\sigma_e/dV$. Experimentally, the two peaks in $\frac{1}{\sigma_o}\frac{d\delta\sigma_e}{dV}$ were never observed. This does not, however, exclude the possibility of their insufficient separation and the small size of the second peak.

Numerical analysis (Teshima, 1974) indicates that the second derivative will not have the two peaks as long as

$$\frac{\Gamma_1^1}{\Gamma_1^2} < 8 + \sqrt{90} \quad \text{at} \quad T = 0\ \text{K} \ .$$

Since the experimentally found parameter Γ ranged from $.4 \leq \Gamma \leq 2.(\text{meV})^2$, it is safe to assume that the condition above is always satisfied.

Nevertheless we have compared some of our data with the predictions of the theory using a three parameter fit. In general, there was no appreciable difference between this fit and the one obtained by assuming a symmetrical junction.

Furthermore, we assume that τ_{ep}, the relaxation time due to electron-phonon interaction is given by eq. (2.12). This is equivalent to an assumption that α^2F behaves linearly for small excitation energies. The justification of this assumption is partly based on the preliminary results of measurements on Mg/Mg and Mg/Au junctions down to 0.3 K. The second derivative characteristics of these junctions have not shown kink in the vicinity of zero, whereas they would if α^2F behaved quadratically for small energies (fig. 2.5). In addition, the theoretical fits using τ_{ep} derived on the basis of the linear α^2F behaviour were superior to those obtained by τ_{ep} of eq. (2.13) and eq. (2.14).

The relaxation time τ_{drift} associated with the magnetic field measurements can be extracted only if both τ_i and τ_B are known. But these are obtained from zero field measurements. The procedure is strictly valid for τ_B which is magnetic field independent. The results prove this assumption to be a correct one.

4.4. Comparison of the Theory with the Experiment

Let us first consider the results of the theory applied on the previously discussed Mg/Mg junction. in fig. 4.6, beside the experimentally determined data points, we show the behaviour of the theoretical curves for three different parameters $\Gamma = 0.4, 0.8, 1.2 \text{ meV}^2$. The peak amplitudes were normalized at 1 K. The dependence of the peak positions on the temperature is well fitted by a theoretical curve with $\Gamma = 0.4 \text{ meV}^2$. In this case, however, the peak amplitudes do not drop as fast as the theory would predict. The second extreme, $\Gamma = 1.2 \text{ meV}^2$, fits the peak amplitudes better at higher temperatures, whereas the peak positions lie below the theoretical curve. A reasonable compromise is to assume that $\Gamma = 0.8 \text{ meV}^2$ represents the best fit.

The theory then predicts a stronger temperature dependence of the peak amplitudes than experimentally observed. Correspondingly the peak positions are at lower biases than expected.

The reasons behind accepting $\Gamma = 0.8 \text{ meV}^2$ as the best fit will be more transparent when we consider the results of the experiments on other junctions. We

Fig. 4.6

Comparison of the experimentally determined peak positions, V_{max} (upper diagram) and peak amplitudes, $\frac{1}{\sigma_o} \left.\frac{d\delta\sigma_e}{dV}\right|_{V_{max}}$ (lower diagram) for a Mg/Mg junction at various temperatures with peak positions and peak amplitudes predicted by the theory.

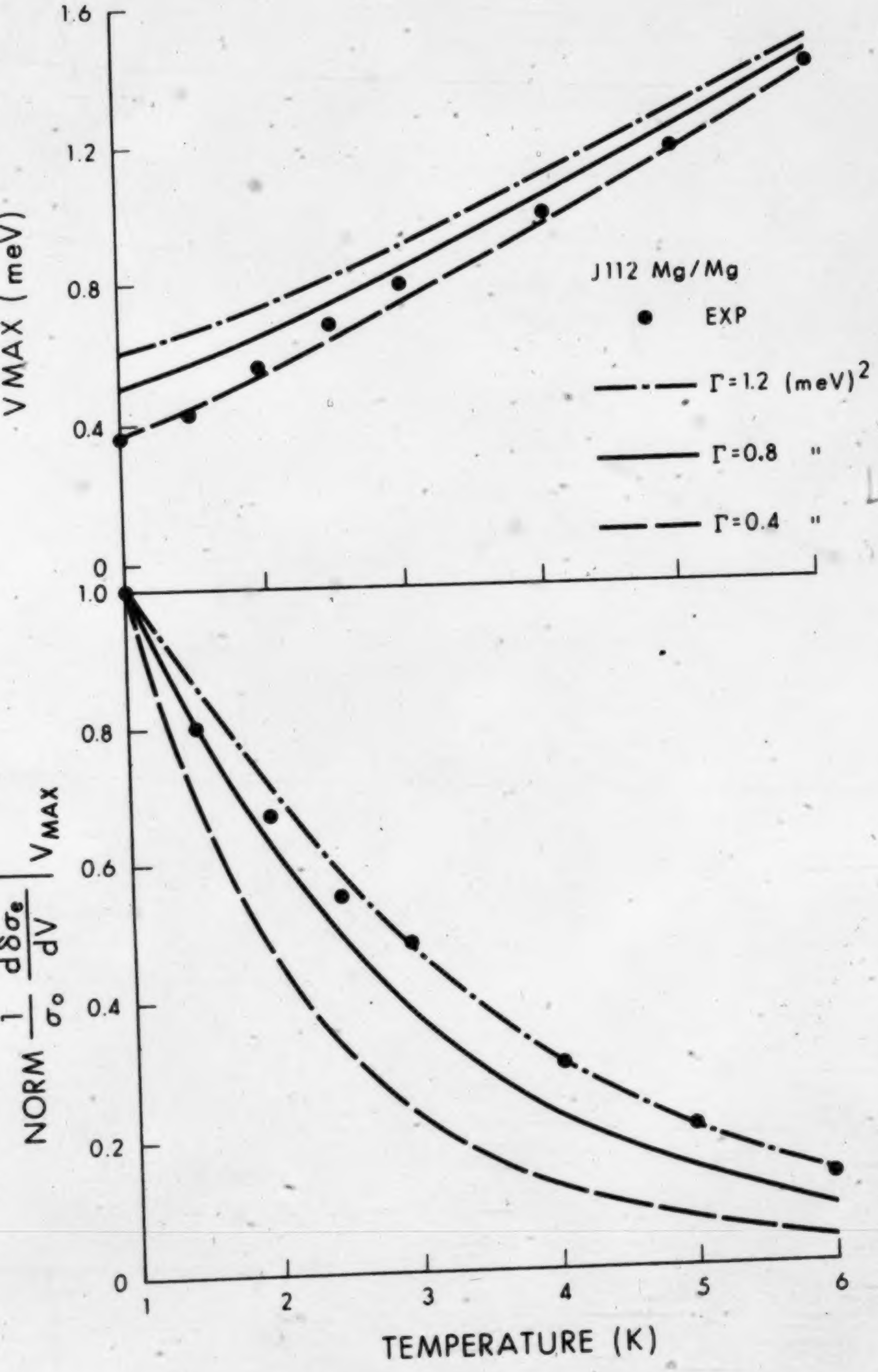
1.6
1.2
0.8
0.4
0
V MAX (meV)
J112 Mg/Mg
● EXP
Γ=1.2 (meV)^2
Γ=0.8 "
Γ=0.4 "
1.0
0.8
0.6
0.4
0.2
0
NORM $\frac{1}{\sigma_o}\frac{d\delta\sigma_e}{dV}\Big|_{V_{MAX}}$
1
2
3
4
5
6
TEMPERATURE (K)

will find that these conclusions apply equally for them.

With $\Gamma = 0.8\ \text{meV}^2$ we have plotted the temperature dependence of the blocking conductance at zero bias and compared it with the experiment (fig. 4.7) the data were normalized at 1 K.

To extract τ_i and τ_B we have to know the value of the electron-phonon coupling constant for Mg. Since to our knowledge there is no available information on it, we have taken it to be equal to $.0015\ \text{meV}^{-1}$. This value is one half of that published for aluminum (Carbotte, Dynes, 1968). This certainly introduces an uncertainty in the determination of τ_i and τ_B. Nevertheless, we feel that this choice is appropriate in obtaining the order of magnitudes involved.

We have then

$$\tau_i = 1.8 \times 10^{-10}\ \text{sec}$$

$$\tau_B = 9.6 \times 10^{-8}\ \text{sec}$$

Using these parameters we can compare the theoretical even part of the second derivative with the measured one. Fig. 4.8 illustrates the fit at T = 1 K and 3 K. The peak amplitude at 3 K reproduces well, while the experimental peak position is shifted to a lower value.

Fig. 4.7

Comparison of the temperature dependent blocking conductance at zero bias for a Mg/Mg junction with the blocking conductance calculated from the theory.

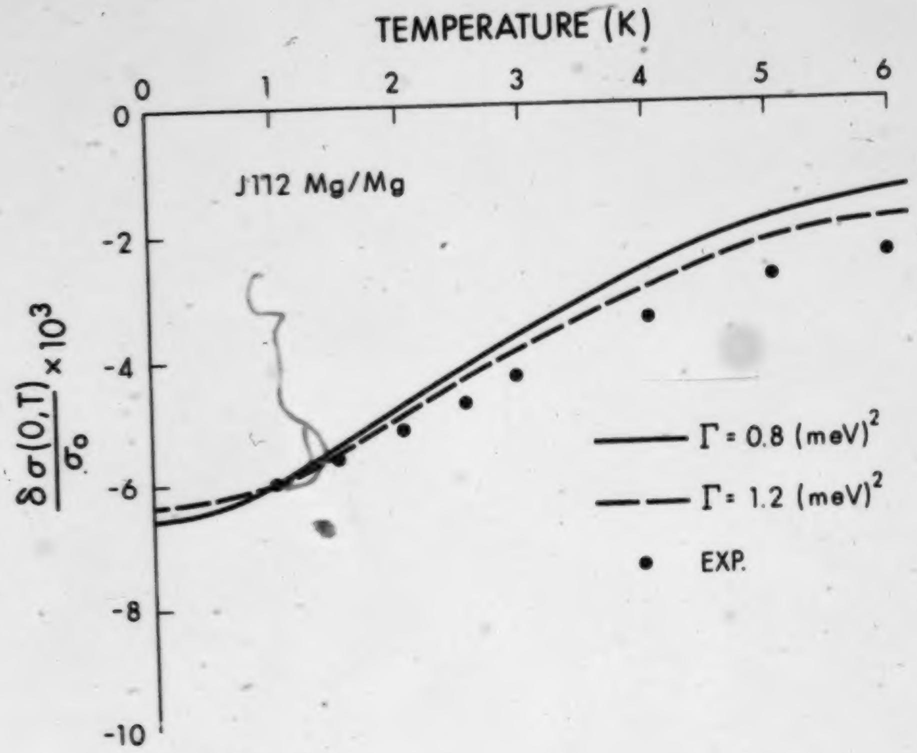
TEMPERATURE (K)
0
1
2
3
4
5
6
0
-2
-4
-6
-8
-10
$\frac{\delta\sigma(0,T)}{\sigma_0} \times 10^3$
J112 Mg/Mg
Γ = 0.8 (meV)^2
Γ = 1.2 (meV)^2
EXP.

Fig. 4.8

Comparison of the experimentally determined $\frac{1}{\sigma_o} \frac{d\delta\sigma_e}{dV}$ for a Mg/Mg junction with $\frac{1}{\sigma_o} \frac{d\delta\sigma_e}{dV}$ predicted by the theory .

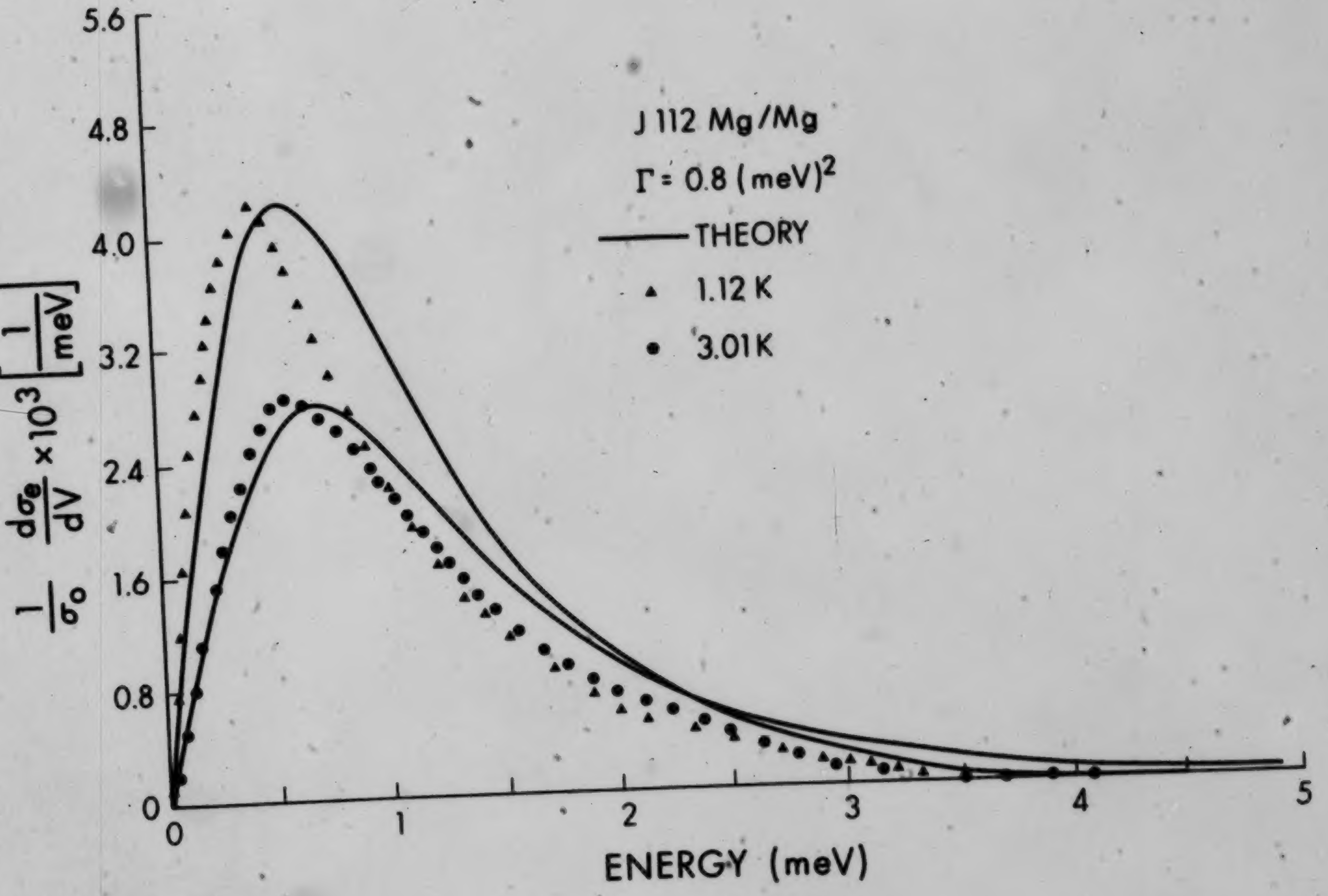
J 112 Mg/Mg
Γ = 0.8 (meV)²
THEORY
1.12 K
3.01 K
$\frac{1}{\sigma_o}\frac{d\sigma_e}{dV} \times 10^3 \left[\frac{1}{meV}\right]$
5.6
4.8
4.0
3.2
2.4
1.6
0.8
0
0
1
2
3
4
5
ENERGY (meV)

Replacing the top Mg layer by an Au counter-electrode has not altered the character of the zero bias anomaly. Figs. 4.9 and 4.10 show the temperature dependence of the conductance of two Mg/N_2/Au junctions. These were prepared on the same substrate with the same Au overlayer. Completing their initial measurement, the junctions were allowed to warm up while they still were kept under a vacuum. After a period of a few days, the junctions were again cooled down and remeasured. The annealing produced a 2.5 fold increase in the resistance of the tunnel junctions. The relative magnitude of the conductance dip, characteristic of the zero bias anomaly, however, has not changed. This documents that the relevant scattering mechanisms which deblock the tunneling electrons were not altered. In fig. 4.11 we show the experimental data for 85 B1 and B2 (annealed) together with the fit obtained by adjusting Γ to 0.6 meV^2. The theory again predicts a stronger temperature dependence for the peak amplitudes. As the temperature decreases the peak positions lie below the theoretical curve. The lineshapes of $\frac{1}{\sigma_o}\frac{d\delta\sigma_e}{dV}$ for T = 1 K and 3 K are shown in the following figure.

According to the theory, metals with infinitely thick electrodes are essentially in equilibrium. This is because the density of final states for the incoming

Fig. 4.9

Temperature dependence of the zero bias conductance anomaly for O85A Mg/N_2/Au

Mg = 30000 Å

Au = 2200 Å

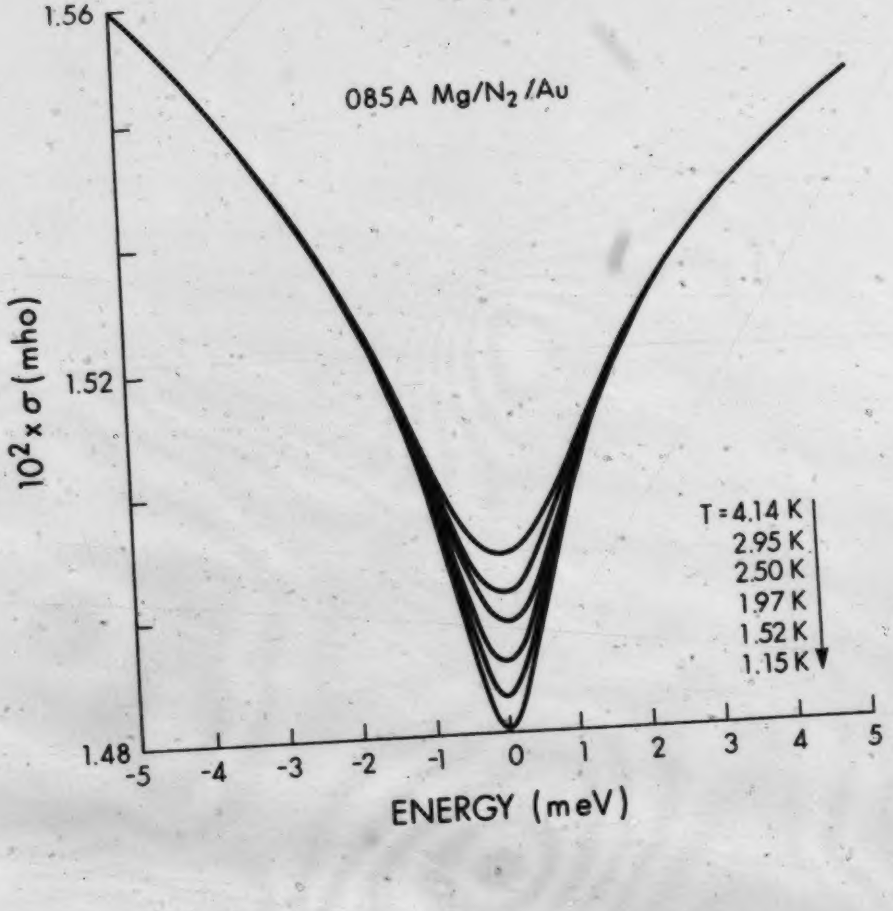
085A Mg/N$_2$/Au
$10^2 \times \sigma$ (mho)
1.56
1.52
1.48
T=4.14 K
2.95 K
2.50 K
1.97 K
1.52 K
1.15 K
-5
-4
-3
-2
-1
0
1
2
3
4
5
ENERGY (meV)

219

Fig. 4.10

Temperature dependence anomaly for O85B

Mg/N_2/Au

Mg = 3000 Å

Au = 2200 Å

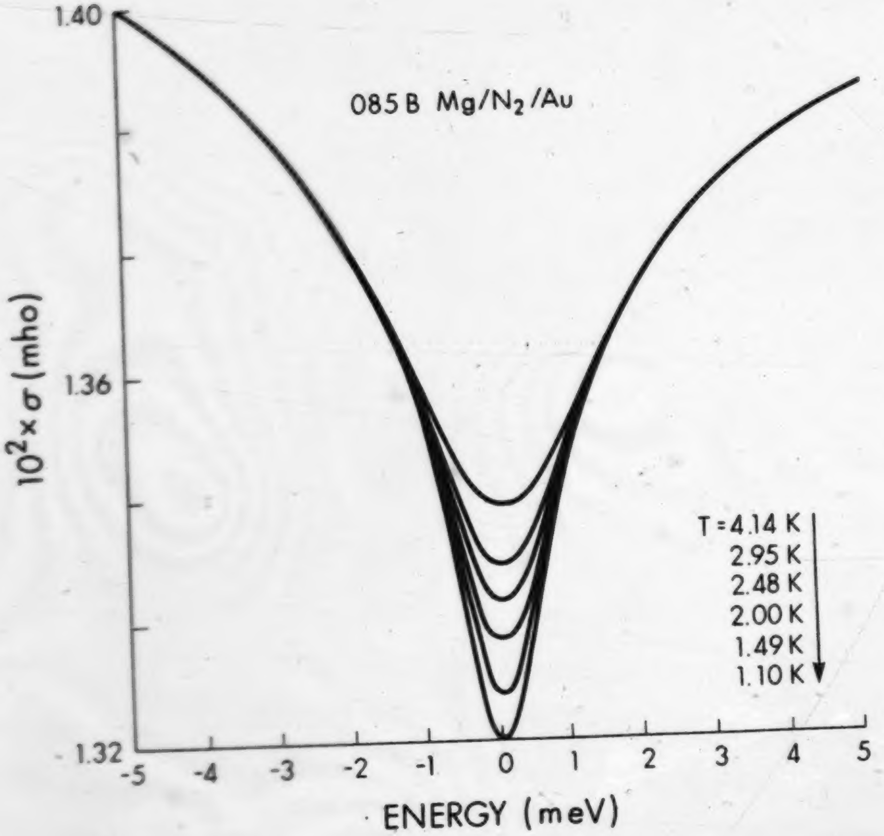
1.40
1.36
1.32
-5
-4
-3
-2
-1
0
1
2
3
4
5
ENERGY (meV)
$10^2 \times \sigma$ (mho)
085 B Mg/N_2/Au
T = 4.14 K
2.95 K
2.48 K
2.00 K
1.49 K
1.10 K

Fig. 4.11

Temperature dependence of peak positions, V_{max} (upper diagram) and peak amplitudes, $\frac{1}{\sigma_o} \frac{d\delta\sigma_e}{dV}\Big|_{V_{max}}$ (lower diagram) of O85, before (B1) and after (B2) annealing. The solid lines represent the theoretical fit.

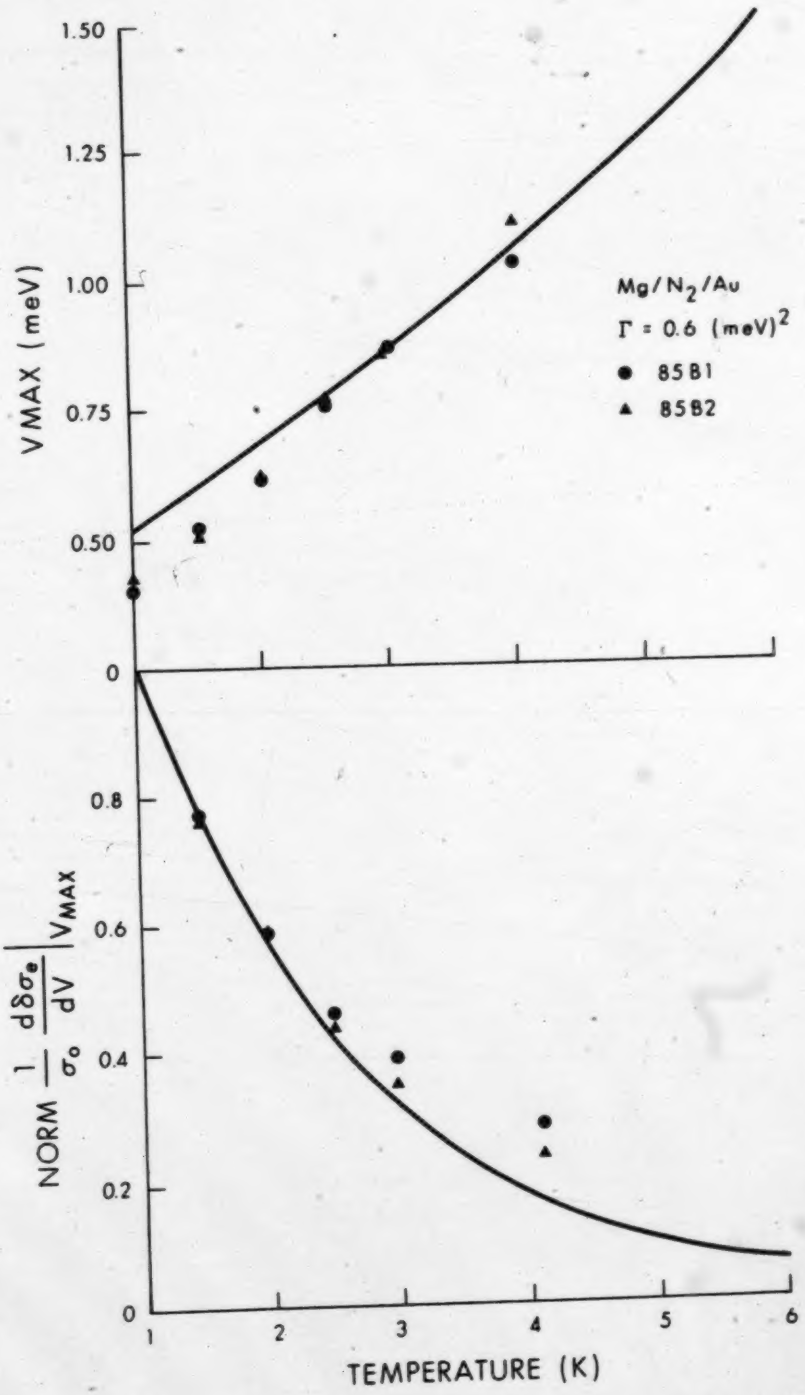
1.50
1.25
1.00
0.75
0.50
0
V MAX (meV)
Mg/N$_2$/Au
Γ = 0.6 (meV)^2
● 85B1
▲ 85B2
0.8
0.6
0.4
0.2
0
NORM $\frac{1}{\sigma_o}\frac{d\delta\sigma_e}{dV}\Big|_{V_{MAX}}$
1
2
3
4
5
6
TEMPERATURE (K)

Fig. 4.12

Comparison of experimental and theoretical $\frac{1}{\sigma_o}\frac{d\delta\sigma_e}{dV}$ for O85B2, Mg/N_2/Au.

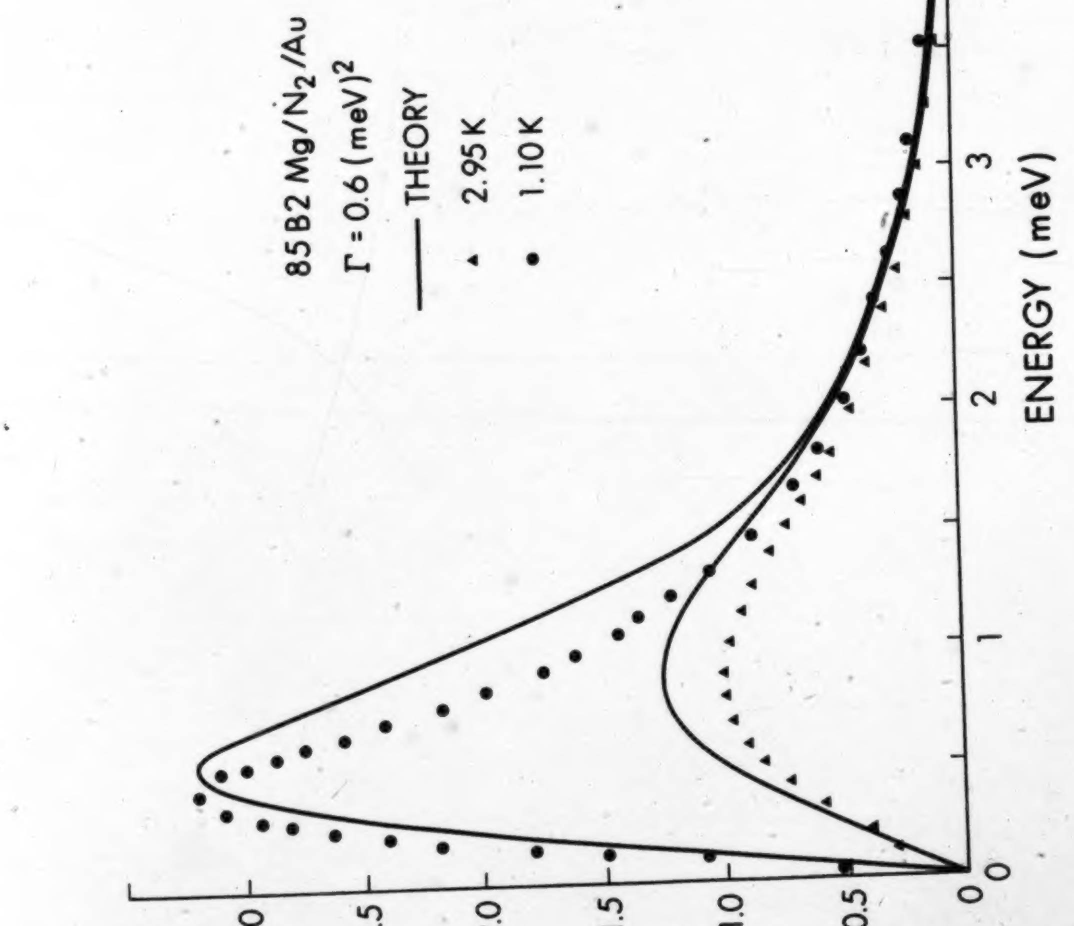
85 B2 Mg/N2/Au
Γ = 0.6 (meV)2
THEORY
2.95 K
1.10 K
ENERGY (meV)
0
1
2
3
4
5
1/go dδσe/dV ×102 [1/meV]
0
0.5
1.0
1.5
2.0
2.5
3.0

electrons is infinite. Mathematically, this is expressed by setting the tunneling time τ_B to infinity. To test this assertion we have prepared double junctions which had one common electrode and in which the counterelectrodes of the same material had different thicknesses. Samples so prepared consistently had smaller zero bias anomalies in junctions with the thicker film. Junctions 85A, 85B are the representative of these. The Au film was 2200 Å thick. The Mg electrode for the junction 85B was 3000 Å thick while for 85A it was 30000 Å thick (fig.4.13). The solid lines represent the theoretical fits. The "thinner" junction 85B was parameterized with $\Gamma = 0.6$ meV^2, giving

$$\tau_B = 1.3 \times 10^{-8} \text{ sec}$$

$$\tau_i = 2.0 \times 10^{-10} \text{ sec.}$$

The "thicker" junction was fitted with $\Gamma = 1.3$ meV^2 yielding

$$\tau_B = 1.0 \times 10^{-8} \text{ sec}$$

$$\tau_i = 1.1 \times 10^{-10} \text{ sec.}$$

Of course, these tests can give only qualitative answers. Meaningful quantitative numbers could be obtained only for metal electrodes with a character of a single grain throughout the entire film thickness. In practice, the evaporated films may grow in layers of different thick-,

Fig. 4.13

Zero bias blocking conductance for two junctions with different thickness of metal electrodes.

(85A - Mg = 30000 Å, Au = 2200 Å)

(85B - Mg = 3000 Å, Au = 2200 Å).

The theoretical fit (solid line) for O85B was calculated with $\Gamma = 0.6$ meV^2. 85A was fitted with $\Gamma = 1.3$ meV^2.

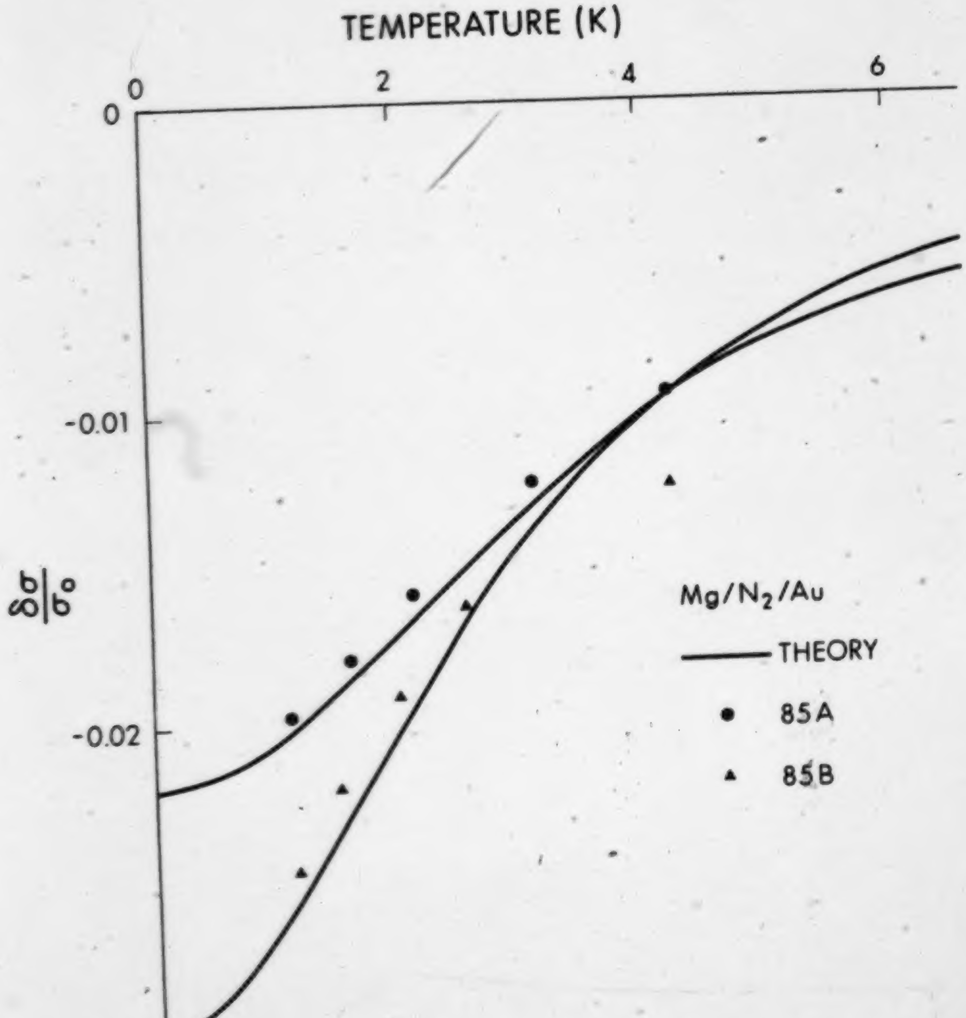
TEMPERATURE (K)
0
2
4
6
0
-0.01
-0.02
-0.03
$\frac{\delta\sigma}{\sigma_0}$
Mg/N$_2$/Au
THEORY
● 85A
▲ 85B

ness and orientation. This then reduces the overall observable effect. The results of this discussion apply equally well to that part of the impurity relaxation time τ_i which is responsible for the diffuse boundary scattering. An investigation of Mg films by an electron microscope revealed that Mg crystallizes in grains, the thickness of which could be equal to the thickness of the whole specimen. This was probably true of films less than 1500 Å (Turner, 1974). The lateral dimensions of the grains ranged between 500-800 Å. The decrease of the zero bias anomaly in junctions with thicker (>1500 Å) films then shows that a fraction of the incoming electrons feels the increased number of grains grown across the whole film.

Similar results have been obtained on Mg/Au junctions having an oxide as its insulating layer. In fig. 4.14 we show a fit for such a junction.

The zero bias anomaly measurements on Mg/Au and Mg/Mg systems have been complemented with investigations on junctions having different electrodes (Pb, Al). We illustrate the results on Al/Al structures. Fig. 4.15 shows a temperature dependence of the conductance dip out on a previously published Al/Al junction (Trofimenkoff, et al, 1972). The data were fitted to the 3 K curve width

Fig. 4.14

Comparison of the experimentally determined peak positions, V_{max} (upper diagram) and peak amplitudes, $\frac{1}{\sigma_o} \frac{d\delta\sigma_e}{dV}\Big|_{V_{max}}$ (lower diagram) for a Mg/O/Au junction at various temperatures with peak positions and peak amplitudes predicted by the theory.

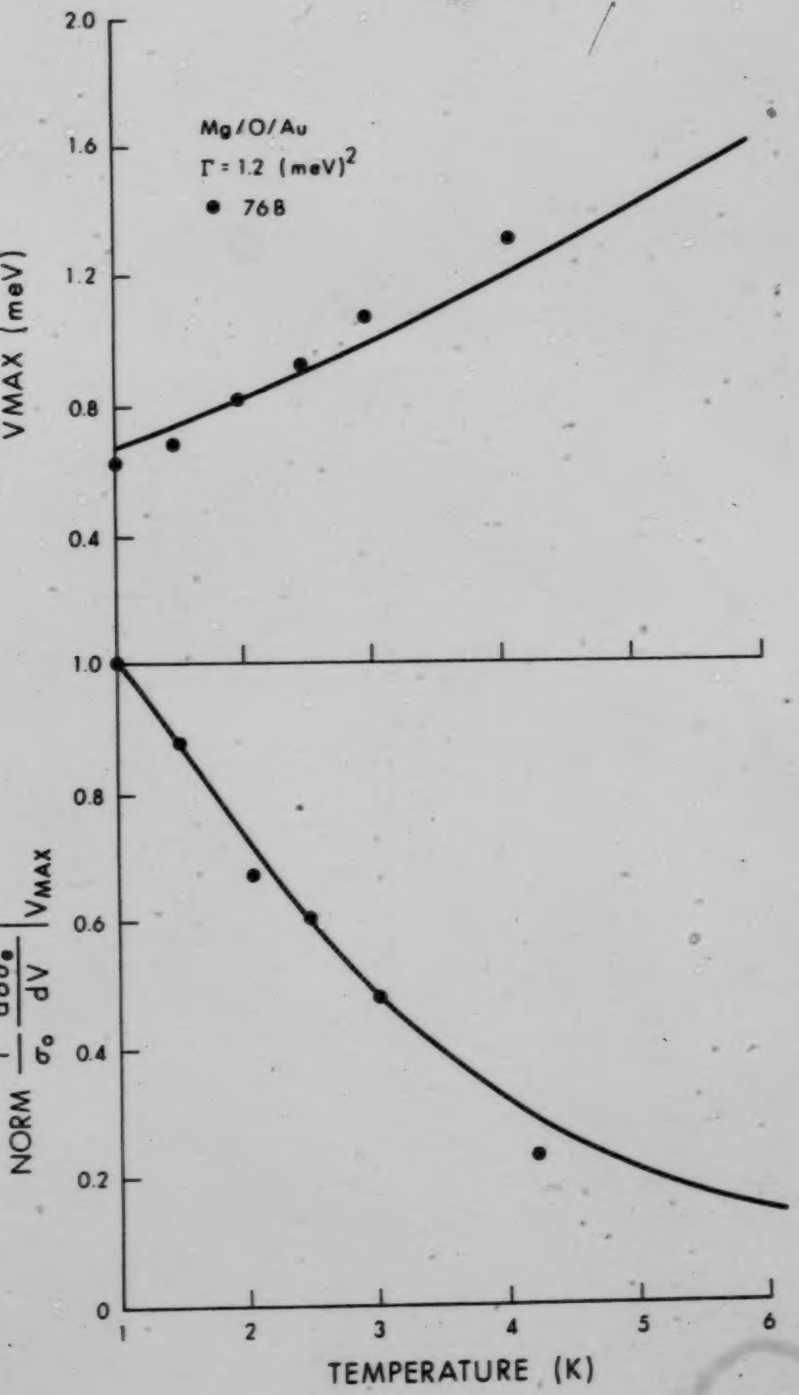
2.0
1.6
1.2
0.8
0.4
1.0
VMAX (meV)
Mg/O/Au
Γ = 1.2 (meV)^2
● 76B
0.8
0.6
0.4
0.2
0
NORM $\frac{1}{\sigma_0}\frac{d\delta\sigma_e}{dV}\Big|_{V_{MAX}}$
1
2
3
4
5
6
TEMPERATURE (K)

Fig. 4.15

Temperature dependent conductance of an Al/Al junction.

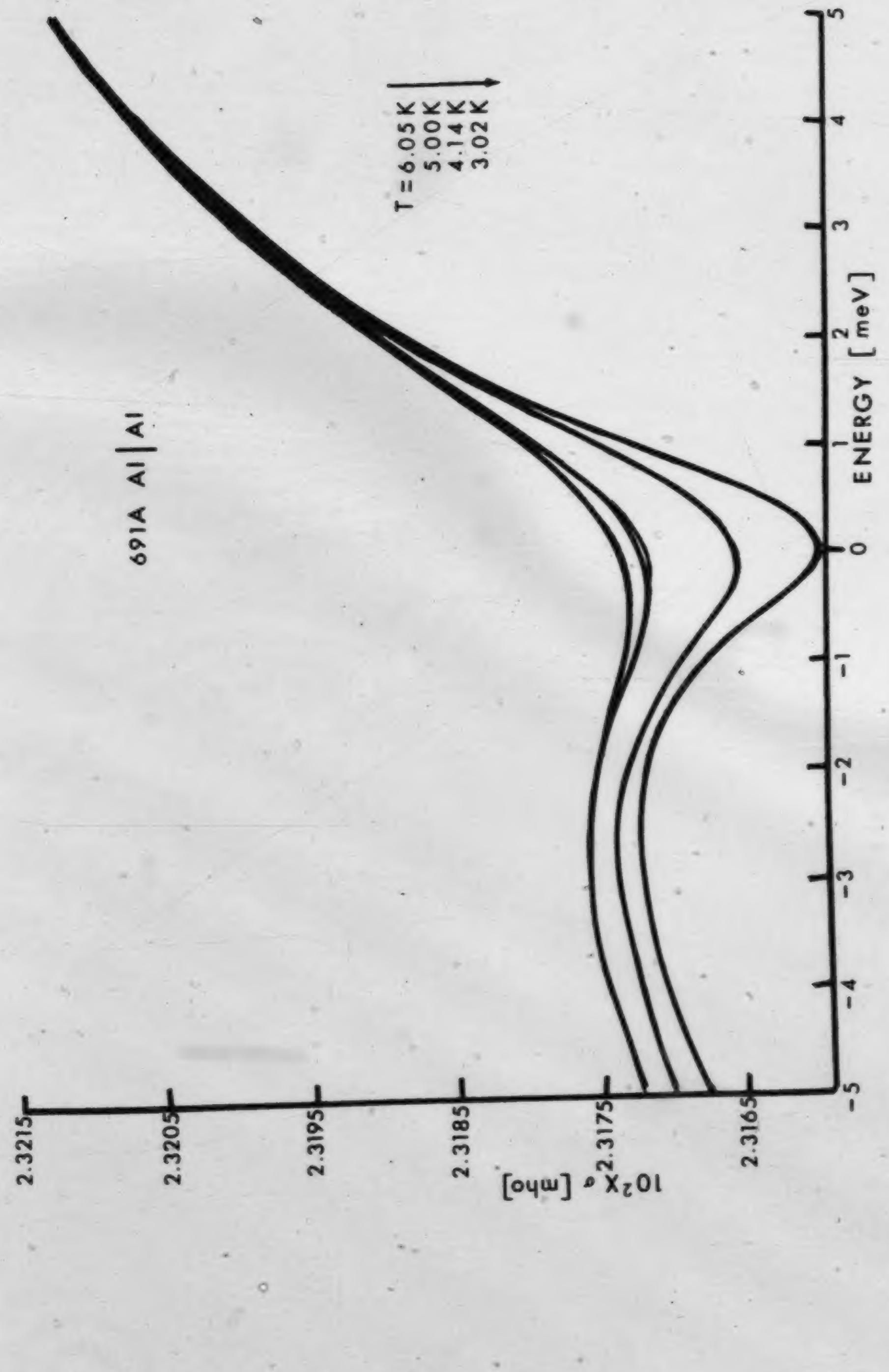
691A Al|Al
T = 6.05 K
5.00 K
4.14 K
3.02 K
2.3215
2.3205
2.3195
2.3185
2.3175
2.3165
10²X_σ [mho]
−5
−4
−3
−2
−1
0
1
2
3
4
5
ENERGY [meV]

$$\tau_B = 1.4 \times 10^{-7} \text{ sec}$$

$$\tau_i = 3.5 \times 10^{-10} \text{ sec}$$

and

$$a = 3 \times 10^{-3} \text{ meV}^{-1}$$

(Carbotte, Dynes, 1968). Figs. 4.16, 4.17 show the resulting fit. In these measurements care had to be taken to separate the decrease in conductivity due to the blocking effect from the one arising from the appearance of superconducting energy gap in the electrode. This is particularly true of thin films, where it is known that the transition temperature increases with decreasing film thickness. We show this effect in fig. 4.18, where at 2 K the Al film (680 Å thick) is already superconducting. The transition temperature of the bulk Al is 1.19 K. In principle a magnetic field could have been used to suppress the appearance of the superconducting phase. But since we wanted to eliminate the influence of the magnetic field on the size of the zero bias anomaly for the subsequent field dependence measurements this has not been done.

The results in the presence of the magnetic field agreed with the predictions of the theory (Sec. 2.5). They have been described earlier (Adler, et al, 1973) and are attached as an Appendix (Appendix II).

Fig. 4.16

Peak height (open circles) and peak position (full circles) vs temperature for an Al/Al junction. The solid line represents the theoretical fit.

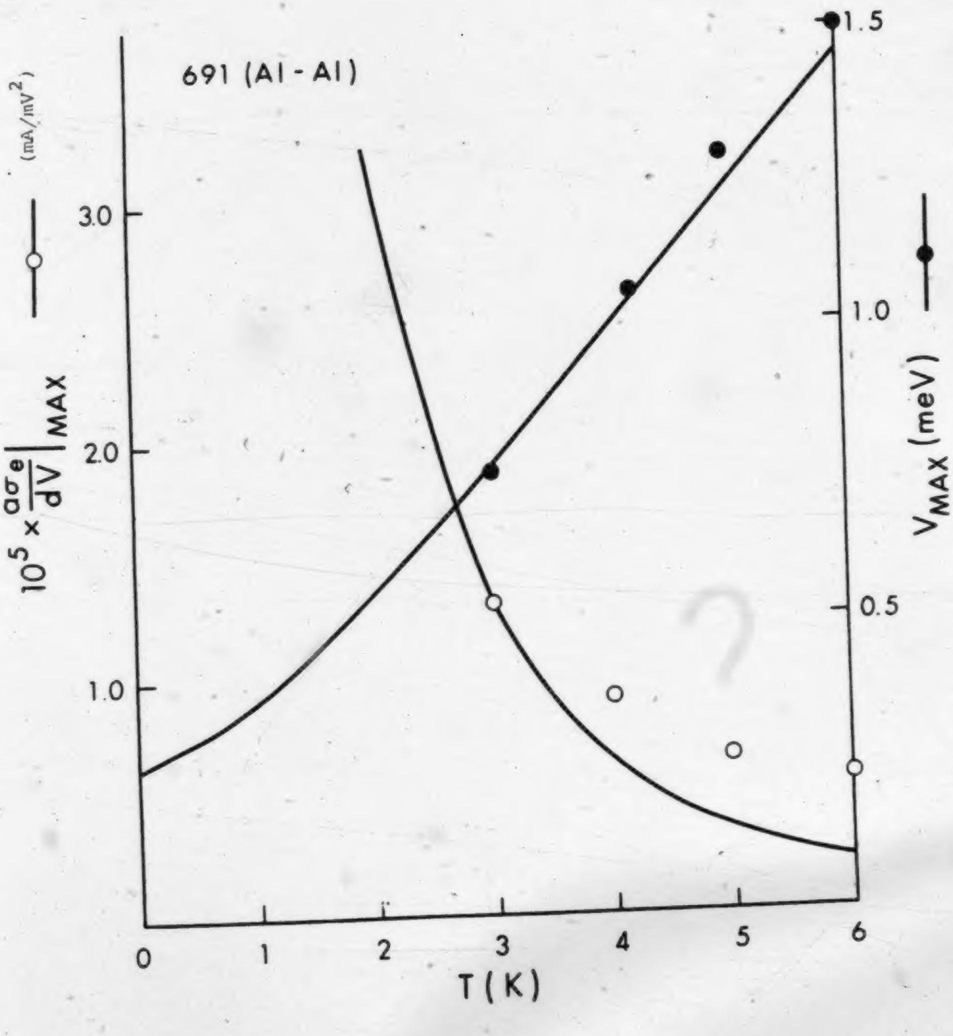
691 (Al - Al)
10^5 × dσe/dV|MAX
(mA/mV²)
3.0
2.0
1.0
1.5
1.0
0.5
VMAX (meV)
0
1
2
3
4
5
6
T (K)
?

Fig. 4.17

$\frac{d\sigma_e}{dV}$ vs V for an Al/Al junction. Solid lines represent data; dashed lines theoretical result for T = 3 K.

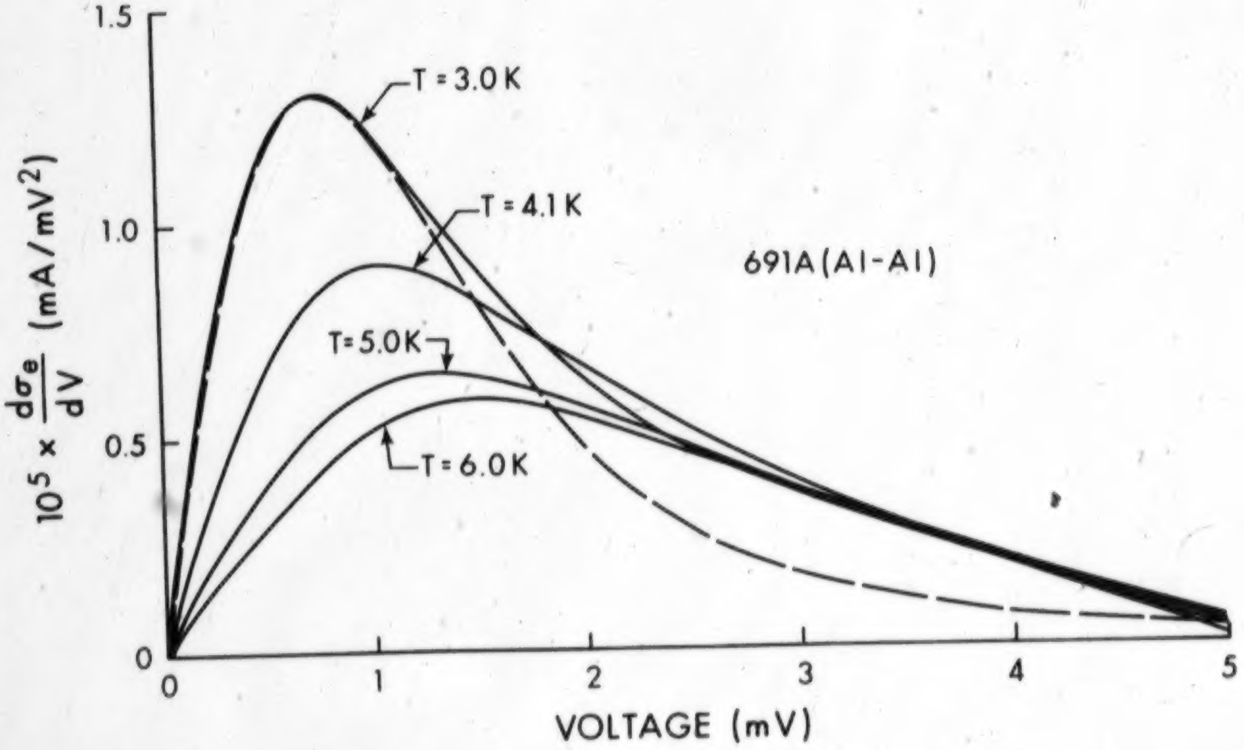

691A(Al-Al)
T = 3.0 K
T = 4.1 K
T = 5.0 K
T = 6.0 K
$10^5 \times \frac{d\sigma_e}{dV}$ (mA/mV^2)
1.5
1.0
0.5
0
0
1
2
3
4
5
VOLTAGE (mV)

Fig. 4.18

Illustration of the appearance of the superconducting energy (at 2 K) gap in an Al/Al junction.

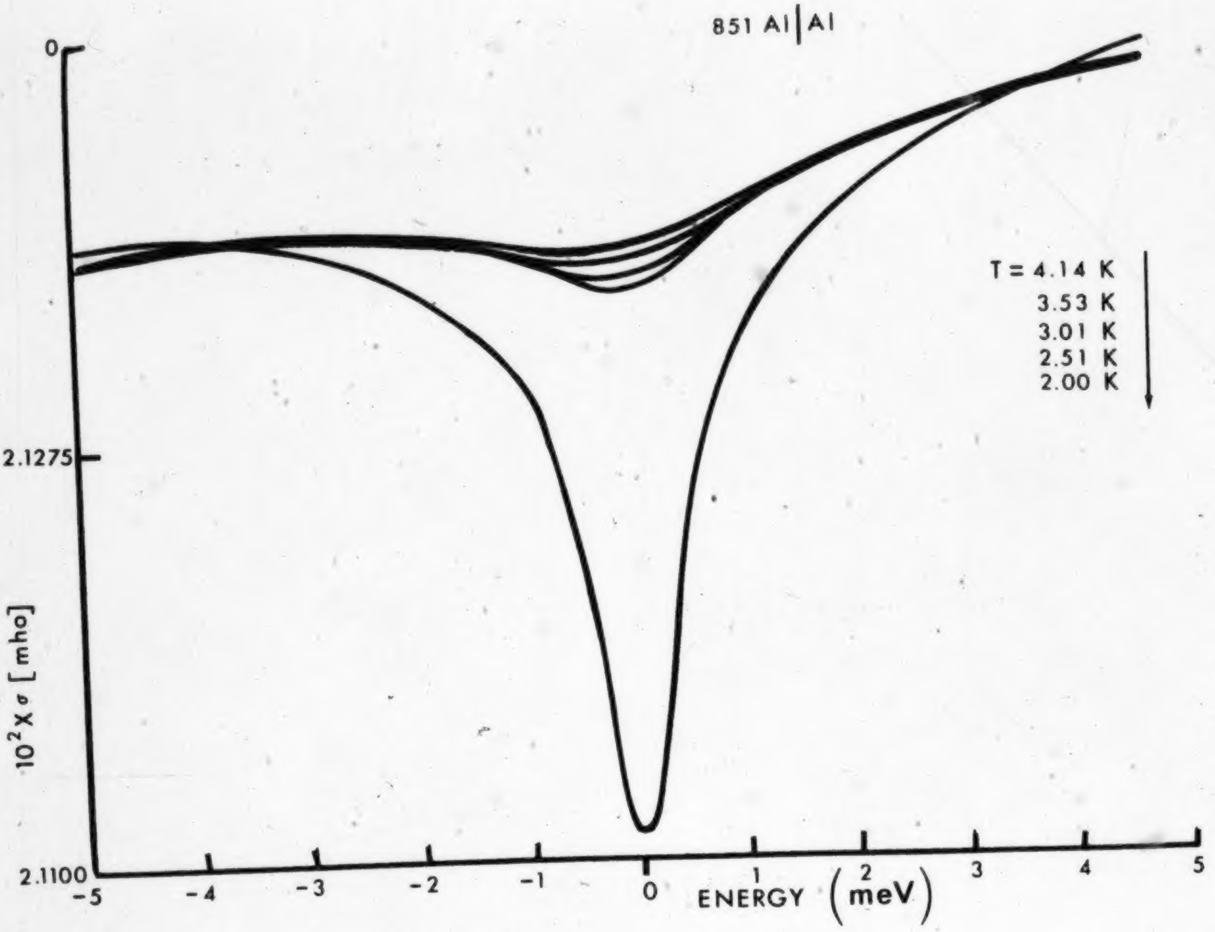
851 Al|Al
0
2.1275
2.1100
$10^2 \times \sigma$ [mho]
−5
−4
−3
−2
−1
0
1
2
3
4
5
ENERGY (meV)
T = 4.14 K
3.53 K
3.01 K
2.51 K
2.00 K

Fig. 4.19

Temperature dependence of the blocking conductance at zero bias for 691 Al/Al and 851 Al/Al. The solid lines are just indicating the linear behaviour.

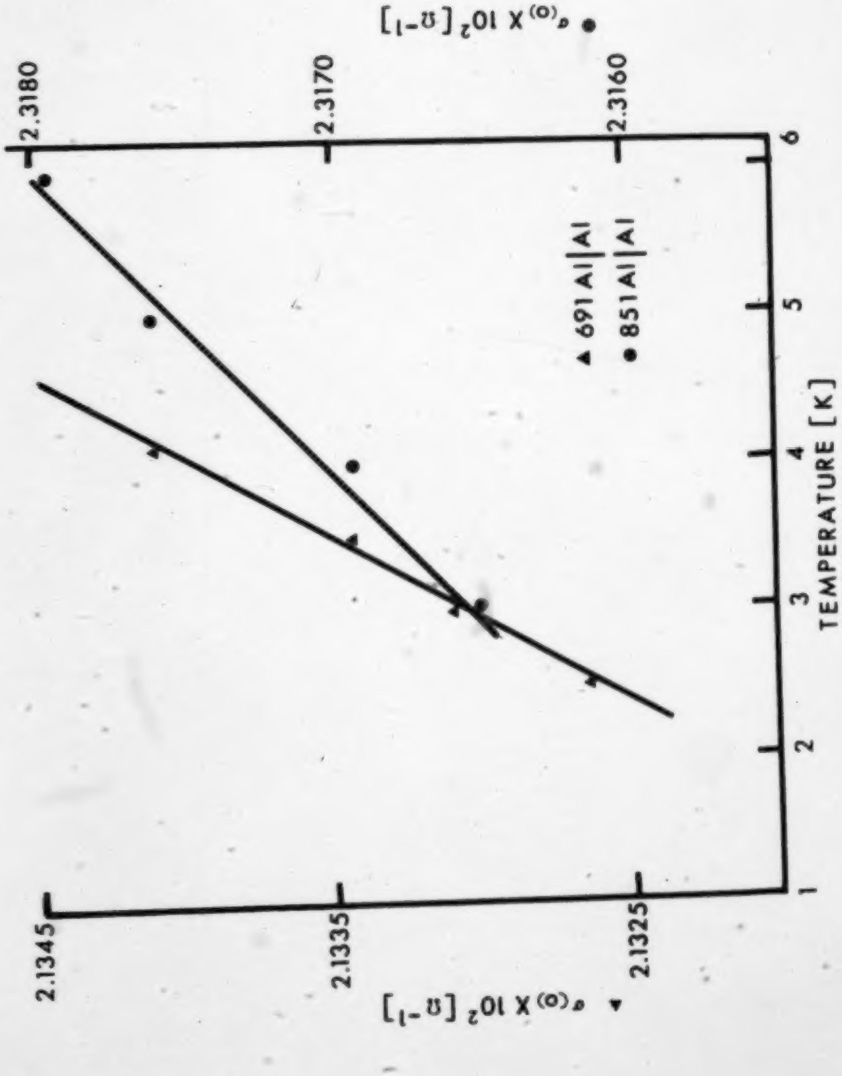
● σ(o) X 10² [Ω-1]
2.3180
2.3170
2.3160
▲ 691 Al|Al
● 851 Al|Al
1
2
3
4
5
6
TEMPERATURE [K]
2.1345
2.1335
2.1325
▲ σ(o) X 10² [Ω-1]

4.5 Discussion

In the last section we have presented the results of the experimental investigations on small conductance decreases around zero bias. These were compared with the predictions of the transport model, based on the non-equilibrium tunneling theory. The temperature dependence of the anomaly was fitted by one parameter, the knowledge of which allowed to extract the impurity relaxation time, τ_i, if the strength of the electron-phonon coupling was known beforehand. The amplitude of the theoretical curve was adjusted to the experimental one with an aid of another parameter, τ_B, related to the barrier penetrability coefficient and the electrode thickness.

The theory, as it stands, predicts a somewhat stronger temperature dependence of the observed peak amplitudes in $d\sigma_e/dV$. The peak positions, at the lowest temperatures, lie approximately 10-20% below the predicted curve. A possible explanation of the observed discrepancies will be given below.

A magnetic field oriented perpendicularly to the direction of the tunneling current reduced the conductance anomaly. This effect was explained on the basis of the Lorentz force induced drift of the electrons with which we associated a relaxation time proportional to the strength of the applied field. No observable changes in the anomaly were observed if the magnetic field was applied parallel to the direction of the current flow.

The behaviour of the conductance with the magnetic field is instrumental in eliminating the structure around zero bias as being due to paramagnetic impurities. It is well known that these can produce either large conductance reductions of the order of 100% and 100 meV wide (Rowell, Shen, 1966) or conductance peaks (Wyatt, 1964) depending on the amount of the deposit and its position with respect to the barrier (Lythall, Wyatt, 1968; El-Semary, Rogers, 1972; Appelbaum, Brinkman, 1970).

Junctions with low impurity concentrations produce conductance peaks which are temperature and magnetic field dependent (Shen, Rowell, 1968; Lythall, Wyatt, 1968). The size of the anomaly is usually of the order of 10%, being a few meV wide. With the application of the magnetic field, the conductance peak first decreases and with higher fields splits into two peaks, the separation of which is proportional to the field. These results have been explained (Anderson, 1966; Appelbaum, 1966, 1967) by considering the interaction between the tunneling electrons and the magnetic impurities. Increasing the amount of the deposit leads to a large conductance reduction which, however, is magnetic field independent (Rowell, Shen, 1968). It is now believed (Wolf, 1974) that this effect is more likely connected with the Giaver-Zeller (Zeller, Giaver, 1969) tunneling, rather than being a manifestation of the interaction between the tunneling electrons and the interacting magnetic impurities (Gupta, Upadhyaya, 1971). The dominant current flow in Giaver-Zeller tunneling is through a two step tunneling process in which an electron first tunnels onto the particle embedded inside the barrier and subsequently tunnels into the second electrode. Since the localization of the electron on the impurity requires an activation energy, this process leads to a strongly non ohmic behaviour. At finite temperatures the zero bias conductivity, $\sigma(0,T)$ is proportional to the number of thermally excited electrons residing on the particle. This is given by

$$\sigma(0,T) \sim \int_0^\infty e^{-E/k_B T} \sim T \qquad (4.10)$$

where E is the activation energy of the excitation.

At this point we call attention to fig. 2.6, where we notice that the zero bias blocking conductance within a certain temperature limit (depending on Γ) is a linear function of the temperature. Thus the behaviour of the small conductance decreases at zero bias which is linear with temperature can be misleading in believing that the tunneling is through particles (Josefowicz, Smith, 1973). A comparison between the observed magnitudes of the corresponding anomalies ($\sim$100% for the two step tunneling vs. <1% for the non-equilibrium effect) and their magnetic field dependence helps to resolve this ambiguity.

Let us turn our attention to the possible sources of observed differences between the theory and the experiment. One of these arises from the fact that the energy and temperature dependent electron-phonon relaxation time was assumed to be momentum independent. There are several sources of anisotropy. The most obvious is the deviation of the Fermi surface sphere. Another results from the anisotropy in the electron-phonon interaction and in the phonon spectrum. Recent calculations (Carbotte, Truant, 1974) have shown that this anisotropy affects strongly the value of the electron-phonon relaxation time. Large variations over the Fermi surface were found even at T = 30 K. For aluminum the ratio of $\tau_{ep}(\theta,\phi,T)/\tau_{ep}(0,0,T)$ can be as high as 10 ($\vec{K} \equiv (k_F,\theta,\phi)$). The anisotropy in the electron-phonon relaxation time suggests a further set of experiments in which the electrons would tunnel into single crystal electrodes having a definite crystalographic orientation. We would expect a certain degree of correlation between the size of the zero bias anomaly and the orientation of the crystal with respect to the incoming electrons.

A more transparent source of a discrepancy arises because of the assumption that phonons created by the relaxing electrons are in equilibrium with the thermally excited phonon gas. The thermalization of the excess phonons was assumed to be immediate with the aid of a perfect heat bath. Thus their further role in the deblocking process has already been described by the previously considered electron-phonon scattering process, leading to a relaxation time given by eq. (2.10). Such a simplification is not always valid. If the lifetimes of the emitted phonons were "long enough" an incoming electron could absorb one of these and thus be scattered into a higher energy level. This results in a removal of the electron from the forward direction, thereby deblocking the occupied state. The process is in sharp contrast with the deblocking considered by the theory previously and being only due to the interaction between the tunneling electrons and thermal phonons.

It is illustrative to consider the order of magnitudes involved in order to obtain an e stimate whether an additional deblocking due to non-equilibrium phonon absorption is possible. The rate of thermalization through the surrounding bath can be characterized by

$$\tau_{bath} = \frac{L}{v_s} \tag{4.11}$$

where L is the film thickness and v_s is the sound velocity in the metal. For a 1000 Å film, and $v_s = 5 \times 10^5$ cm/ρ, $\tau_{bath} = 2 \times 10^{-11}$ sec. The relaxation time of phonons due to their absorption by electrons at T = 0 K is given by equation (4.12) (Truell, et al, 1969)

$$\frac{1}{\tau_{ph-e}} = \frac{2}{9} \frac{E_f^2}{\pi \rho_o v_s} \left(\frac{m}{\hbar^2}\right)^2 \varepsilon \tag{4.12}$$

where ρ_o represents the density of the metal. At 1 meV and $\rho_o = 10\rho/cm^3$, $E_f = 10$ eV, $v_s = 5 \times 10^5$ cm

$$\tau_{ph-e} = 2 \times 10^{-10} \text{ sec} .$$

This is comparable to τ_{bath} and the relaxation time of electrons due to their interaction with the equilibrium phonon gas. It follows that electrons can be additionally deblocked by scattering with the non-equilibrium phonon gas. Thus in steady state we should solve a coupled system of Boltzmann transport equations relating the non-equilibrium situation in the phonon and electron gas.

$$\frac{\partial N}{\partial t} = 0 = \left(\frac{\partial N}{\partial t}\right)_{scatt} + \left(\frac{\partial N}{\partial t}\right)_{ph-e} \tag{4.13}$$

$$0 = \left(\frac{\partial f}{\partial t}\right) = 0 = \left(\frac{\partial f}{\partial t}\right)_{tunneling} + \left(\frac{\partial f}{\partial t}\right)_{e-ph} + \left(\frac{\partial f}{\partial t}\right)_{scatt} \tag{4.14}$$

The interpretation of different terms in eqs. (4.13) and (4.14) is obvious.

The solution of the coupled equations is beyond the scope of the present work. Instead of this, let us see what possible results can one deduce on the basis of the previous considerations. First of all we can crudely estimate the importance of the additional deblocking mechanism. Let us assume that the effective relaxation time of electrons due to their interaction with phonons can be written as

$$\frac{1}{\tau} \sim \frac{1}{\tau_{No}} + \frac{1}{\tau_{\delta N}} \tag{4.15}$$

where $N = No + \delta N$. $\tau_{No} = \tau_{ep}$ - gives the part of the lifetime relaxation which is associated with the equilibrium phonon distribution (eq. 2.10). Setting $\tau_{\delta N} = \tau_{ph-e}$ (eq. 4.12) we further assume that the non-equilibrium phonons relax only by a scattering with the transmitted electrons. The amount of relaxation due to excess of phonons is negligible only if $\tau_{\delta N} >> \tau_{No}$. At $T = 0$ K, recalling eqs. (2.12), (4.12), this is satisfied for

$$\varepsilon \gg \frac{\hbar}{\pi a} \cdot \frac{E_f^2\, m^2}{2\pi\rho_o v_s \hbar^4} \qquad (4.16)$$

$$\varepsilon \gg .3 \text{ meV}$$

for the typically used quantities. Practically then at ~3 meV, the contribution of non-equilibrium phonons to deblocking is minimal.

Secondly at T = 0 K we expect that the size of the conductance dip at zero bias is unaffected by the incorporation of the non-equilibrium phonons into the theory. This follows from the fact that at zero bias there are no non-equilibrium phonons created since the tunneling current is zero. As voltage is imposed across the junction the zero bias anomaly decreases sharper because of the additional deblocking mechanism previously neglected by the theory. This leads to a shift of V_{max}, the peak position in $d\sigma_e/dV$, to a lower bias with a simultaneous increase in the peak amplitude. With increasing temperatures, the influence of the non-equilibrium phonons is minimized by a greater thermal phonon population.

All these results point to correction factors which when included in the theory could explain the observed experimental discrepancies. Since the nature of this discussion is purely qualitative, it is impossible to present exact values of these.

CHAPTER 5

RESONANT ELECTRON TUNNELING

5.1 Introduction

The measurements of zero bias anomalies on some junctions of Mg/oxide/Mg, Mg/oxide/Au and Mg/nitride/Au have produced characteristics which had marked differences from those shown in the previous chapter.

As a representative of junctions of this unusual behaviour we show a temperature dependence of $\frac{1}{\sigma_o}\frac{d\sigma}{dV}$ for junction 877A (fig.5.1). Note the usual set of peaks close to zero bias reflecting the discussed blocking effect with very weak additional structures seen at -3.5 meV and +1.8 meV. The structure as compared to the background is less than 5%, with the background itself being of the order $\sim 5\times 10^{-3}$ meV^{-1}. The order of magnitudes involved in observation of such effects again documents the necessity of measurements at lowest attainable temperatures and modulations to avoid thermal and instrumentational smearing. The calculated relaxation times for the junction 877A agree well with the relaxation times for samples without the additional structures.

The set of unexpected peaks in $\frac{1}{\sigma_o}\frac{d\sigma}{dV}$ prompted an investigation as to their physical origin and resulted

Fig. 5.1

Illustration of a junction having weak additional structure in the derivative of the conductance.

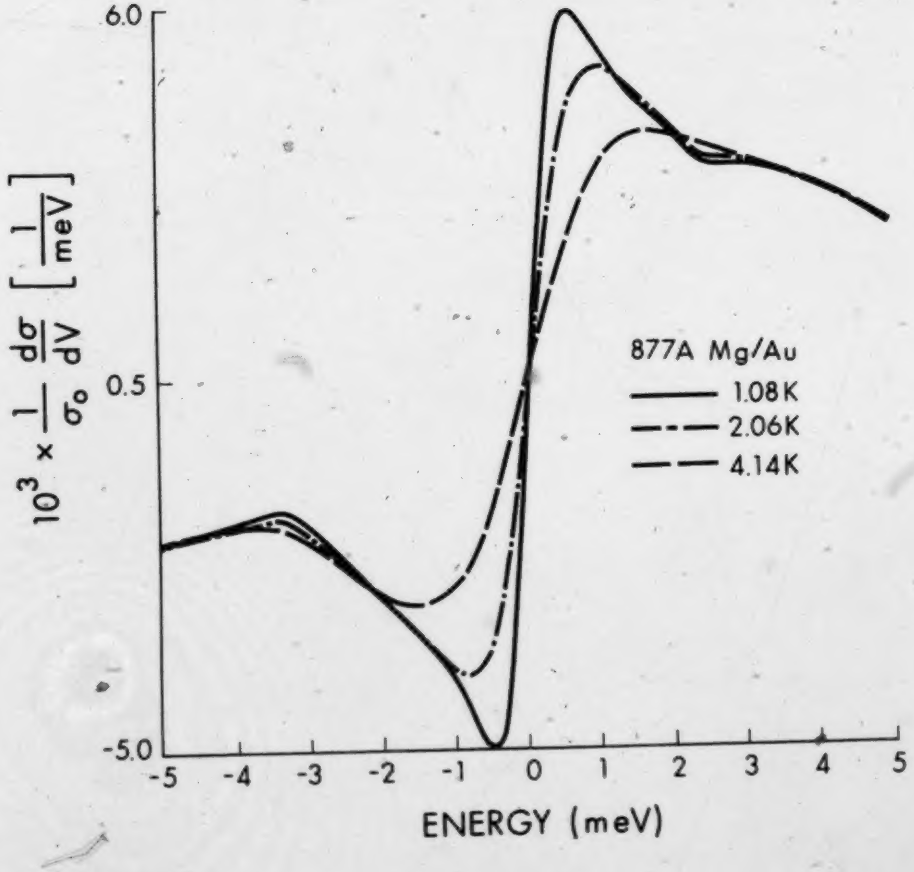
6.0
0.5
-5.0
$10^3 \times \frac{1}{\sigma_o} \frac{d\sigma}{dV} \left[\frac{1}{meV}\right]$
-5
-4
-3
-2
-1
0
1
2
3
4
5
ENERGY (meV)
877A Mg/Au
1.08K
2.06K
4.14K

in the present chapter. To substantiate our possible explanation of the observed effect we find it appropriate to present first the results of the experiments on junctions showing the new oscillatory structure.

5.2 Experimental investigations of oscillations

The occurrence of the new structure was not restricted to junctions of Mg/Au type. In fact, we have observed the additional peaks in $\frac{d\sigma}{dV}$ in Mg/oxide/Mg and Mg/oxide/Pb junctions. In fig. 5.2 we present a $\frac{d\sigma}{dV}$ characteristics for Mg/oxide/Mg junction with peaks which are better resolved and are more numerous in the same voltage range as compared to fig. 5.1. The corresponding conductance curve is shown on the next fig. 5.3 with noticeable changes in its shape close to $\frac{d\sigma}{dV}$ peak positions. It is interesting to note that in one of our earlier measurements on Mg/oxide/Pb junctions we have seen a structure similar to the presently investigated one which at the time of measurement were considered to be due to the noise in the junction.

The appearance of a structure in Mg/Au and Mg/Pb junctions gave rise to a suspicion that it is connected either with the Mg electrode or with its insulating oxide. In view of this fact, we have decided to investigate the

Fig. 5.2

Conductance vs energy for a Mg/Mg junction having oscillations.

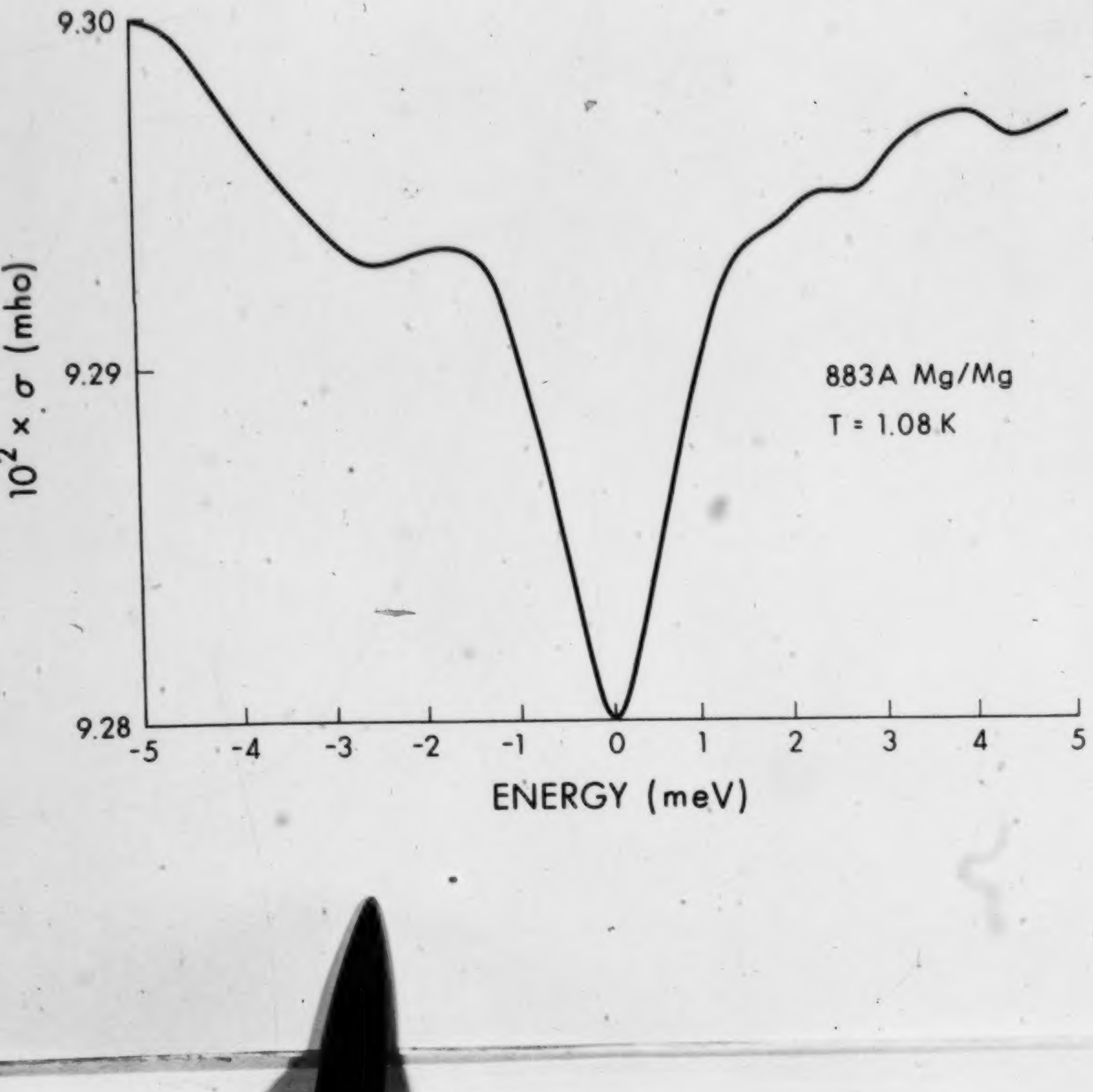

9.30
9.29
9.28
$10^2 \times \sigma$ (mho)
-5
-4
-3
-2
-1
0
1
2
3
4
5
ENERGY (meV)
883A Mg/Mg
T = 1.08 K

Fig. 5.3

Derivative of the conductance for a Mg/Mg having oscillations

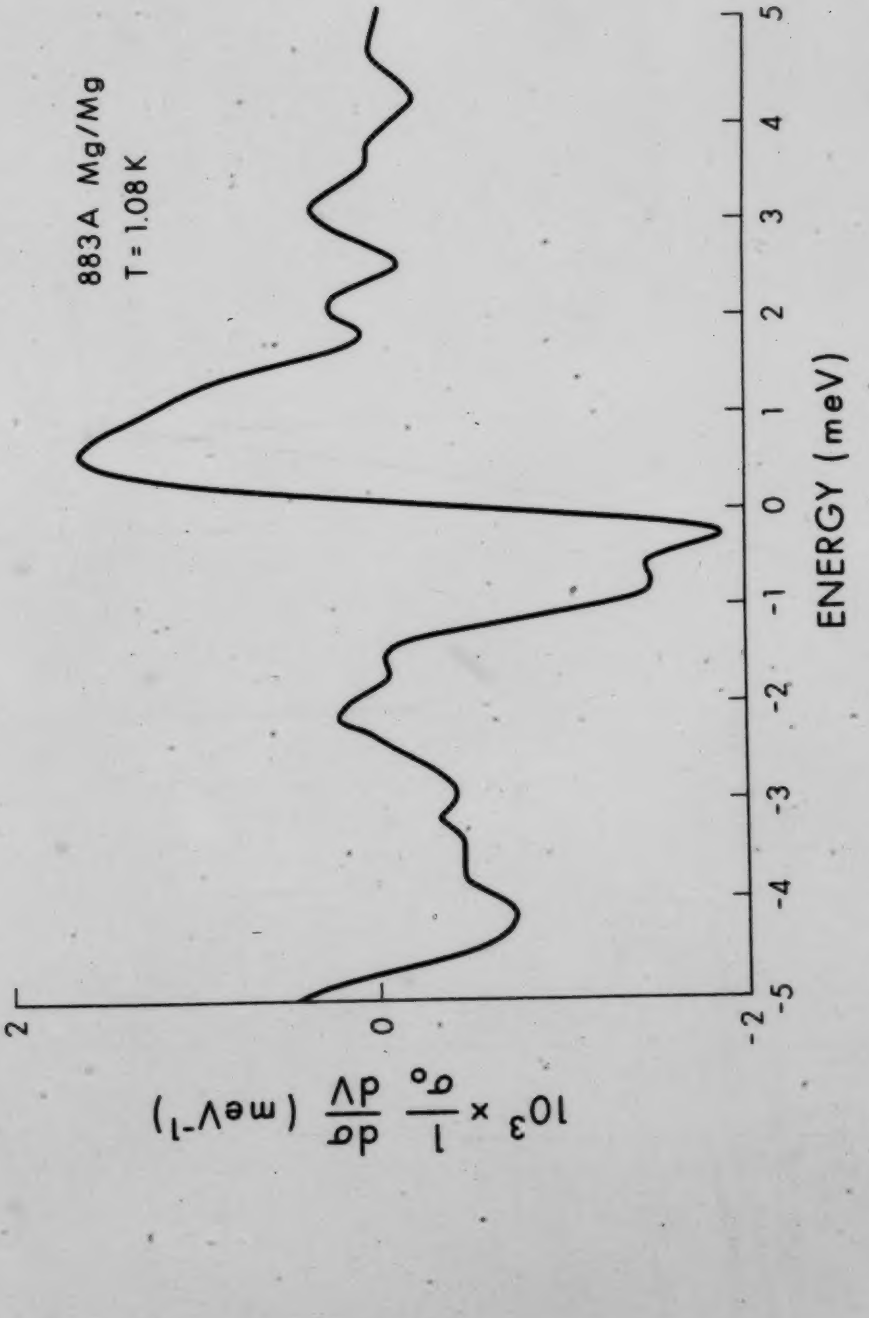
883 A Mg/Mg
T = 1.08 K
ENERGY (meV)
-5
-4
-3
-2
-1
0
1
2
3
4
5
$10^3 \times \frac{1}{\sigma_o} \frac{d\sigma}{dV}$ (meV^{-1})
2
0
-2

new effect on Mg/Au junctions since the likelihood of their successful preparation proved to be the greatest. We have accepted the observation of phonon emission either in Mg electrode (Adler, 1969) or in MgO (when applicable) (Adler, 1969) as a sufficient proof that the measured current was due to tunneling. Since the peaks in $d\sigma/dV$ tend to have an oscillatory character, we shall henceforth refer to them as "oscillations".

The existence of oscillations in tunnel junctions was independent of the techniques of sample preparation as described in Chapter 3, and the occurrence of the additional structure even in junctions prepared under identical experimental conditions was unpredictable. We have considered the thickness of the electrodes, junction area, the chemical composition of the barriers, evaporation rates, glow discharge currents, oxidation (nitrification) times and pressures as variables which could have influenced the final properties of the tunnel junctions. The magnesium film thickness ranged between 700-30000 Å with the gold counterelectrode of 600-3000 Å and junction areas of .01-.05 mm^2. The evaporation rates varied from 10 Å/sec to 1000 Å/sec at pressures of 2×10^{-6} atm. The combined effects of the glow discharge current, oxidation (nitrification) time and pressure are reflected on the tunnel junction resistance which in our samples ranged between 15-8000 Ω at He^4 temperatures. The decision to make junctions with nitride barriers was taken with a hope of altering the barrier composition and thus possibly changing the physical properties of the metal-barrier interface which we thought to be responsible for the appearance of the oscillations.

In fig. 5.4 to fig. 5.12 we present some typical characteristics we have obtained while measuring the properties of Mg/Au junctions having magnesium oxide or nitride as their insulating barriers.

To illustrate the effect of the temperature smearing, we show $\frac{1}{\sigma_o}\frac{d\sigma}{dV}$ measured at 1 K and 4 K for a junction with weak oscillations (fig. 5.4). First we notice a decrease in the blocking effect due to the elevated temperature with a continuous smearing of the resolved peaks (at 1 K) into the smooth and wide background curve at 4 K. The slight overshooting of the 1 K curve at -5 meV with respect to the background is due to the oscillatory peak at -3.6 meV. The total variation of the conductivity between 0 - 5 meV at 1 K, represents only 4 parts in 10^5.

The most drastic oscillatory behaviour was observed in 875B Mg/oxide/Au. The 4 K curve (fig. 5.5)

Fig. 5.4

Illustration of the effect of the temperature on the size of the oscillations in $\frac{1}{\sigma_o} \frac{d\sigma}{dV}$.

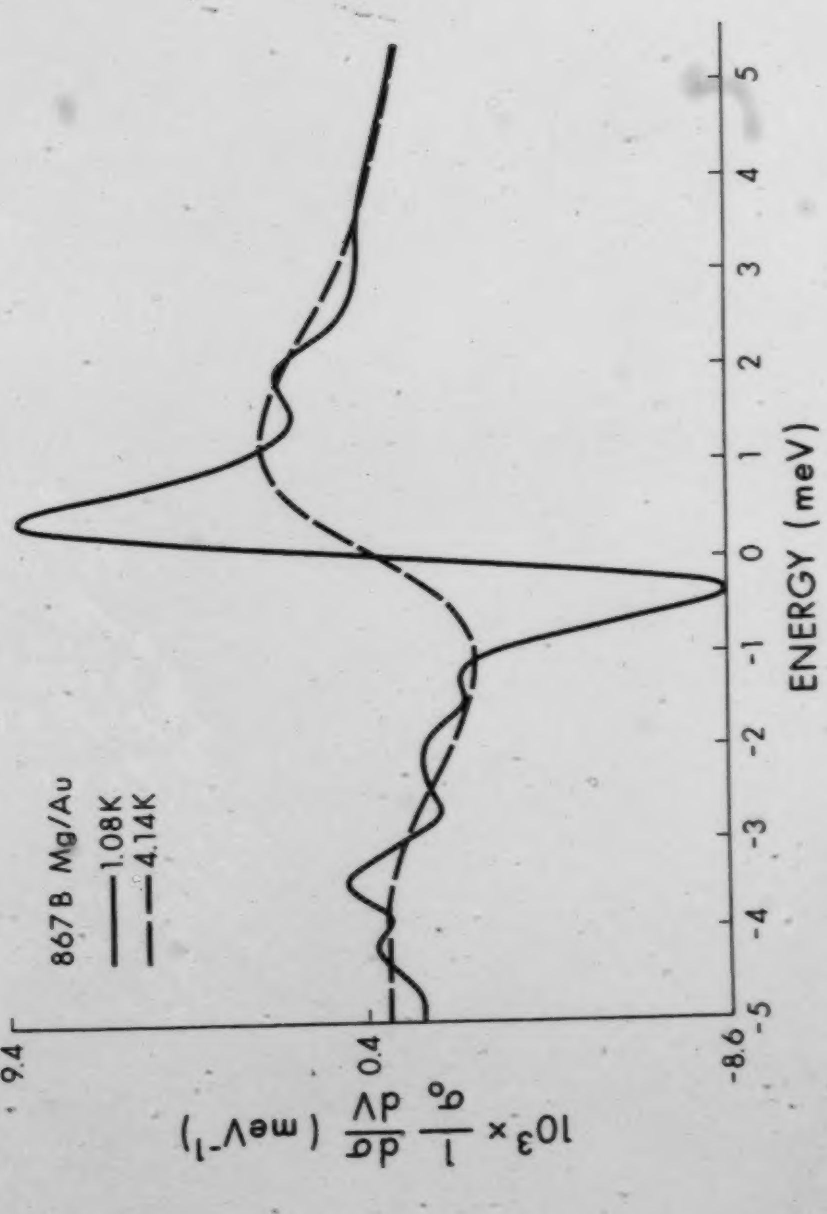
867 B Mg/Au
1.08K
4.14K
$10^3 \times \frac{1}{g_0}\frac{dg}{dV}$ (meV^{-1})
9.4
0.4
-8.6
-5
-4
-3
-2
-1
0
1
2
3
4
5
ENERGY (meV)

Fig. 5.5

Illustration of a junction having well resolved oscillatory peaks in the conductance. The effect of the temperature smearing is shown as well.

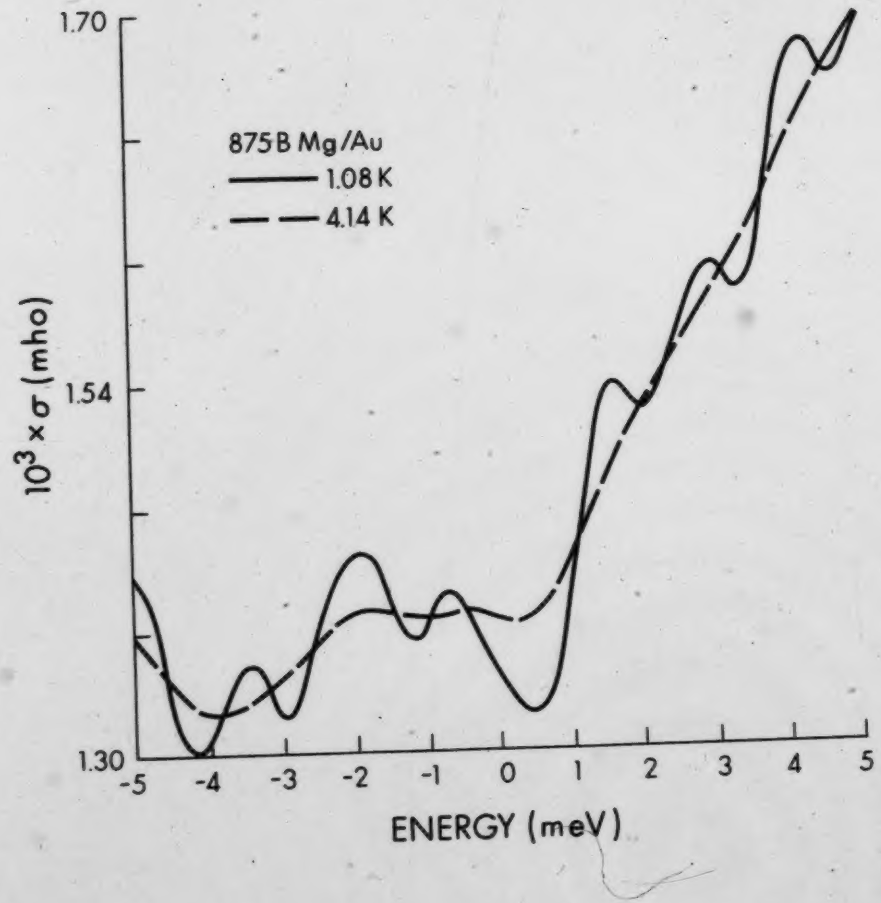
875B Mg/Au
1.08 K
4.14 K
1.70
1.54
1.30
$10^3 \times \sigma$ (mho)
-5
-4
-3
-2
-1
0
1
2
3
4
5
ENERGY (meV)

Fig. 5.6

The conductance resp. derivative of the conductance vs energy for 875B Mg/Au measured to ±25 meV. The arrows indicate the expected phonon emission threshold.

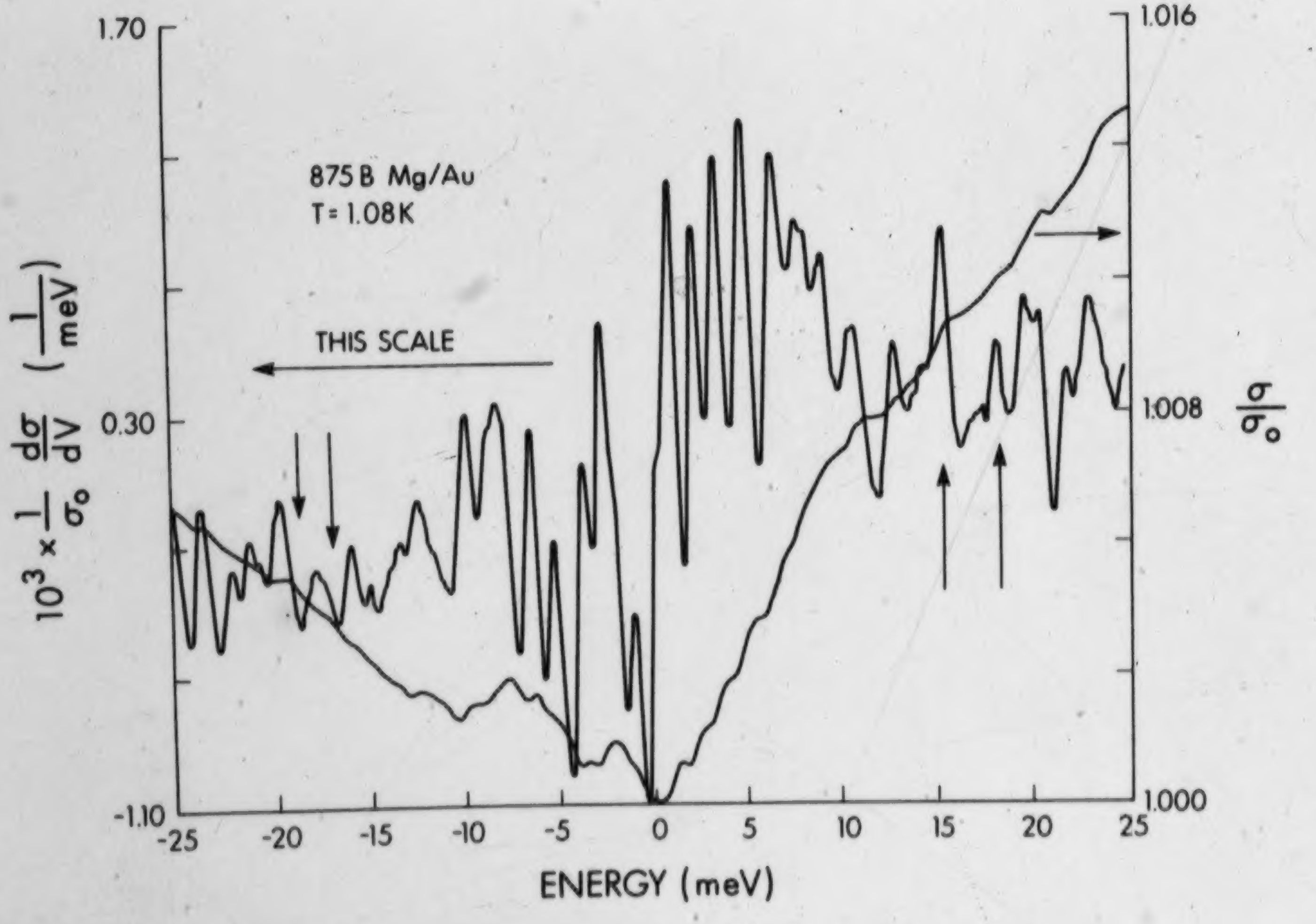
875 B Mg/Au
T= 1.08K
THIS SCALE
1.70
0.30
-1.10
$10^3 \times \frac{1}{\sigma_o}\frac{d\sigma}{dV}$ $\left(\frac{1}{meV}\right)$
1.016
1.008
1.000
$\frac{\sigma}{\sigma_o}$
-25
-20
-15
-10
-5
0
5
10
15
20
25
ENERGY (meV)

again passes smoothly through the oscillations which are strongly pronounced at the lowest temperature. In contrast to the previously seen kinks in fig. 5.3 the conductivity curve now displays a set of humps almost equally spaced. The asymmetric offset at zero bias is probably due to the oscillatory background. The regularly well resolved oscillations persisted to almost ±10 meV beyond which they started to diminish in size (fig. 5.6). The arrows indicate the expected phonon emission threshold in Mg. For the positive applied bias the conductivity curve has a series of steplike increases which are almost smeared into the structureless background beyond 10 meV. Since the slope of the curve is smaller on the negative side the structure still retained its humplike behaviour as seen previously in fig. 5.3.

Finally, for an illustration we present a junction having a nitride as its barrier showing oscillations in ±25 meV region. The 4.2 K curve is again superimposed to show the effect of the temperature smearing (figs. 5.7, 5.8).

An important result which contributed to a possible explanation of the tunneling curves was obtained by an adsorption of hydrocarbon molecules inside the insulating layer during the barrier formation. Junctions

Fig. 5.7

Illustration of the oscillations in a $Mg/N_2/Au$ junction measured to ±25 meV. The arrows indicate the expected phonon emission threshold.

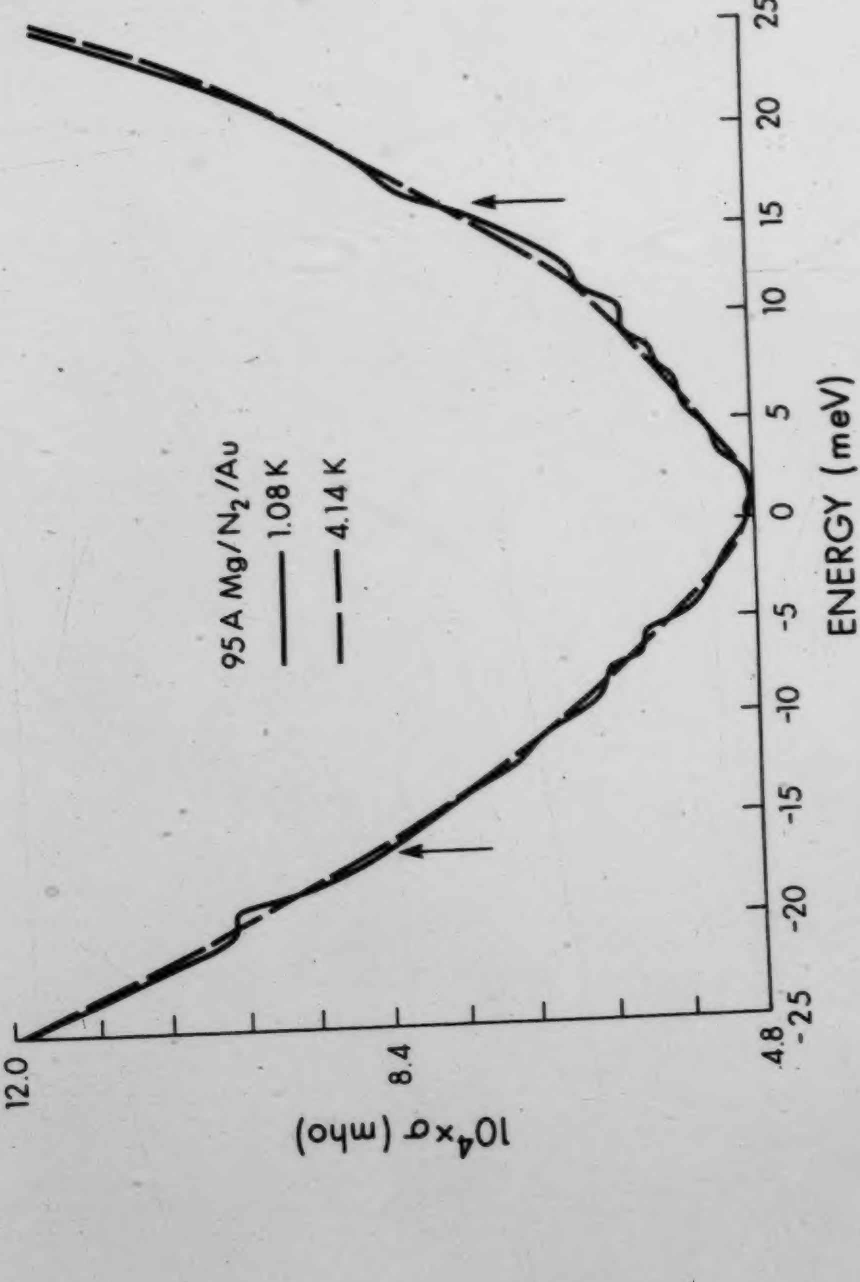
95 A Mg/N_2/Au
1.08 K
4.14 K
ENERGY (meV)
-25
-20
-15
-10
-5
0
5
10
15
20
25
12.0
8.4
4.8
$10^4 \times \sigma$ (mho)

Fig. 5.8

Derivative of the conductance vs energy for a $Mg/N_2/Au$ junction.

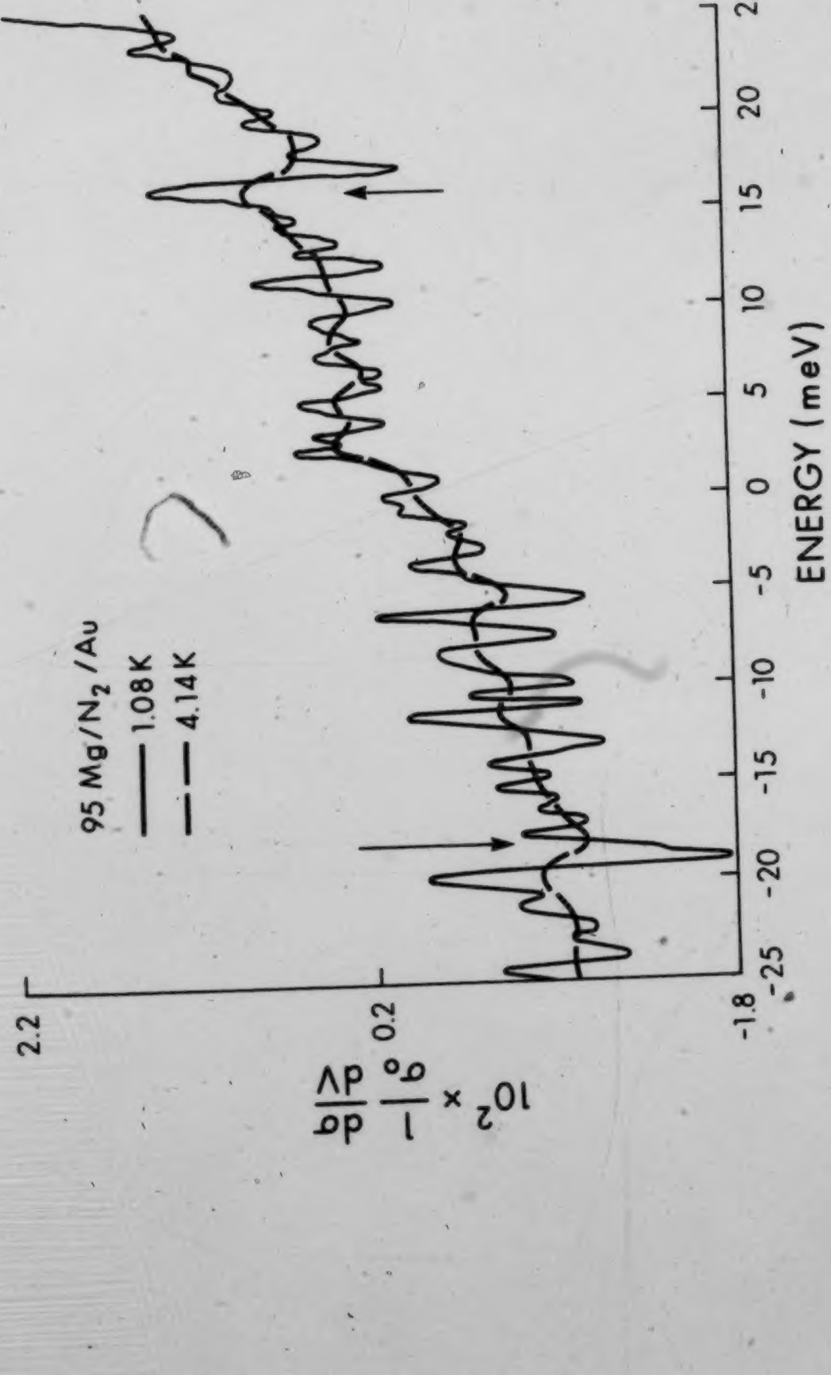
95 Mg/N$_2$ /Au
1.08 K
4.14 K
2.2
0.2
-1.8
$10^2 \times \frac{1}{g_0} \frac{dg}{dV}$
-25
-20
-15
-10
-5
0
5
10
15
20
25
ENERGY (meV)

so prepared were subjected to oil vapours during oxidation (nitrification) by passing the oxygen (nitrogen) gas through a flask containing light machine oil heated close to its boiling point. The presence of adsorbed molecules of hydrocarbons inside the barrier drastically affected the tunneling barrier with respect to the occurrence of the oscillations. In all junctions of this type no additional structure superimposed on the background curve was seen.

The verification of the oil adsorption was performed by an observation of the inelastic spectrum of the junction at bias range where previously reported (Jacklevic and Lambe, 1968) hydrocarbon peaks were located.

To gain further insight into the nature of the oscillations we have tried to alter the properties of the junctions by an application of external perturbations such as annealing the junctions to room temperatures, applying voltages up to 1000 meV across the junctions and polarizing the interface by passing DC currents along its adjoining electrode. We hoped that by correlating the newly obtained results with characteristics measured before the application of the external influences we could extract additional information which would help to interprete our data. Such an effort proved to be quite fruitful as it will be seen on the following figures.

Junction 080B when measured after an initial cooldown to 1 K had oscillations in its characteristics. These, however, disappeared upon annealing the junction to room temperature while still keeping it in a vacuum (figs.5.9-5.10). The annealing produced a 36% decrease in junction resistance, while the change in resistance over the spanned voltage region approximately remained the same (1.93% and 2.02%). The sharper conductivity increase around zero bias reflects the tail of the first smeared oscillation. In contrast to this result, an application of 700 meV (Mg positive) across another junction for 1 hour produced a stronger structure which in the earlier measurement was weakly visible (fig. 5.11). Besides the better resolved structure, there is a slight shift in peak positions (fig. (5.12). The relative change of the conductance at zero bias $(\sigma_{4.2}(0) - \sigma_{1.1}(0))/\sigma_{1.1}(0) = 0.0145$ due to zero bias anomaly in both cases remained the same implying that the boundary and impurity scattering mechanisms which helped to deblock the tunneling electrons in the metal electrodes were not altered. Thus only a change in electron transition rate $1/\tau_B$ is responsible for the change in the junction resistance (from 210.97Ω to 201.86 at 1 K).

Similar results were obtained by passing a DC current along the bottom (Mg) or top (Au) electrode.

Fig. 5.9

Comparison of the conductance curves for 080B Mg/Au before and after annealing.

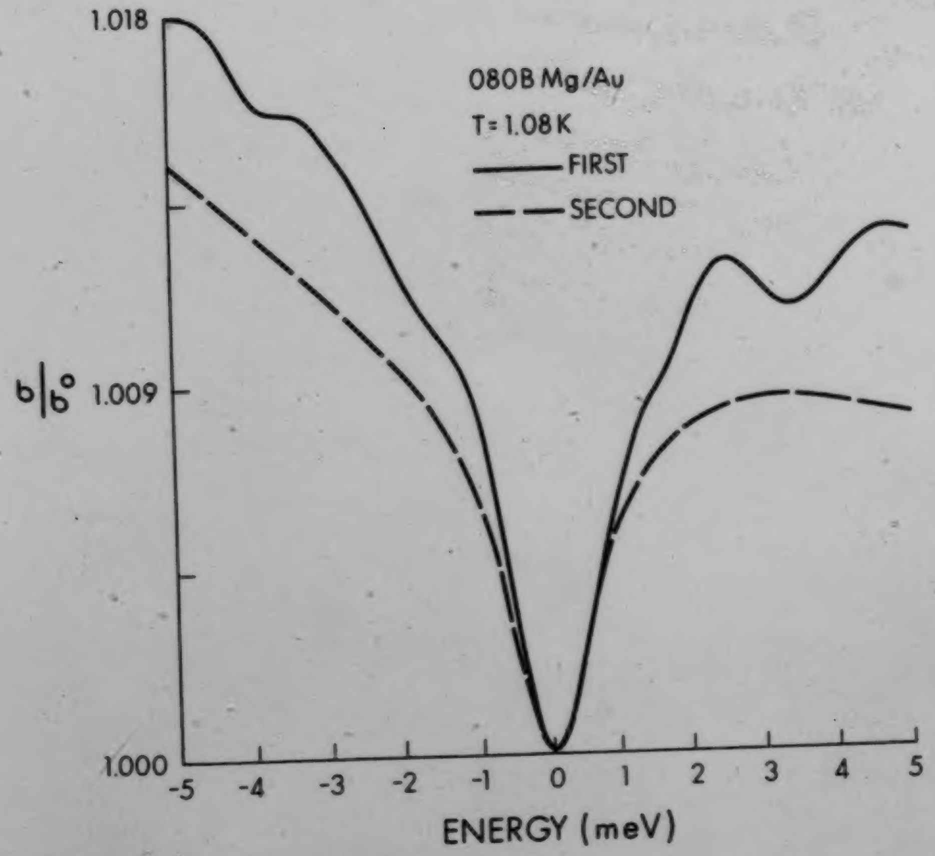
1.018
1.009
1.000
b|b°
080B Mg/Au
T= 1.08 K
FIRST
SECOND
-5
-4
-3
-2
-1
0
1
2
3
4
5
ENERGY (meV)

Fig. 5.10

Comparison of the derivative of conductance curves for 080B Mg/Au before and after annealing.

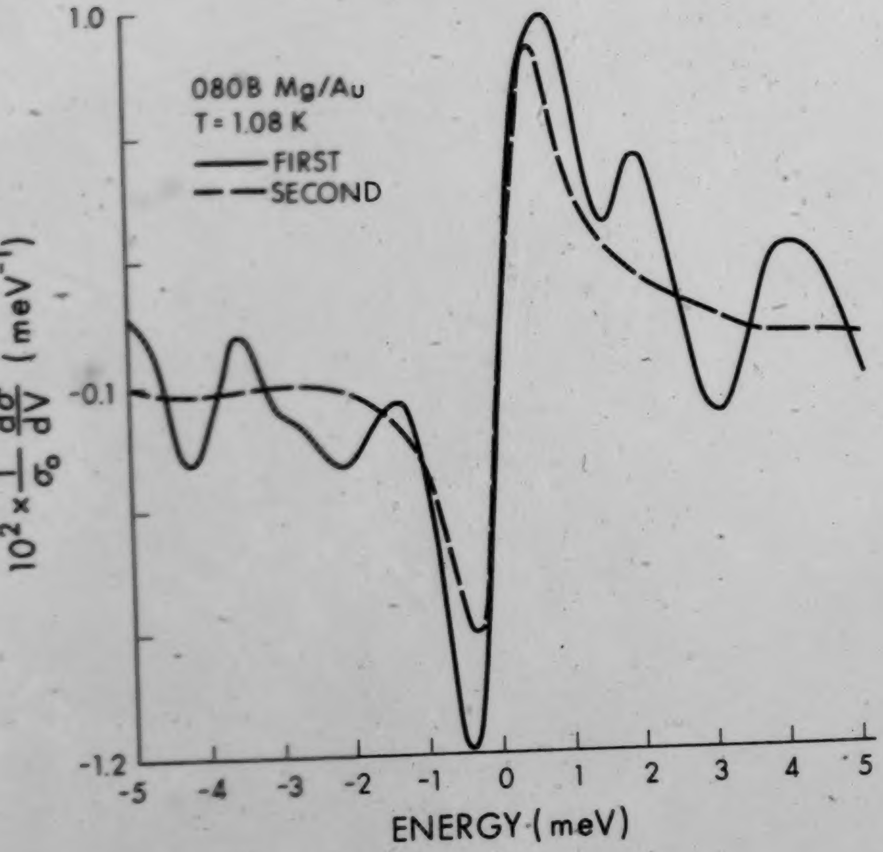
1.0
-0.1
-1.2
080B Mg/Au
T = 1.08 K
FIRST
SECOND
$10^2 \times \frac{1}{\sigma_0}\frac{d\sigma}{dV}$ (meV^{-1})
-5
-4
-3
-2
-1
0
1
2
3
4
5
ENERGY (meV)

Fig. 5.11

Comparison of the conductance curves for J107B Mg/N_2/Au before and after applying high bias across the junction.

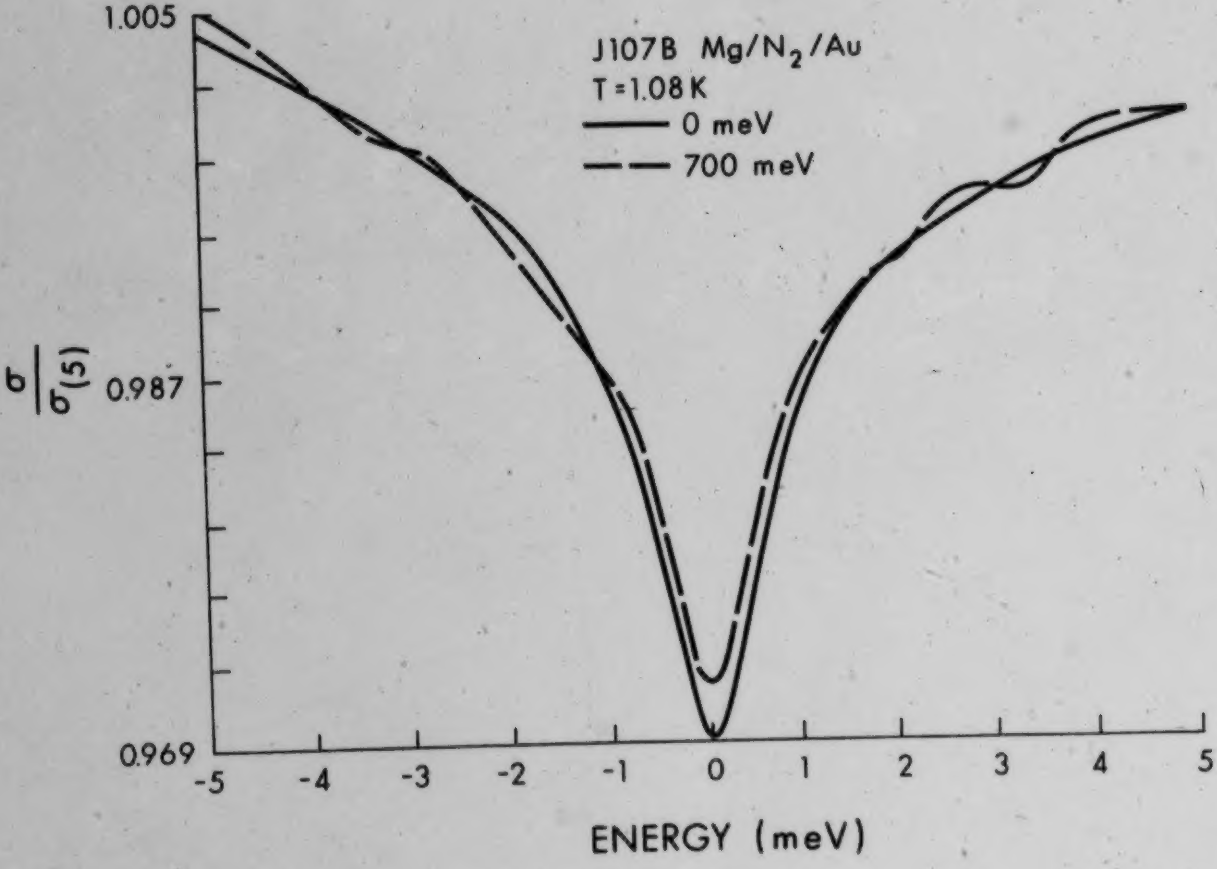
J107B Mg/N_2/Au
T=1.08 K
0 meV
700 meV
$\frac{\sigma}{\sigma(5)}$
1.005
0.987
0.969
-5
-4
-3
-2
-1
0
1
2
3
4
5
ENERGY (meV)

Fig. 5.12

Comparison of the derivative of the conductance curves for J107B Mg/N_2/Au before and after applying high bias across the junction.

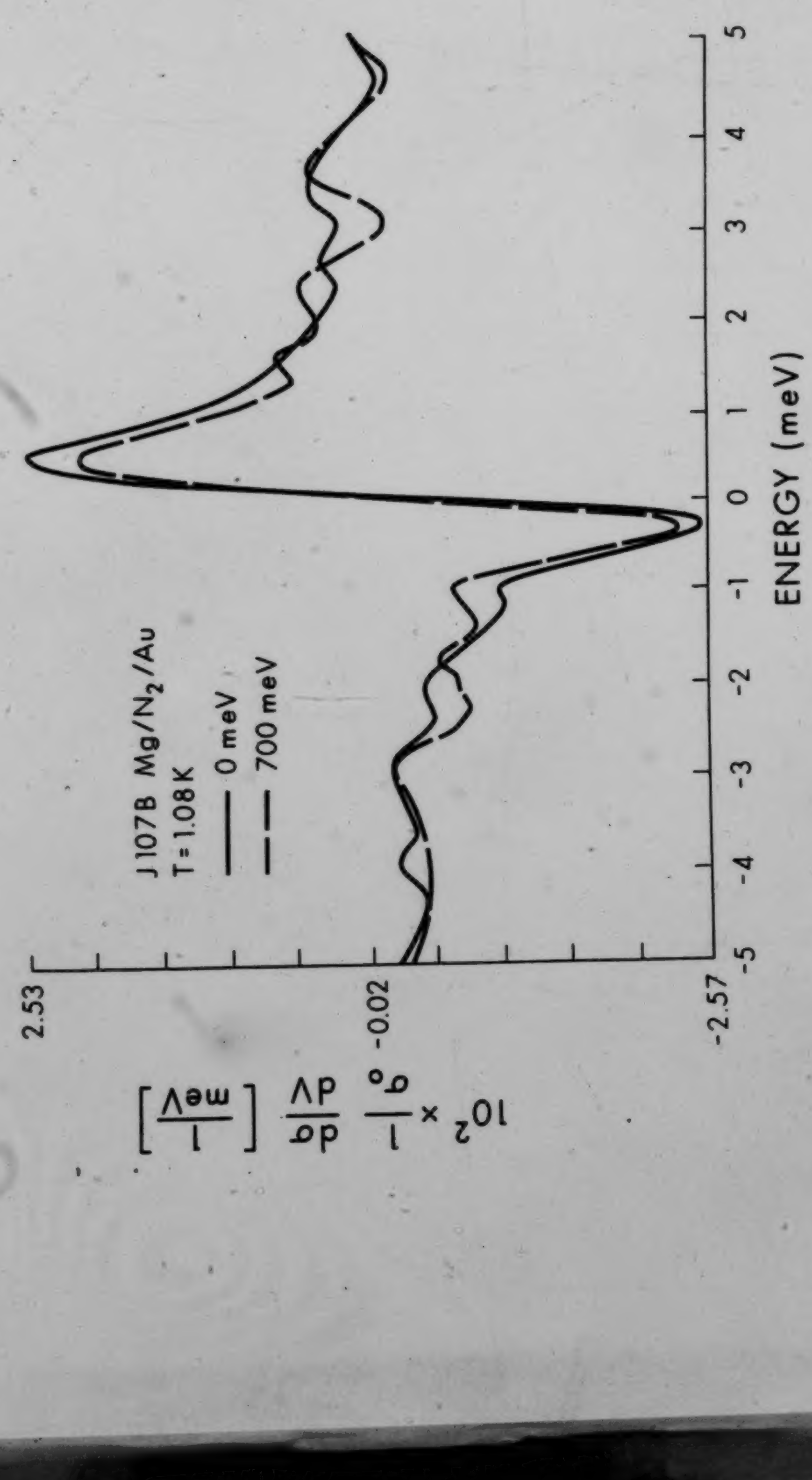
J107B Mg/N_2/Au
T=1.08K
0 meV
700 meV
$10^2 \times \frac{1}{g_0} \frac{dg}{dV} \left[\frac{1}{meV}\right]$
2.53
-0.02
-2.57
-5
-4
-3
-2
-1
0
1
2
3
4
5
ENERGY (meV)

With increasing currents the resistance of the junctions continuously increased. We interprete this as being due to the burning of thin edges across the junction area (Adler, Kreuzer, 1972). Simultaneously with this effect we have seen a change in the oscillation pattern of the junctions.

The information revealed from the above quoted results represents the main line along which the analysis and the interpretation of the data will be performed. In the next section we shall consider this and suggest a physical model which can explain the appearance of the new structure.

5.3 Analysis of the experimental data

Through the results of the experimental investigations on Mg/Au and Mg/Mg junctions a new electron transfer mechanism was established which enhanced the conductivity of the tunnel junctions. The existence of the associated structure was found to be independent of the thickness of the electrodes and of the barrier. The most probable bias region of the occurrence of the structure was found to be within 25 meV of the zero bias. In some junctions, however, the oscillations persisted up to ±100 meV. Since the amplitudes of the oscillations rapidly decreased with increasing temperatures the measurements had to be done at the lowest attainable temperatures.

The appearance of oscillations in $d\sigma/dV$ with an apparent periodicity of 0.8-2.7 meV led to an early speculation that the observed effect was due to resonances associated with the presence of the electron standing waves in Mg (Jacklevic et al, 1972). According to Jacklevic et al, the experimental observation of the box quantization requires a preparation of films with a very high purity and smoothness. This limited the thickness of Mg films in their experiments to 150 Å - 500 Å. To promote smoothness, the films had to be deposited onto substrates cooled to -100°C - 150°C, with a subsequent warmup to room temperature to achieve recrystallization. In contrast to this procedure our Mg films, 700 Å - 30000 Å thick, were evaporated onto substrates held at room temperature. We would then expect that the stringent conditions imposed on the observation of the standing waves were not reached. Furthermore, correlation between the thickness of the film and the peak separations in $d\sigma/dV$ has not been successful. For instance, film thicknesses of 25000 Å - 30000 Å are needed in order to resolve oscillations with a periodicity of ∿1 meV. This thickness range is well above the thickness of the Mg film in junction 875 (700 Å), in which the oscillations were the most pronounced from all our samples. These considerations then point to a conclusion that the structure in our junctions could not be connected with Jacklevic type resonances.

In order to gain further insight into the nature of oscillations, the tunnel junctions were subjected to the influence of external perturbations. As indicated in the last section, a thermal cycling, an application of high biases across the junction or a flow of a DC current along the electrodes produced irreversible changes in the junctions which resulted in the new tunneling characteristics. These could be repeatedly traced over, unless a new perturbation was reapplied. We have to mention, though, that the aging effects in thin films associated with the thermal cycling often led to a destruction of the tunnel junction. The same was true of the applied DC bias, resulting in the dielectric breakdown of the insulator. Nevertheless, we feel that the measurements performed on different samples revealed enough information for their mutual intercomparison.

We attribute the changes in the tunnel junctions as being due to modifications of the tunneling layer or of the interface. We further assume that the structure of the metal electrodes has not been altered. This is supported by an observation that the relative size of the conductance anomaly between 1 K and 4 K did not change, even though the oscillatory pattern in the tunnel characteristics did so. The new tunneling curves may either reflect a change in the barrier profile arising from the additional growth of the insulating layer (Pollack, Morris, 1964) with a simultaneous change in the tunneling path or result from the spatial redistribution of impurities inside the barrier. Due to the exponential dependence of the transmission probability on the thickness and height of the barrier the first two effects merely alter the magnitude of the tunneling current which in turn determines the structureless background (Simmons, 1963; Stratton, 1962).

A considerable variation in the detailed behaviour of the junctions even for samples prepared under identical condition suggests that the structure is connected with the impurity content of the insulating layer. Clearly, the inelastic impurity assisted tunneling (Jacklevic, Lambe, 1968) associated with the vibronic excitation of the impurity has to be excluded. This follows since it is not expected that the inelastic conductivity enhancement threshold could be changed by annealing or by an applied DC bias (Geiger et al, 1969). The presence of an impurity inside the tunneling layer, however, often leads to a possibility of a resonant-two step tunneling process. This will happen if the impurity provides an attractive potential which may have a bound state within the barrier (Giaver-Zeller, 1968; Parker, Mead, 1969; Gadzuk, 1970; Duke, 1972). Then under favourable conditions a new tunneling channel can open up, in which the tunneling electron goes from the metal to the adsorbed impurity where it is partially localized and then tunnels through the reduced barrier into the second electrode. The degree of electron localization is very important in distinguishing between two possible processes. An impurity state with a deep and narrow attractive potential can lead to a capture of the tunneling electron with a characteristic lifetime longer than the barrier tunneling time.

A subsequent decay of the bound state with the transmission of the electron into the second electrode is essentially equivalent to Giaver-Zeller tunneling. A uniform distribution of bound state energies then leads to a large temperature dependent resistance peak. In contrast,the effect on the impurity potential on the tunneling electron can be such that it will allow only for a resonant buildup of the electron wave function in the potential well with localization times shorter than the tunneling times. This will lead to an increase in the electron probability amplitude inside the forbidden region, resulting in a greatly enhanced barrier transmission coefficient. We believe that this type of the electron resonant transmission is responsible for the structure resolved in our tunnel characteristics. It is then appropriate to consider a model which explicitly shows how such resonances can affect the conductivity of the tunnel junctions.

5.4 Resonant tunneling through impurity states

For simplification let us consider a tunneling process in which the insulating layer contains only one impurity, having an allowed energy level of a magnitude eV_o, inside the barrier. For further simplification let us assume that the metal electrodes are at 0 K and that the barrier potential can be represented by its average value Φ (fig. 5.13a). As the bias is established between the two electrodes the Fermi levels separate and the impurity level shifts linearly with the electric field. Past the threshold voltage

$$V = |V_o| + V \cdot \frac{r}{\ell}$$

(where r is the position of the impurity, ℓ, thickness of the barrier) the impurity lies above the Fermi level of the right hand electrode. In this case a new tunneling channel opens up in which electrons can tunnel from

Fig. 5.13

Schematic potential for a junction having a single impurity in the middle of the barrier:

a) no applied voltage

b) sufficient applied voltage so that the resonance channel is opened.

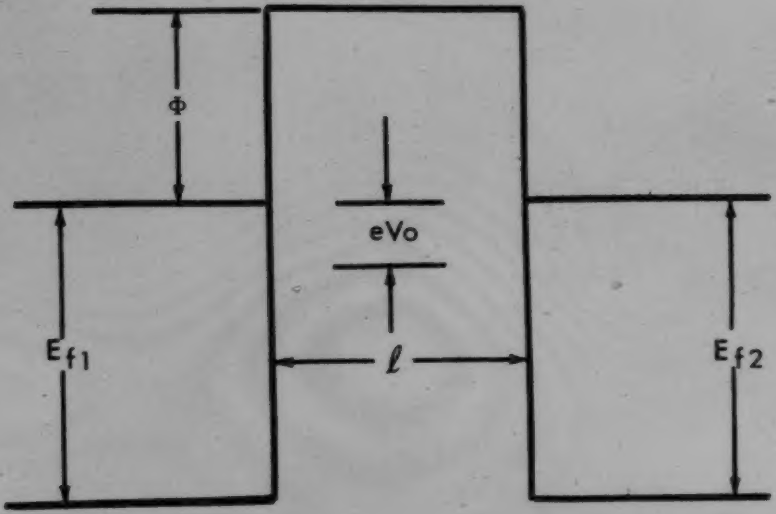
Φ
eVo
ℓ
E f1
E f2

a

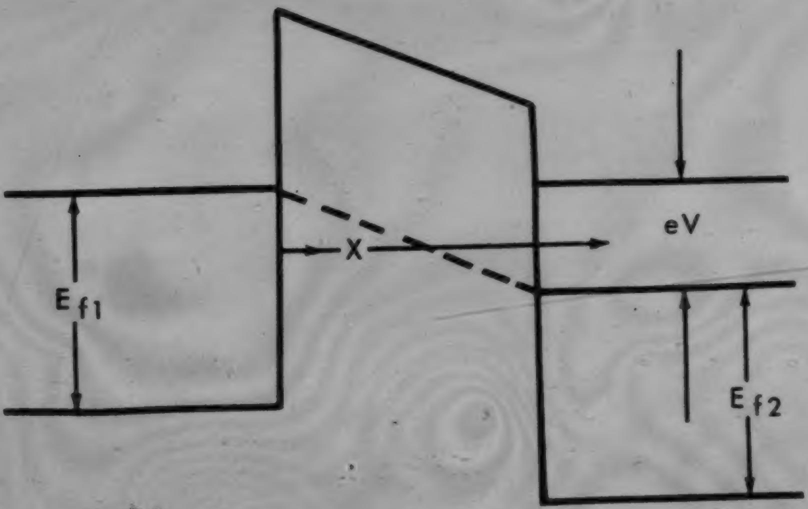

b

left to the impurity and then from the impurity to the right (fig.5.13b).

Let us consider what happens to the wave function of an electron with energy equivalent to the trapping level. The incoming wave after penetration decays exponentially inside the barrier. As it approaches the trap it resonates with a large amplitude inside the potential well. After a partial localization it decays again exponentially towards the other side of the barrier. By moving the potential well to the middle of the barrier the amplitude of the incoming wave can be made equal to that of the outgoing wave (Bohm, 1964). For electron energies different from the resonance level the wave function decays exponentially in the usual way while passing through the barrier.

Gadzuk's (Gadzuk, 1970) treatment of the described model gives the following expression for the ratio of conductivities with and without the trapping center:

$$\frac{\sigma_R}{\sigma_N} = \frac{N_i A_i}{A_s} \cdot \frac{1}{2} \exp(\ell \sqrt{\frac{2m}{\hbar^2}} \Phi^{\frac{1}{2}}) \cdot \theta(|V| - 2|V_o|) \qquad (5.1)$$

where it was assumed that the resonance occurs in the low voltage region ($eV << \Phi$) and that the impurity lies in the mid-plane of the barrier. N_i represents the number of impurities with an effective cross section A_i. A_s gives the junction area. $\theta(x)$ is a usual step function. Setting $N_iA_i/A_s = 1$, $\Phi = 1$ eV, $\ell = 30$ Å the ratio of σ_R/σ_o at the threshold of impurity assisted tunneling is $\sigma_R/\sigma_N = 2 \times 10^{16}$. However, in real situation this favourable ratio is reduced considerably by smallness of N_iA_i/A_s.

The calculation of the resonant conductivity with a single impurity is a great simplification of the tunneling problem. In practice the impurities are distributed over the whole volume of the insulating layer. It is then reasonable to expect that the resonance levels will be smeared out and the sharp conductivity increase will be further reduced. Gadzuk's calculation shows that the smearing effect indeed reduces the conductivity increase. Fig. 5.14a illustrates the ratio of the distributed impurity conductance to the clean junction as a function of applied voltage, treating the impurity level parametrically ($N_iA_i/A_s = 1$). Fig. 5.14b shows the effect of the barrier width on σ_R/σ_N. The broadening of σ_R/σ_N is due to the presence of a finite electric field in the barrier which shifts the bound state energy of an impurity by an amount of the order of the voltage drop at the corresponding impurity site. To avoid complete blurring of the resonance effect it is important that the impurity has an energy level close to the Fermi level and that it is located in a few

Fig. 5.14

The ratio of distributed impurity conductance to the clean junction conductance as a function of voltage:

a) impurity level treated parametrically

b) thickness of the barrier treated parametrically.

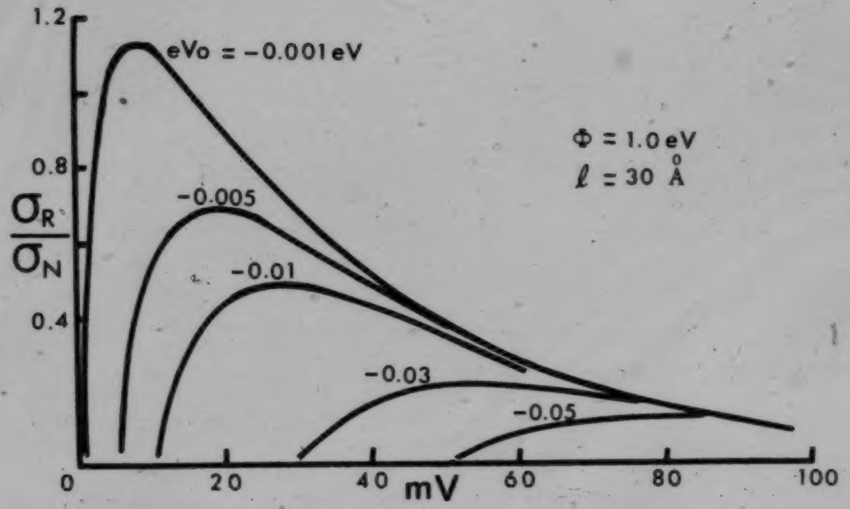
1.2
0.8
0.4
$\frac{\sigma_R}{\sigma_N}$
eVo = −0.001 eV
−0.005
−0.01
−0.03
−0.05
Φ = 1.0 eV
ℓ = 30 Å
0
20
40
60
80
100
mV

a

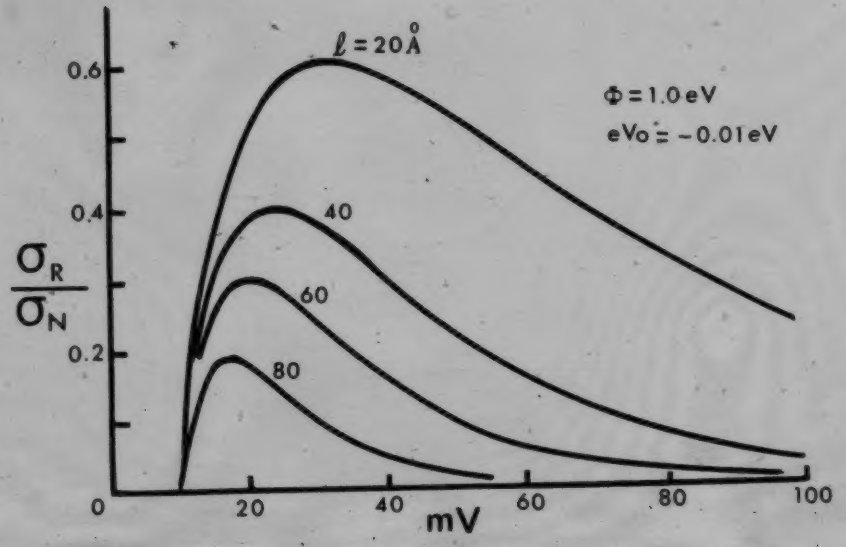
0.6
0.4
0.2
$\frac{\sigma_R}{\sigma_N}$
ℓ = 20 Å
40
60
80
Φ = 1.0 eV
eVo = −0.01 eV
0
20
40
60
80
100
mV

b

neighbouring atomic planes inside the barrier. Impurity clusters lying near the interface yield a contribution which is very asymmetric with respect to the applied bias. This follows because the shift of the energy level with the applied voltage is polarity dependent.

We should note that the presented treatment is one dimensional and assumes that the impurity has only one resonance level. In reality the attractive potential associated with the impurity can have more than one allowed level with a result that the tunneling characteristics will show a series of peaks which may or may not interact with each other to bring in additional smearing effect. A three dimensional treatment by Hurault (Hurault, 1971) of the resonant electron tunneling predicts that the transmission coefficient varies as a Lorentzian with the peak at the resonance energy level. The width of the Lorentzian is equal to the width of the virtual bound state

$$|T_R|^2 \sim \frac{\Gamma^2}{(E - E_R)^2 + \Gamma^2} \times |T_{imp}|^2$$

where E_R is the resonant level, Γ - width of the level and $|T_{imp}|^2$ is the resonance enhancement factor dependent on the position of the impurity and its concentration. A calculation by Combescot (Combescot, 1971) confirms Hurault's result.

5.5 Discussion

On the basis of the experimental evidence presented in section 5.3 we have concluded that the interaction between the tunneling electron and the trapped impurity is responsible for the appearance of the additional structure in our tunnel junctions. Schmidlin (Schmidlin, 1965) analyzed the effect of the trapping centers on the barrier profile and found that throughout a low voltage region a positive ion substantially reduces the barrier high in its locality At large biases the effect of the impurity is "smothered" out if the ion is close to the positive electrode. The local decrease of the barrier height around the impurity can then be instrumental in establishing a resonant transmission of electrons across the barrier via intermediate energy levels existing inside the barrier.

With these considerations, the changes produced in the general behaviour of the junctions by annealing or by applying a DC bias can readily be explained by allowing the charged impurities to migrate through the insulator. The change in the oscillatory pattern while a current was passed along the electrode is attributed to a redistribution of charges existing at the metal-insulator interface.

A convincing confirmation of the resonant impurity assisted tunneling arises from the observation of the behaviour of the localized energy levels under the influence of a magnetic field. In fig. 5.15 we show the second derivative curve of a previously shown junction (fig. 5.9) measured at 0 kG and 60 kG, with a field oriented parallel to the tunneling current. The characteristics were obtained after the junction was annealed at room temperature. Even though the oscillations when compared to the first measurement did not seem to exist, a 10 fold increase in sensitivity resolved the weak structure. The prominent feature of the 60 kG curve in fig. 5.15 is the appearance of two peaks at ∿5 meV as a result of the spin splitting of the previously degenerate atomic level (0 kG). The effective g factor obtained from the separation is g = 2.75. With the exception of the peak at ∿16 meV which is identified with inelastic phonon emission (Klein et al, 1973) the other peaks appear to be shifted or broadened under the influence of the magnetic field. A small energy difference in the separation of the peak at 5 meV suggests that the strength of the magnetic field was not sufficient to achieve complete spitting of the other atomic levels. Esaki et al (Esaki et al, 1968) reported a similar observation of localized energy levels in the forbidden gap of PbTe. Oscillations

Fig. 5.15

Illustration of the spin splitting of an impurity level.

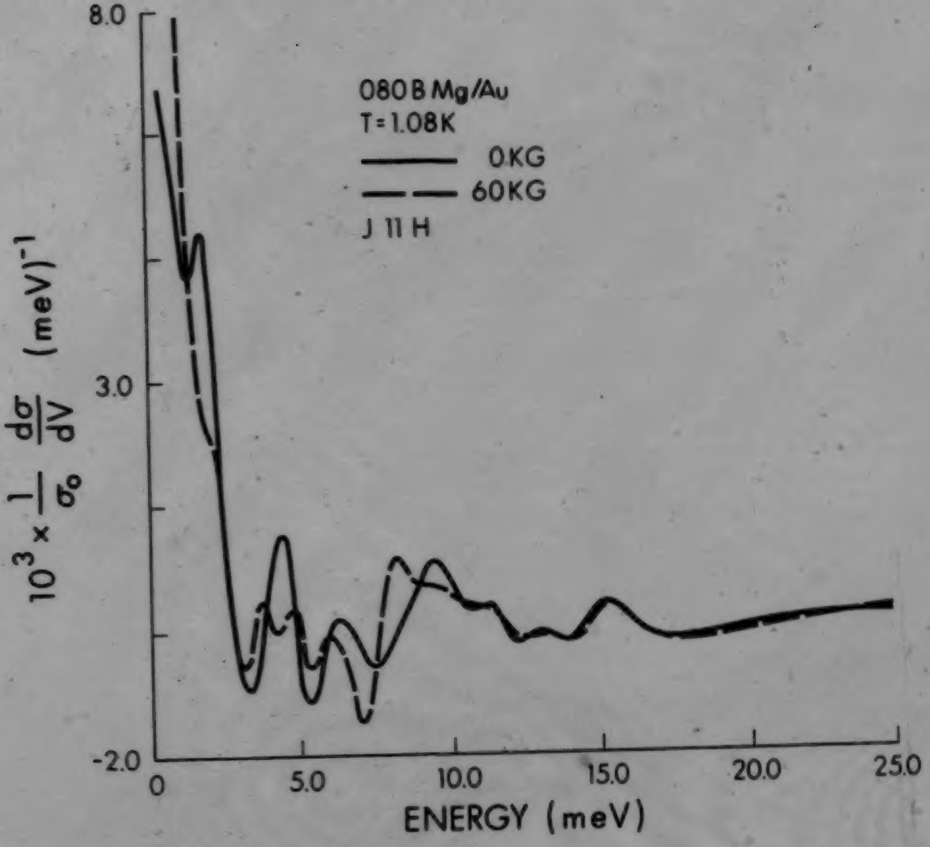
080B Mg/Au
T=1.08K
0KG
60KG
J 11 H
$10^3 \times \frac{1}{\sigma_o}\frac{d\sigma}{dV}$ (meV)$^{-1}$
8.0
3.0
-2.0
0
5.0
10.0
15.0
20.0
25.0
ENERGY (meV)

J

in the tunnel characteristics of Pb/O/Pb were reported as well (Yanson et al, 1971). These were directly correlated with the impurity contamination of the barrier by a layer of uracil. It was assumed that tunneling through localized energy levels was responsible for the occurrence of the oscillations.

The discussion in the preceding section shows that the effect of the impurities is most pronounced if they are distributed in a few atomic planes which are well separated within the depth of the insulator. The sharpness and the separation of the experimentally observed peaks then leads to a conclusion that the impurities do not interact strongly with each other. The lifetimes broadening of the atomic levels of the order of 1 meV gives an estimate on the localization time of an electron inside the potential well. The time on the order of 6×10^{-13} sec is comparable to the accepted magnitudes of the barrier transmission times (Gadzuk, Lucas, 1973; Thornber et al, 1967). Recall that we have "ab initio" required such a relationship. The bias region of the occurrence of the oscillations confirms the theoretical prediction that their observation is more likely if the intermediate energy levels are situated in the vicinity of the Fermi level.

Even though the origin of the impurities has not been established a few considerations may help to elucidate this question. The observation of a structure in Mg junctions irregardless of the top electrode and of the barrier leads to two possibilities or a combination of both. Into the first category we classify a contamination of the barrier (while it was grown) by foreign atoms. This includes the unavoidable adsorption of residual gases inside the vacuum system. Shen (Shen, 1968) suggested that various impurities (Al, Ni, Pt) can be introduced into the insulating layer if the glow discharge method is used for the barrier formation. The contamination was caused by materials sputtered from the electrodes. The Sn-Pb and Sn-Sn junctions showed several sharp, peaklike 1% structures in the conductance of the tunnel junctions which he identified with randomly distributed energy states in the barrier.

The second possibility leads to an assumption that the insulating barrier intrinsically contains trapping centers arising from its nonstoichiometric growth (Fisher-Giaver, 1961; Pollack, Morris, 1964; Esaki, et al, 1968; Sasaki, 1960). Stevenson and Hensley (Stevenson, Hensley, 1961) concluded that MgO tends to exist in the form of an n-type semiconductor. The donors responsible for this behaviour were similarly associated with the nonstoichiometric composition of the oxide. We suggest further experiments in which the procedure of sample preparation would be altered in order to eliminate the suspected reasons behind the contamination of junctions. We, similarly, leave open the answer for the disappearance of the oscillations with the oil doping of the junctions. We suggest either a binding of uncompensated Mg ions into complex organic molecules or a much simpler reason , arising from preventing the sputtering of materials from the discharge electrodes by formation of a thin layer of oil on the surface of the electrodes.

CHAPTER 6

TUNNELING INTO BISMUTH

6.1 Quantum size effect in Bi

There has been a considerable interest in Bi, both theoretical and experimental (Fal'kovskij,1968). Its interesting properties result largely from its carriers which are very light and few in number. The fermi level of the electrons is ∿25 meV (holes ∿ 11 meV) and the effective mass along some crystal direction is two or three orders of magnitude smaller than the free electron mass (Fal'kovskij,1968). Consequently the electronic de Broglie wavelength can be as large as 300 Å or 400 Å. In comparison the de Broglie wavelength in metals is on the order of the lattice period which is at the most a few Å. If the de Broglie wavelength of the conduction electrons becomes comparable to the physical dimensions of the sample, the electronic energy spectrum should become discrete (quantum size effect) with the separation between the energy levels being determined by the sample thickness (Tavger, Demikhovskij, 1969). The main features of size quantization can be derived from a model in which the electrons and the holes are regarded as independent particles moving in an infinite square well potential. The single particle wave function for a film of thickness L_z can then be written as

$$\psi n\, k_x k_y = \left(\frac{2}{L_z L_x L_y}\right)^{1/2} \sin \frac{n\pi z}{L_z}\,.$$

$$\cdot \exp(ik_x . x + ik_y . y) \qquad (6.1)$$

where $0 \le z \le L_z$, and the film has infinite dimensions in the y and z directions. The corresponding energy spectrum is

$$Enk_x k_y = n^2 E_o + \frac{\hbar^2 k_x^2}{2m_x} + \frac{\hbar^2 k_y^2}{2m_y} \qquad (6.2)$$

where

$$E_o = \frac{\hbar^2 \pi^2}{2m_z L_z^2}$$

$$n = 1,2,3,....$$

Thus while in a bulk crystal, the electron states are given by points which fill the Fermi sea quasi-continuously; in a thin film the Fermi surface breaks up into allowed subsheets parallel to k_x-k_y plane. Each subsheet corresponds to a discrete value of the wave vector along the quantized direction of the film (Garcia, et al, 1972). These consequences have been investigated with regard to electrical conductivity, optical properties, galvanomagnetic phenomena, paramagnetic susceptibility, superconductivity and tunneling phenomena (Tavger, Demikhovskij, 1969; Larson, 1971).

One of the possible methods of direct experimental observation of the quantization of the transverse motion energy in a film is the use of tunneling of the electrons in a sandwich made of the investigated films (Gogadze, Kulik, 1965; Kümmel, 1968). In the tunnel junction, the films of quasi-discrete energy spectrum are separated by a potential barrier. When an external field is turned on, the energy levels of one film shift relative to the levels of the other film. Assuming elastic transmission,the current through the barrier will arise whenever the populated levels of one film lie opposite the free levels of the other film. As a result, a current-voltage characteristic in the form of a series of peaks is obtained. The period of oscillations is approximately

$$\Delta E = \frac{\pi\hbar}{L_z}\sqrt{\frac{2E_f}{m^*}} \qquad (6.3)$$

where m* is the effective mass of the carrier. The upper bound on the amplitude of the oscillations is estimated to be

$$\frac{I^{osc}}{I_{non}} \leq \frac{\Delta E}{E_f} \qquad (6.4)$$

(Gogadze, Kulik, 1965). It is illustrative to estimate the order of magnitudes involved. In order that the oscillations would be observable let us require that

$$\frac{I^{osc}}{I_{non}} \sim 10^{-1} \quad .$$

This depending on the Fermi energy puts an upper limit on the thickness of the film. Table 6.1 illustrates the calculated values of the required thickness and correspondingly obtained periods of oscillations, ΔE.

Table 6.1

Thickness and periodicity of oscillations

Material	m*	E_f	Required thickness	Calculated ΔE
typical metal	m_o	1 eV	120 Å	98 meV
Bi electrons	10^{-2} m_o	25 meV	7400 Å	2.50 meV
Bi holes	0.7 m_o	15 meV	1140 Å	1.50 meV

m_o is the mass of the free electrons.

The thickness range in Bi is considerably relaxed because of the small Fermi levels and light masses of the carriers. Thus according to theoretical predictions it is possible to observe the QSE directly by tunneling. However, it is obvious that this favourable prediction is further minimized through thermal smearing and scattering of the carriers by impurities and diffuse boundaries. It is then necessary to keep the films sufficiently homogeneous and pure. Tunneling into single crystals or films containing large grains of well defined orientation therefore increases the likelihood of the observation of the QSE. The existence of quantized energy levels in thin metal films was well documented through ingenious interpretation of tunneling results of Jacklevic et al (Jacklevic et al, 1971). They have noticed that even though the required smoothness of the metal films is not experimentally feasible, certain energy levels (for instance at the band edge) are stationery with respect to thickness perturbations. These then are easily determined by tunneling experiments.

A direct observation of the quasi-discrete energy level spectrum by tunneling was claimed by Russian experimentalists(Korneev et al, 1970; Lutskii et al, 1966). Korneev et al have observed oscillations in Ag-Bi structures in which the electrodes were condensed onto two separate mica substrates and pressed together. The measurements were performed at nitrogen temperatures. The thickness of Bi films was greater than 1000 Å. Lutskii et al reported the observation of the QSE in structures in which the thickness of the Bi films ranged between 800-1300 Å. In both cases the steplike increases in the tunnel characteristics allowed a successful correlation with the thickness of the film.

The purpose of our experiments was to reproduce these results through tunneling experiments in systems containing Bi films in which the insulating layer was formed by a solid dielectric.

6.2 General considerations

The investigations were performed on Al/Bi, Mg/Bi, Bi/Bi and Bi/Pb junctions. They were prepared according to the procedure described earlier (section 3.2). The substrates usually were heated to 80°C by a resistive heater in order to promote formation of large grains in the evaporated film. Even though Bi films evaporated onto glass slides generally are polycrystalline, the trigonal axes of their grains are usually within 20% of the film normal (Komnik, Bukhstab, 1968). Condensation of Bi films onto heated mica creates larger crystallites, the trigonal axes of which are perpendicular to the substrate (Komnik, Pilipenko, 1971). Hauser and Testardi (Hauser, Testardi, 1968) reported similar observations. Electron microscope study showed that the lateral sizes of the microcrystals were on the order of 1500 Å - 3000 Å. The extent of grain formation was not very critical on the evaporation rate. The annealing of films during oxidation did not increase the grain sizes appreciably (20%-30%).

The thickness of Bi electrodes ranged between 1500 Å - 15000 Å. Films thinner than 1500 Å after oxidation had very high resistances (>5 kΩ). Junctions made of these in most cases were not stable and were easily destroyed by biasing them only to a few meV. The counterelectrodes of Al, Mg, Pb were approximately 1000 - 5000 Å thick.

The detection of an energy gap in Pb by tunneling gave us a confidence that the dominant mechanism of a current transport across the oxide of Bi was due to tunneling. The observation of inelastic phonon assisted tunneling in Bi/Bi samples similarly led us to believe that by oxidation of Bi in oven we could prepare "good" tunnel junctions.

6.3 Discussion of results

Early measurements on Bi/Bi junctions showed a reproducible oscillatory type structure in the vicinity of zero bias. We illustrate this in figs. 6.1 and 6.2. Fig. 6.1 shows the conductance curves for three Bi/Bi junctions. The Bi films in junctions 007 and 016 were 5000 Å thick. The films in 001 were 4000 Å thick. The corresponding derivatives $d\sigma/dV$ are in the next figure (fig. 6.2). The amplitudes

Fig. 6.1

Conductance vs energy for three Bi/Bi junctions. The thicknesses of films were following :-

001 - 4020 Å/4020 Å
007 - 5360 Å/5360 Å
016 - 5420 Å/5360 Å

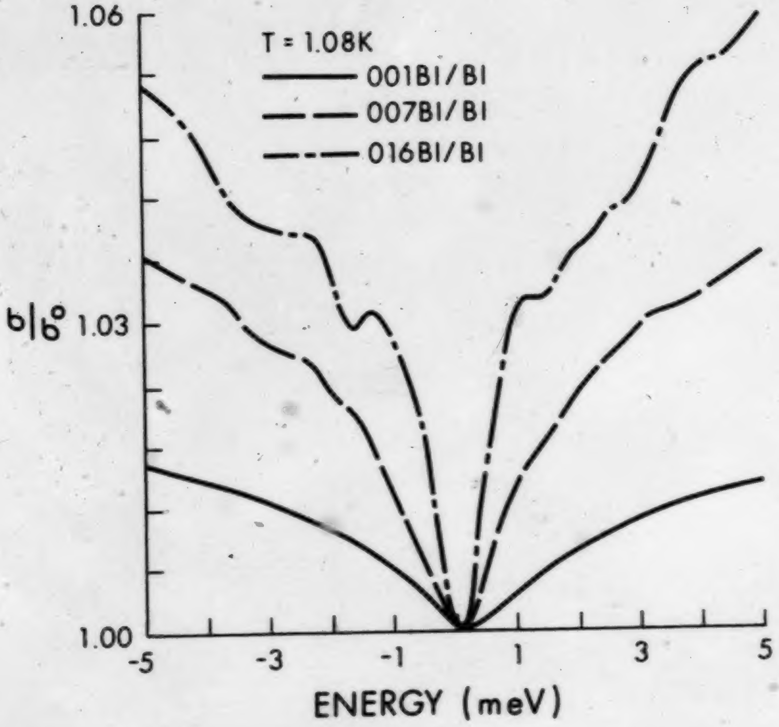
T = 1.08K
001BI/BI
007BI/BI
016BI/BI
σ/σ₀
1.06
1.03
1.00
-5
-3
-1
1
3
5
ENERGY (meV)

Fig. 6.2

dσ/dV vs energy for three Bi/Bi junctions

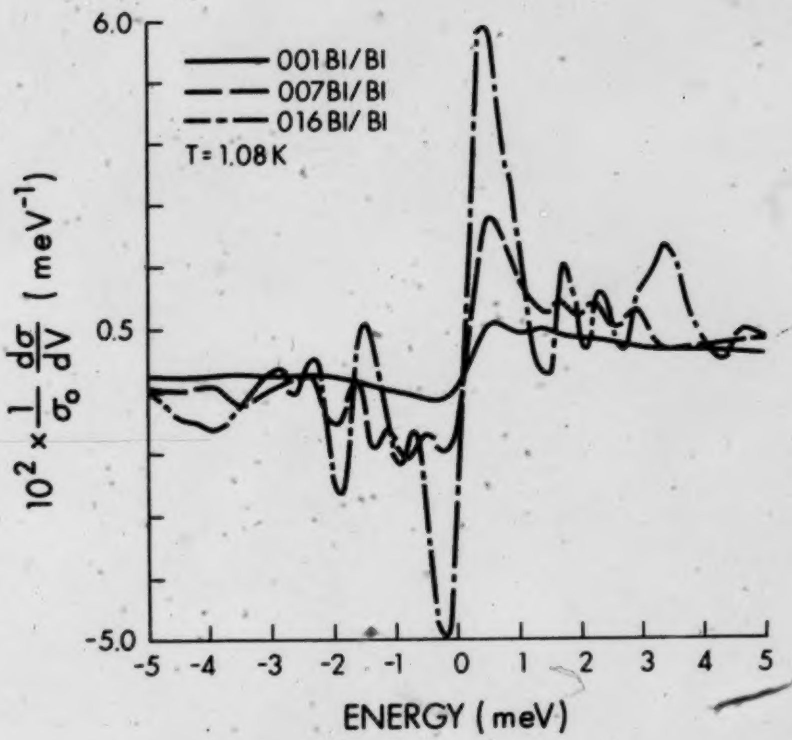
001 BI/BI
007 BI/BI
016 BI/BI
T = 1.08 K
6.0
0.5
-5.0
$10^2 \times \frac{1}{\sigma_o}\frac{d\sigma}{dV}$ (meV^{-1})
-5
-4
-3
-2
-1
0
1
2
3
4
5
ENERGY (meV)

of oscillations in 001, in comparison to the two other junctions, are small and barely visible. For positive applied voltages (top film positive) the oscillations had practically the same periodicity. This, however, was not true for the bias voltages of negative polarity (top film negative). The explanation of this effect is probably due to difference in the film structure, since the bottom films were always subjected to an annealing.

Fig. 6.3 illustrates dσ/dV for 007 in a greater detail. The general features of oscillations seen in fig. 6.3 were well reproduced even in junctions where the electrodes were 15000 Å thick. In all samples the regular oscillations always disappeared beyond the phonon emission threshold at 3 meV (Rowell et al, 1969). Taking into account this reproducibility we believe that the structure cannot be connected with impurity assisted tunneling discussed in Chapter 5. However, since the periodicity of oscillations did not change with increased thickness of Bi films, we can immediately conclude that the structure cannot be connected with the observation of quantum size effect.

Fig. 6.3

dσ/dV vs energy for 007 Bi/Bi shown separately

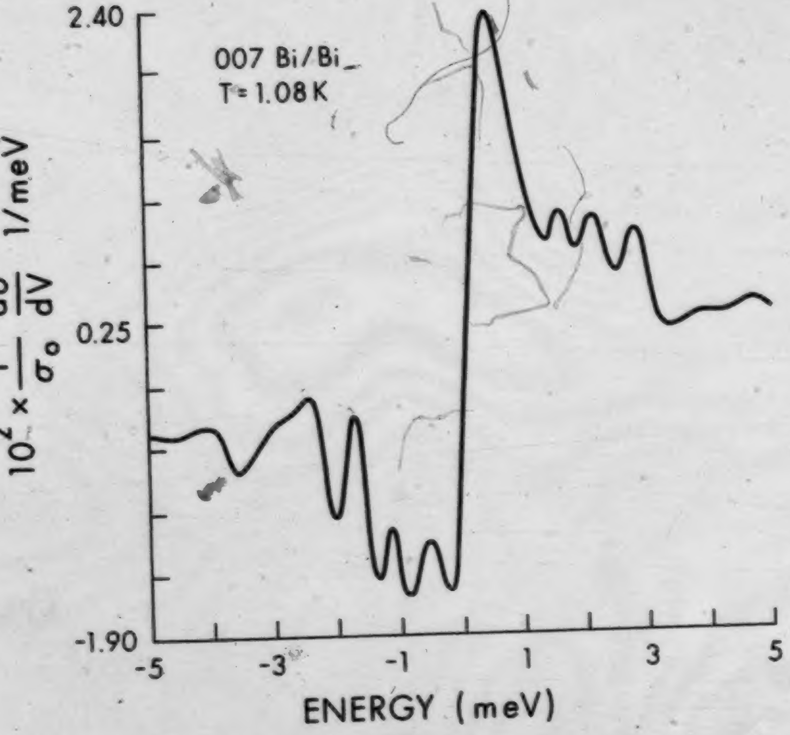
007 Bi/Bi
T=1.08 K
2.40
0.25
-1.90
$10^2 \times \frac{1}{\sigma_o}\frac{d\sigma}{dV}$ 1/meV
-5
-3
-1
1
3
5
ENERGY (meV)

6.4 Phonons in Bi

The observation of phonon emission by tunneling in carefully prepared single crystals of Bi has been reported by Esaki et al (Esaki, et al, 1968a). The conductance characteristics of $Bi/Al_2O_3/Au$ tunnel junctions, in which Bi was oriented along its trigonal axis, showed a set of humps located approximately at 3±1 meV, 6±1 meV, 10±1 meV and 14±1 meV, regardless of the polarity of applied voltage. These were correlated with previously measured phonon energies of the four propagation modes in the trigonal direction (Kotov et al):

transverse acoustic (TA) = 4.8 meV ,
longitudinal acoustic (LA) = 7.4 meV ,
transverse optic (TO) = 12.6 meV ,
and longitudinal optic (LO)= 13.4 meV ,

at the Brillouin zone boundary,

and TO = 9.2 meV and LO = 12.5 meV

at the zone center.

Peaks in $d\sigma_e/dV$ at 3 and 12 meV reflecting the inelastic excitation of Bi phonons in Al/Bi junctions were observed by Rowell et al (Rowell, et al, 1969).

Results similar to those quoted above were obtained in our samples as well. However, in contrast

Fig. 6.4

Observation of inelastic phonon assisted tunneling in a Bi/Bi junction prepared on mica. The numerals show the location of phonon peaks.

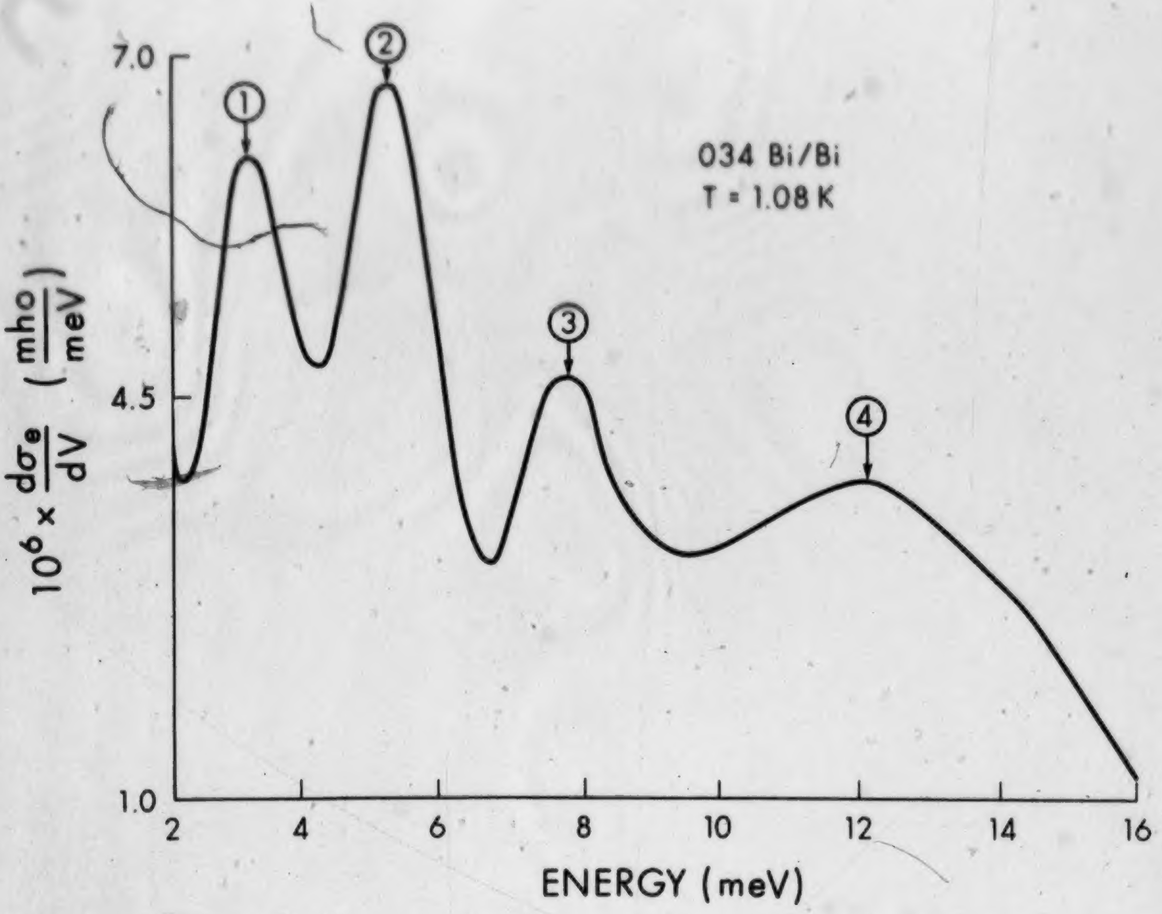
034 Bi/Bi
T = 1.08 K
①
②
③
④
7.0
4.5
1.0
$10^6 \times \frac{d\sigma_e}{dV}$ $\left(\frac{\text{mho}}{\text{meV}}\right)$
2
4
6
8
10
12
14
16
ENERGY (meV)

Fig. 6.5

Observation of inelastic phonon assisted tunneling in a Mg/Bi junction. The numerals show the location of phonon peaks.

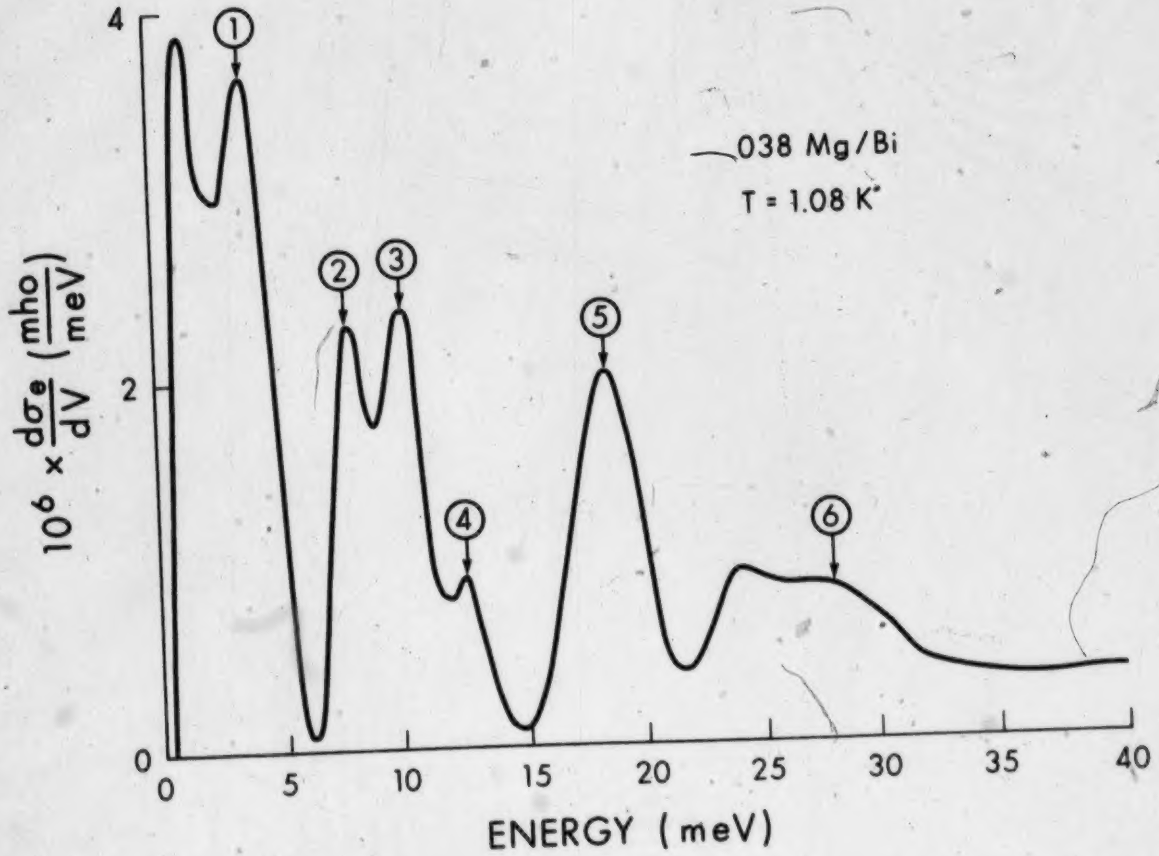
038 Mg/Bi
T = 1.08 K
$10^6 \times \frac{d\sigma_e}{dV} \left(\frac{mho}{meV}\right)$
4
2
0
ENERGY (meV)
0
5
10
15
20
25
30
35
40
①
②
③
④
⑤
⑥

Fig. 6.6

Observation of inelastic phonon assisted tunneling in an Al/Bi junction. The numerals show the location of phonon peaks.

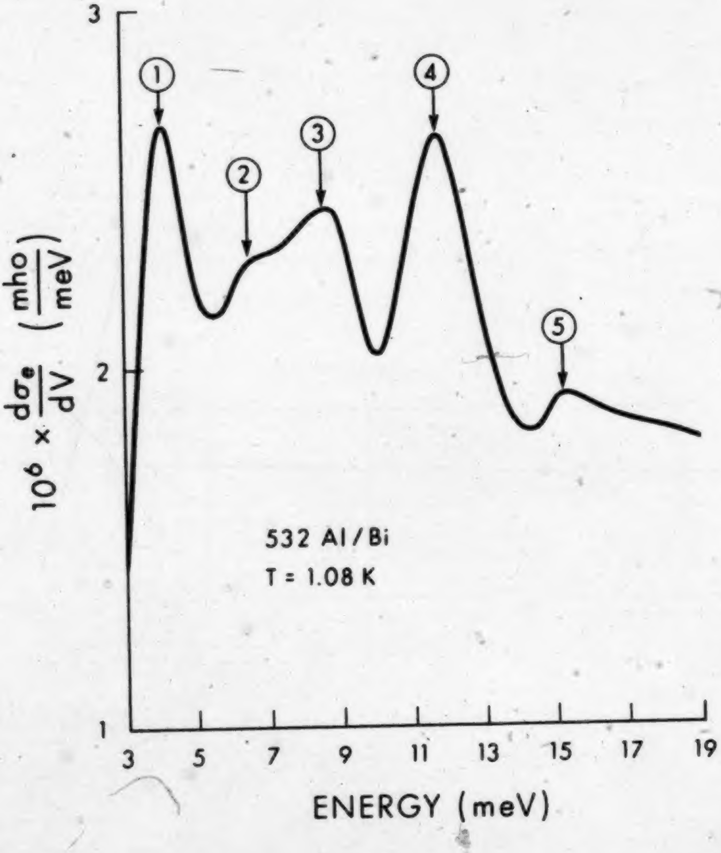
3
2
1
$10^6 \times \frac{d\sigma_e}{dV} \left(\frac{mho}{meV}\right)$
①
②
③
④
⑤
532 Al/Bi
T = 1.08 K
3
5
7
9
11
13
15
17
19
ENERGY (meV)

to the observation of Rowell et al, we were able to detect phonons which energetically lie between 3 and 12 meV.

According to Esaki et al junctions with polycrystalline Bi films did not exhibit the fine phonon structure in their tunnel characteristics. Furthermore, they did not see any structure in junctions, the resistances of which were below 5 kΩ. In comparison the resistances of our samples were less than 5 kΩ. The detection of phonons in our polycrystalline Bi films therefore complements the results of Esaki et al.

The assignments of phonon emission thresholds according to Kotov et al are following :-

Table 6.2

Identification of phonon peaks in Bi/Bi junction

Peak number	Position (meV)	Possible identification	Cryst. direction
1	3.1	LA	2 fold axis
2	4.8	TA	3 fold axis
3	7.8	LA	3 fold axis
4	12.3	TO,LO	3 fold axis

Similar identification is performed in a Mg/Bi junction (fig. 6.5).

Table 6.3

Identification of phonon peaks in Mg/Bi

Peak number	Position (meV)	Possible identification	cryst. direction
1	3.3	LA	2 fold axis
2	7.7	LA	3 fold axis
3	9.7	TO	3 fold axis
4	12.4	TO,LO	3 fold axis
5	18.4	transverse Mg	
6	27.5	longitudinal Mg	

The unmarked peak is due to zero bias anomaly.

Finally, we present the results of tunneling into an Al/Bi junction (fig. 6.6).

Table 6.4

Identification of phonon peaks in Al/Bi

Peak number	Position (meV)	Possible identification	Cryst. direction
1	3.7	LA	2 fold axis
2	6.5	TA	3 fold axis
3	8.5	LA?	3 fold axis
4	11.4	LO	2 fold axis
5	15.1	2 phonon processes?	

When determining the exact peak positions above a small correction factor (.18 meV) due to superconductivity of the Al-electrode was subtracted from the experimentally measured peak positions. The peak at 6.5 meV is identified only tentatively in the view of uncertainty in exact determination of maximum in $d\sigma_e/dV$. The peak at 8.5 meV is above the LA phonon (7.3 meV) emission threshold. Both peaks, however, at 4.2 K merged into a broad shoulder around 8 meV which is in the vicinity of the excitation energy of the LA phonon. The common feature of all three samples is the appearance of phonon peaks in the vicinity of 3 and 12 meV. This suggests that the coupling between electrons and phonons is strongest at these energies. We expect that the resolution of phonon peaks at different energies depends on the size and orientation of grains comprising the evaporated Bi film.

6.5 Other interesting effects

In connection with attempts to observe QSE in Bi we have performed tunneling experiments in which the junctions were biased up to 500 meV. All Al/Bi and Mg/Bi junctions have shown the characteristic W-shape (Fig. 6.7). The Bi/Bi junctions on the other hand show the more parabolic shape associated with

Fig. 6.7

Normalized conductance vs energy for typical Al/Bi, Mg/Bi and Bi/Bi junctions. The Mg/Bi curve has been displaced upwards by 0.2 for clarity. Negative bias indicates that the bottom layer is negative with respect to the counterelectrode.

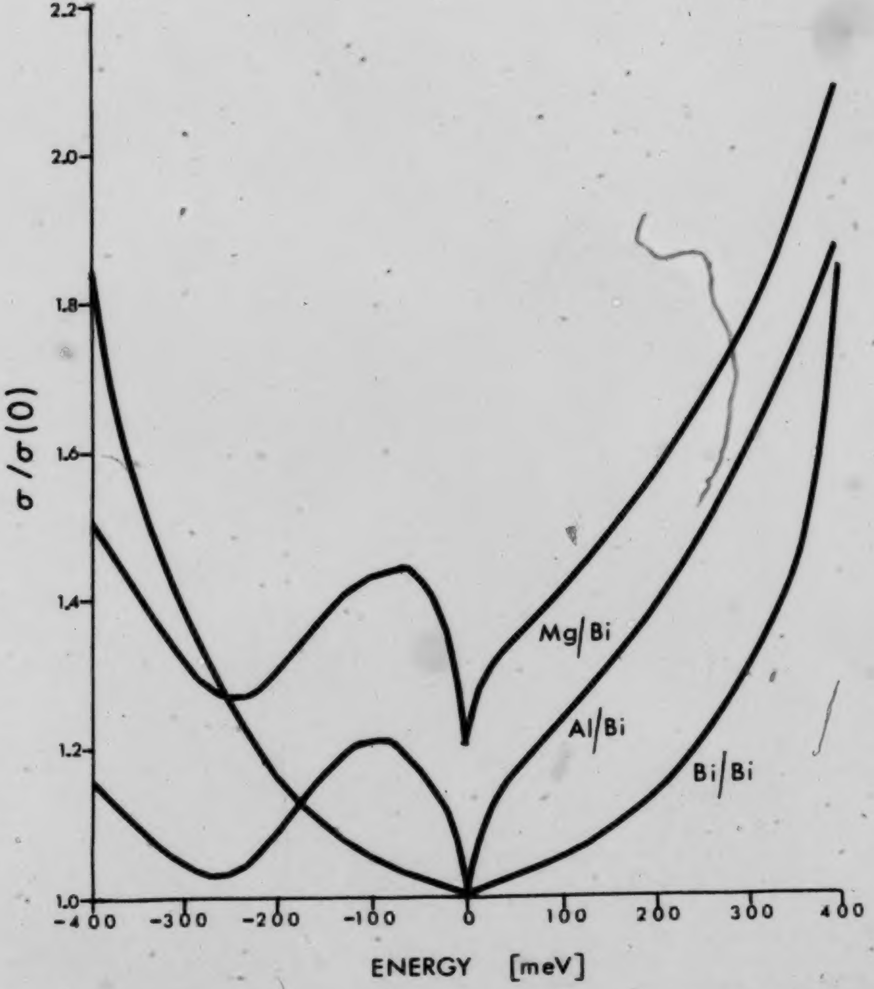
2.2
2.0
1.8
1.6
1.4
1.2
1.0
$\sigma/\sigma(0)$
-400
-300
-200
-100
0
100
200
300
400
ENERGY [meV]
Mg/Bi
Al/Bi
Bi/Bi

symmetrical tunnel junctions. We feel that the W-shape arises from the large difference in Fermi energies between the base layer and Bi counter-electrode.

In the intermediate energy range (<100 meV) we have observed a structure in Bi/Bi, Mg/Bi, Bi/Pb and Pb/Bi junctions which in certain extent correlated with the known band edges of Bi determined by other observers (Hauser, Testardi, 1968; Esaki et al, 1965).

CHAPTER 7

SUMMARY AND CONCLUSIONS

7.1 Discussions

The experimental work presented in this thesis is divided into three chapters.

In Chapter 4 we have presented the results of measurements of small conductance decreases occurring around zero bias. A recent theory (Trofimenkoff et al, 1972) has explained these through non-equilibrium treatment of the tunneling process. In particular, the related structure in σ and $d\sigma/dV$ have been accounted for by the blocking of otherwise available electron states due to finite electron relaxation times in metal electrodes. The theory assumes that the deblocking of occupied states is through scattering of electrons via lattice vibrations and impurities. These processes are characterized by a temperature and energy dependent electron-phonon relaxation time τ_{ep} and a constant impurity scattering time, τ_i. The temperature dependence of the zero bias anomaly is described only by one parameter Γ, the knowledge of which allows one to extract the impurity scattering time τ_i, if the strength of the electron-phonon interaction is known beforehand.

We have performed detailed measurements on Mg/Mg, Mg/Au and Al/Al junctions and found that the theory agrees well with experiment. A magnetic field oriented perpendicularly to the direction of tunneling current reduced the conductance anomaly. This effect was explained on the basis of Lorentz force induced drift of tunneling electrons with which we have associated a scattering time, τ_{drift}, proportional to the strength of applied field. No observable changes in the anomaly were detected if the magnetic field was applied parallel to the tunneling current.

While investigating the zero bias anomaly we have observed additional oscillatory type structure in characteristics of some tunnel junctions. The structure was found to exist in Mg/Mg, Mg/Au and Mg/Pb type junctions, irregardless of electrode thickness and barrier preparation. With the aid of external perturbations the properties of junctions could be irreversibly altered resulting in new characteristics. Adsorption of hydrocarbons during formation of barrier layer prevented the appearance of oscillations. From these observations we have concluded that a contamination of the insulating layer by charged impurities is responsible for the observed structure. It was suggested that the impurities could alter the barrier profile in such a way as to allow for a resonant transmission of tunneling electrons. The effect of external perturbations is then understood on the basis of rearrangement of impurities inside the barrier. Another possible explanation of the observed effect arises if we consider a creation of space charge trapping clusters, which could be instrumental in capture of tunneling electrons. However, until the exact nature of impurity contamination is not found, the results of discussion given in Chapter 5 will remain purely speculative.

In Chapter 6 we have briefly commented on an unsuccessful attempt to observe quantized energy levels of Bi by tunneling. As a byproduct of measurements, we have observed the excitation of phonons in polycrystalline Bi films with Bi/Bi, Mg/Bi and Al/Bi junctions. These results augment the previously published data and simultaneously provide better resolution for some of the observed peaks. The high energy conductance curves (∿500 meV) of Al/Bi and Mg/Bi junctions displayed the usual W-shape associated with such junctions. On the other hand, Bi/Bi junctions showed characteristics which are typical of symmetrical junctions. This interesting result requires further experiments for its proper interpretation.

7.2 Suggestions for further work

Concerning the zero bias anomaly we propose to investigate these areas as possible extensions of the presented work.

Evaluate the dependence of the zero bias anomaly on the crystal structure of the metal electrons. In particular, we would expect a correlation between the magnitude of the conductance dip and the anisotropy in the electron-phonon relaxation time. This, of course, requires a preparation of single crystal junctions. We include here the dependence of the zero bias anomaly on film thickness. The experimental results gave qualitative agreement with the theory. A more detailed investigation should possibly extract the amount of blocking due to decreased film thickness. In connection with this we suggest backing of electrodes with a silver layer in order to change the amount of specular scattering.

A further study should show the effect of alloying on the size of zero bias anomaly. With such experiments we can change not only the impurity scattering time τ_i, but the electron-phonon coupling strength as well.

Finally, as it has already been shown (Wattamaniuk, 1972) the non-equilibrium aspect of the electron tunneling can be extended to include a tunneling into superconducting metals. In particular, for the case of two identical superconductors, the continuous increase in the tunnel current just above twice the gap edge (T ≠ 0 K) has been explained as due to blocking of the incoming quasi-particles. It should be noted that the quasi-equilibrium theory predicts a discontinuous jump which is experimentally not observed. Further experiments are needed to clarify this situation.

Regarding the impurity assisted tunneling, the objective of further experiments is to determine the origin of barrier contamination. This requires a different method of barrier formation; thermally grown barrier eliminates a possibility of contamination through sputtering action during glow discharge. Experiments should be performed in order to determine a mechanism by which adsorption of hydrocarbons in the insulating layer prevents the occurrence of oscillations.

Since our attempts to observe the quantized energy levels directly by tunneling have failed we suggest further experiments in which surface roughness of Bi films is minimized and better controlled. This includes tunneling into single crystals of Bi.

Furthermore, tunneling in Bi/oxide/metal and metal/oxide/Bi type junctions appears to be a unique method of proper identification of a structure in characteristics of these junctions.

BIBLIOGRAPHY

Adler, J.G. and Jackson, J.E., Rev. Sci. Instr. 37, 1049 (1966).

Adler, J.G., Phys. Lett. 29A, 675 (1969a).

Adler, J.G., Sol. State Commun. 7, 1635 (1969b).

Adler, J.G. and H.J. Kreuzer, Can. J. Phys. 22, 2842 (1972).

Adler, J.G. and Straus, J., Technical Report, University of Alberta, 1974, unpublished .

Allen, P.B. and Cohen, M.L., Phys. Rev. B 1, 3929 (1970).

Anderson, P.W., Phys. Rev. Lett. 11, 95 (1966a).

Anderson, P.W., Phys. Rev. Lett. 17, 95 (1966b).

Appelbaum, J.A., Phys. Rev. Lett. 17, 91 (1966).

Appelbaum, J.A., Phys. Rev. 154, 633 (1967).

Appelbaum, J.A. and Brinkman, W.F., Phys. Rev. B 2, 907 (1970).

Appelbaum, J.A. and Shen, L.Y.L., Phys. Rev. B 5, 544 (1972).

Bardeen, J., Phys. Rev. Lett. 6, 57 (1961).

BenDaniel, D.J. and Duke, C.B., Phys. Rev. 152, 683 (1966).

BenDaniel, D.J. and Duke, C.B., Phys. Rev. 160, 697 (1967).

Bohm, D., in Quantum Theory (Prentice Hall, Inc., New York, 1951), pp. 283-295.

Brinkman, W.H., Dynes, R.C. and Rowell, J.M., J. Appl. Phys. 41, 1915 (1970).

Burstein, E., Lundquist, S., eds., Tunneling Phenomena in Solids (Plenum Press, New York, 1969).

Carbotte, J.P. and Dynes, R.C., Phys. Rev. 172, 476 (1968).

Carbotte, J.P. and Truant, P.T., Can. J. Phys. 52, 618 (1974).

Chen, T.T. and Adler, J.G., Sol. State Commun. 8, 1965 (1970).

Combescot, R., J. Phys. C: Solid St. Phys. 4, 2611 (1971).

Dijk, H. van, Durieux, M., Clement, J.R. and Logan, J.K., The "1958 He^4 Scale of Temperatures", NBS Monograph 10, June 17, 1960.

Duke, C.B., Tunneling in Solids (Academic Press, New York, 1969).

Duke, C.B., Phys. Rev. 159, 632 (1967).

Duke, C.B., Kleinman, G.G. and Stakelon, T.E., Phys. Rev. B 6, 2389 (1972).

El-Semary, M.A. and Rogers, J.S., Phys. Rev. Lett. 42A, 79 (1972).

El-Semary, M.A., Kaahwa, Y. and Rogers, J.S., Solid State Commun. 12, 593 (1973).

Esaki, L. and Stiles, P.J., Phys. Rev. Lett. 14, 902 (1965).

Esaki, L., Stiles, P.J. and Chang, L.L., Phys. Rev. Lett. 20, 1108 (1968a).

Esaki, L., Chang, L.L., Stiles, J.P., O'Kane, D.F. and Wiser, Nathan, Phys. Rev. 167, 637 (1968b).

Eschbach, H.L. and Kruidhof, W.E., Vacuum Microbalance Techn. 3, 207 (1965).

Fal'kovskij, L.A., Sov. Phys. Uspekhi, 1, (1968).

Fisher, J.C. and Giaver, I., J. Appl. Phys. 32, 172 (1961).

Frenkel, J., Phys. Rev. 36, 1604 (1930).

Gadzuk, J.W., J. Appl. Phys. 41, 286 (1970).

Gadzuk, J.W. and Lucas, A.A., Phys. Rev. B 7, 4470 (1973).

Garcia, N., Kao, Y.H., and Strongin, Myron, Phys. Rev. 5, 2029 (1972).

Geiger, A.L., Chandrasekhar, B.S. and Adler, J.G., Phys. Rev. 188, 1130 (1969).

Giaver, I., and Zeller, H.R., Phys. Rev. Lett. 20, 1540 (1968a).

Giaver, I. and Zeller, H.R., Phys. Rev. Lett. 21, 1385 (1968b)

Gogadze, D.G.A. and Kulik, I.O., Sov. Phys. Sol. State 7, 345 (1965).

Goy, P. and Castaing, B., Phys. Rev. B 7, 4409 (1973).

Gupta, N.M. and Upadhyaya, U.N., Phys. Rev. B 4, 2765 (1971).

Hapase, M.G., Tare, V.B. and Biswas, A.B., Acta Metallurgica 15, 131 (1967).

Harrison, W.A., Phys. Rev. 123, 85 (1961).

Hartman, T.E., J. Vacuum Tech. 3, 28 (1965).

Hauser, J.J. and Testardi, L.R., Phys. Rev. Lett. 20, 12 (1968).

2

Holland, L., in Vacuum Deposition of Thin Films (Chapman and Hall Ltd., 1961) pp. 74-78.

Hurault, J.P., J. de Physique 32, 421 (1971).

Jacklevic, R.C. and Lambe, J., Phys. Rev. Lett. 17, 1139 (1966).

Jacklevic, R.C. and Lambe, J., Mikkor, M. and Vassell, W.C., Phys. Rev. Lett. 26, 88 (1971).

Jacklevic, R.C. and Lambe, J., Mikkor, M. and Vassell, W.C., Solid State Commun. 10, 199 (1972).

Josefowicz, J. and Smith, H.J.T., Can. J. Phys. 51, 597 (1973).

Klein, J. Léger, A., Belin, M., DéForneau, D. and Sangster, M.J.L., Phys. Rev. 7, 2336 (1973).

Komnik, F. Yu. and Bukhstab, E.I., Sov. Phys. JETP 27, 34 (1968).

Komnik, F. Yu. and Pilipenko, V.V., Sov. Phys. Cryst. 16, 352 (1971).

Korneev, D.N., Lutskii, V.N. and Elinson, M.I., Sov. Phys. Solid State 12, 1049 (1970).

Kotov, B.A., Okuneva, N.M. and Plachenova, E.L., Sov. Phys. Solid State 11, 1615 (1970).

Kümmel, R., Zeitschrift fur Physik 213, 282 (1968).

Larson, D.C., in Physics of Thin Films, ed. by Francombe, Hoffman (Academic Press, New York, 1971), pp. 137-143.

Lutskii, V.N., Korneev, D.N. and Elinson, M.I., Sov. Phys. JETP 4, 179 (1966).

Lythall, D.J. and Wyatt, A.F.G., Phys. Rev. Lett. 20, 1361 (1968).

Maissel, L.I., and Glang, R., in Handbook of Thin Film Technology (McGraw-Hill, 1970) pp. 14-18.

Miles, J.L. and Smith, P.H., J. Appl. Phys. 34, 2109 (1963).

Parker, G.H. and Mead, C.A., Phys. Rev. 184, 780 (1969).

Penley, C., Phys. Rev. 128, 596 (1962).

Pollack, S.R. and Morris, C.E., J. Appl. Phys. 35, 1503 (1964).

Rowell, J.M. and Shen, L.Y.L., Phys. Rev. Lett. 17, 15 (1966).

Rowell, J.M., J. Appl. Phys. 40, 1211 (1969).

Rowell, J.M., McMillan, W.L. and Feldman, W.L., Phys. Rev. 180, 658 (1969).

Sasaki, Y., J.Phys. Chem. Solids 12, 177 (1960).

Sawatari, Y. and Arai, M., Jap. J. Appl. Phys. 7, 560 (1968).

Schmidlin, F.W., J. Appl. Phys. 37, 2823 (1966).

Shen, L.Y.L., Phys. Rev. Lett. 21, 361 (1968).

Simmons, J.G., J. Appl. Phys. 34, 1973 (1963a).

Simmons, J.G., J. Appl. Phys. 34, 2581 (1963b).

Sommerfeld, A. and Bethe, H.A., in Handbuch der Physik, S. Flugge ed. (Springer-Verlag, Berlin, 1933), Vol. 24, p.150.

Sommers, H.S., Rev. Sci. Instrum. 25, 793 (1954).

Steckelmacher, W., in Thin Film Microelectronics ed. by Holland, L. (John Wiley & Sons, New York, 1965), p.193.

Stevenson, R.J. and Hensley, E.B., J. Appl. Phys. 32, 1661 (1961).

Stockbridge, C.D., in Vacuum Microbalance Techniques, ed. by Behrndt, K. (Plenum Press, New York, 1966), vol. 5, p.193.

Stratton, R., J. Phys. Chem. Solids 23, 1177 (1962).

Tavger, B.A. and Demikhovskij,V. Ya., Sov. Phys. Uspekhi 11, 644 (1969).

Teshima, R., Private communication (1974).

Thornber, K.K., McGill, T.C. and Mead, C.A., J. Appl Phys. 38, 2384 (1967).

Tolansky, S., in Surface Microtopography (Longmans Green and Co., Ltd., 1960).

Trofimenkoff, P.N., Kreuzer, H.J., Wattamaniuk, W.J. and Adler, J.G., Phys. Rev. Lett. 29, 597 (1972).

Truell, R., Elbaum, C. and Chieck, B.B., Ultrasonic Methods in Solid State Physics (Academic Press, New York, 1969) pp. 290-294.

Tsui, D.C., Phys. Rev. Lett. 22, 293 (1969).

Tsui, D.C., Dietz, R.E. and Walker, L.R., Phys. Rev. Lett. 27, 1729 (1971).

Turner, P.S., Private communication (1974).

Vaisnys, J.R., McWhan, D.B. and Rowell, J.M., J. Appl. Phys. 40, 2623 (1969).

Vrba, J., Tunneling into Weakly Coupled Films of Al and Sn in Proximity (Ph.D. thesis, University of Alberta, 1971).

Wattamaniuk, W.J., Nonequilibrium Effects in Tunnel Junctions (Ph.D. thesis, University of Alberta, 1973).

Wilkins, J.W., Lecture notes on; Observable Many-Body Effects in Metals (Nordita, 1968).

Wolf, E.L., Nonsuperconducting Electron Tunneling (Academic Press, to be published, 1974).

Wyatt, A.F.G., Phys. Rev. Lett. 13, 401 (1964).

Yanson, I.K., Verkin, B.I., Ostrovskii, L.I., Teplitskii, A.B. and Skhlyarevskii, O.I., Zhetf. Pis. Red. 14, 40 (1971).

Zeller, H.R. and Giaver, I., Phys. Rev. 181, 789 (1969).

PREVIOUSLY COPYRIGHTED MATERIAL,

IN APPENDIX I, LEAVES 219-225,

NOT MICROFILMED.

High Resolution Electron Tunneling Spectroscopy, by J.G. Adler, T.T. Chen, and J. Straus, Department of Physics, University of Alberta, Edmonton, Alberta, Canada. Reprinted from The Review of Scientific Instruments, Vol. 42, No. 3, 362-368, March 1971.

APPENDIX II

Reprinted from
SOLID STATE COMMUNICATIONS

PREVIOUSLY COPYRIGHTED MATERIAL,

IN APPENDIX II, LEAVES 227-229,

NOT MICROFILMED.

Size Effect in the Magnetic Field Dependence of Nonequilibrium Electron Tunneling, by J.G. Adler, H.J. Kreuzer and J. Straus, Department of Physics, University of Alberta, Edmonton, Canada. Reprinted from Solid State Communications, Vol. 13, pp. 939-941, 1973. Pergamon Press. Printed in Great Britain.